

Ab initio Investigations
on H Bonded
Molecular Clusters



Dissertation

zur Erlangung des Doktorgrades der Naturwissenschaften (Dr. rer. nat.)
der Fakultät IV
- Chemie und Pharmazie -
der Universität Regensburg

vorgelegt von

Dominik Schemmel

aus Stuttgart

Regensburg 2010

Promotionsgesuch eingereicht am:	17. September 2010
Tag des Kolloquiums:	12. November 2010
Diese Arbeit wurde eingeleitet von:	Prof. Dr. Martin Schütz
Promotionsausschuss	
Vorsitzender:	Prof. Dr. Jörg Daub
Erstgutachter:	Prof. Dr. Martin Schütz
Zweitgutachter:	Prof. Dr. Bernhard Dick
Drittprüfer:	Prof. Dr. Arno Pfitzner

Die Ergebnisse dieser Arbeit sind bereits veröffentlicht worden:

Kapitel 2

D. Schemmel and M. Schütz

"Phenol-water_{1≤n≤3} revisited: An ab initio study on the photophysics of these clusters at the level of coupled cluster response theory"

Journal of Chemical Physics, **127**, 174304 (2007), doi: 10.1063/1.2794037

Ausgewählt für: *Virtual Journal of Biological Physics Research*, **14/10** (2007).

Kapitel 3

D. Schemmel and M. Schütz

"The 2-naphthol-water₂ cluster: Two competing types of hydrogen-bonding arrangements"

Journal of Chemical Physics, **129**, 034301 (2008), doi: 10.1063/1.2952271

Kapitel 4

D. Schemmel and M. Schütz

"Molecular aniline clusters. I. The electronic ground state"

Journal of Chemical Physics, **132**, 174303 (2010), doi: 10.1063/1.3419505

Kapitel 5

D. Schemmel and M. Schütz

"Molecular aniline clusters. II. The low-lying electronic excited states"

Journal of Chemical Physics, **133**, 134307 (2010), doi: 10.1063/1.3488227

Kapitel 6

D. Hoppe, D. Schemmel, M. Schütz and A. Pfitzner

"Nb and Ta adduct compounds: Connecting d⁰ metal chlorides and phosphorus sulfide cages"

Chemistry - A European Journal, **15**, 7129-7138 (2009),
doi: 10.1002/chem.200900370

Acknowledgements

First I thank Prof. Dr. Martin Schütz for the supervision of my doctoral studies. I am very grateful for his expert advice and all his time and support.

I am indebted to Dr. Diana Hoppe and Prof. Dr. Arno Pfitzner for fruitful cooperation and all their ideas, expertise and dedication.

I am grateful to all my instructors in the field of theoretical and physical chemistry. This work would not have been possible without outstanding teachers sharing their knowledge and fascination for science.

I thank my colleagues Dr. Denis Usvyat, Dr. Uwe Birkenheuer, Dr. Keyarash Sadeghian, Dr. Danylo Kats, Marco Lorenz, Stefan Loibl, Thomas Merz and Katrin Freundorfer for their support, friendliness, and the time we shared. I am grateful to Klaus Ziereis for helping me whenever technical difficulties appeared.

Financial support from the Deutsche Forschungsgemeinschaft (DFG) is gratefully acknowledged.

This thesis is dedicated with love and gratitude to my family and friends.

Contents

1	General introduction	3
1.1	Preface	3
1.2	Experiment	5
1.3	Theory	7
1.3.1	Synopsis	7
1.3.2	Supermolecule method	9
1.3.3	Coupled cluster model	10
1.3.4	MP2 and CC2	11
1.3.5	Spin component scaled methods	12
1.3.6	Local approximation	13
1.3.7	Density fitting approximation	13
1.4	Overview	14
2	Phenol-water_{1≤n≤3} clusters	15
2.1	Introduction	15
2.2	Computational Methods	18
2.3	Results and Discussion	19
2.3.1	Minimum energy geometries	20
2.3.2	Conical Intersection and Proton Transfer	30
2.4	Conclusions	32
3	2-Naphthol-water₂ clusters	33
3.1	Introduction	33
3.2	Computational methods	35
3.3	Results and discussion	36
3.3.1	S ₀ minimum-energy geometries	37
3.3.2	S ₁ minimum-energy geometries	43
3.3.3	Excitation energies and transition moments	48
3.3.4	Vibrational modes	52
3.4	Conclusions	52
4	Aniline clusters in the electronic ground state	55
4.1	Introduction	55

Contents

4.2	Computational methods	57
4.3	Nomenclature	59
4.4	Results and Discussion	61
4.4.1	Structures and interaction energies	61
4.4.2	Vibrational frequencies of the N–H stretch modes	68
4.5	Conclusions	69
5	The low-lying electronic excited states of aniline clusters	71
5.1	Introduction	71
5.2	Computational methods	73
5.3	Results and Discussion	74
5.3.1	The aniline dimer, An ₂	74
5.3.2	The aniline trimer, An ₃	79
5.4	Conclusions	83
6	Adducts of tantalum chlorides and phosphorus sulfide cages	85
6.1	Introduction	85
6.2	Computational methods	86
6.3	Results and Discussion	87
6.3.1	Constitution and packing	87
6.3.2	Conformation	89
6.3.3	Bond lengths	91
6.3.4	Alternative coordination modes	95
6.4	Conclusions	100
7	Summary	103
	Bibliography	106

1 General introduction

1.1 Preface

Starting from the time of the ancient Indians and Greeks we know about the concept that the microscopic world around us is built of smallest units. Two and a half millenia later there is no doubt that the matter around us is composed of distinct molecules and macromolecular structures which themselves are consisting of nuclei and electrons. This gluing of the atoms to extended structures is due to the formation of chemical bonds, i.e. a stable equilibrium of the electrons and nuclei in their mutual electric fields.

However, regarding the macroscopic behavior of gases and liquids, even our daily experiences tell us that also attractive and repulsive forces between the molecules have to be present, since the world around us can neither be arbitrarily compressed nor evaporated. Starting from the nineteenth century this topic has been addressed by science. Whereas the ideal gas law assumes non interacting and non colliding molecules, starting with van der Waals and his famous corrections to this equation, the field of intermolecular interactions has been founded.

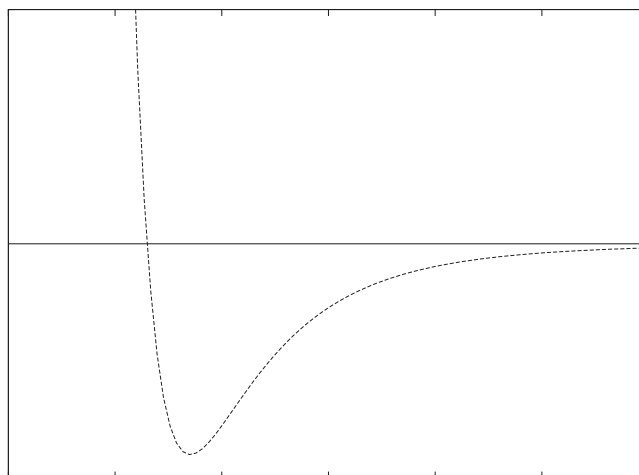


Figure 1.1: Exemplary intermolecular potential function.

1 General introduction

A typical intermolecular potential curve can be estimated as seen in figure 1.1. The steep incline at small distances shows that the volumes of the interacting molecules refuse to penetrate each other. At very large distances, the interaction is zero, being conform with the good applicability of the ideal gas law on describing gases of low density. At intermediate distances, attractive forces and a minimum can be assumed, reflecting the observation that a gas can condense into a liquid, because the molecules tend to glue to each other. Usually the depth of the minimum is shallower than that of a chemical bond, since a phase transition can take place without altering the bonding patterns in the molecules. Whereas the binding energy of the weakest covalent bonds start at approximately 50 kcal/mol, the intermolecular binding energies lie in the range of a few kcal/mol only.

Interestingly, the presence of intermolecular forces eminently influences our view on our environment. They are not only crucial for the description of the fluids, but also influence chemical reactions in solvents. The vast field of biochemistry mainly describes systems and reactions in aqueous solution. The macroscopic properties of elastic polymers and the folding of proteins are all governed by intermolecular forces. Furthermore the biological phenomena such as the climbing abilities of the Tokay geckos rely on weak intermolecular interactions [1]. There are numerous further examples.

From the physical point of view, the intermolecular interactions can be divided into meaningful parts [2–4]. This can be seen when we try to apply Rayleigh-Schrödinger perturbation theory on two non interacting subsystems. The perturbation in this case is the electron repulsion between the subsystems and the Hamiltonian is the sum of the Hamiltonians of the two subsystems. This is known as the polarization theory. Consequently the wavefunction (in the zeroth order of perturbation) is the product of the wavefunctions of the subsystems. In the first order, one obtains the electrostatic energy. This can be interpreted as the interaction energy of static charge distributions of the subsystems. In the second order, the polarization energy and the dispersion energy are obtained. The polarization interaction means the influence of the field of one subsystem on the other subsystem. This type of interaction always is attractive. The term dispersion describes the electron correlation between the subsystems, which leads to mutually induced density fluctuations in each subsystem. All these contributions can be approximated at large separations as power laws of distance with negative exponents.

It turns out that the polarization theory suffers from severe drawbacks. Not only the perturbation series diverges in higher orders, also the theory is qualitatively wrong at intermediate and short distances. The reason for this is, that the wavefunction of the system is antisymmetric under the exchange of two electron belonging only to the same subsystem. The approach however assumes a product

wavefunction, so that the electron exchange between the subsystems is symmetrical, which is incorrect for fermions such as electrons. To remedy this problem, the antisymmetry between the subsystems needs to be enforced. Among other theories formulated, the field of the symmetry-adapted perturbation theories (SAPT) is rather successful. Here the antisymmetry between the subsystems is corrected a posteriori [2, 5–8]. A plethora of different approaches exist, but generally a set of additional correction terms to terms already known from the polarization theory are obtained. In the first order the exchange-repulsion energy describes on the one hand the attractive tunneling of electrons between the subsystems, but on the other hand the repulsive situation due to the Pauli principle, when the electrons of the same spin but from different subsystems attempt to occupy the same space. In the second order the corrections differ from theory to theory, but can generally be seen as the exchange corrections to polarization and dispersion. These short-range contributions to the energy vanish exponentially, and thus can be neglected at large distances. Still, the convergence problem remains unsolved. The SAPT can be implemented as a double perturbation theory, using inter- and intramonomer perturbations [9]. Modern implementations up to second order, such as DF-DFT-SAPT [10] or local EOM-CCSD [11] offer an accuracy for the interaction energy similar to the "golden standard" of quantum chemistry, CCSD(T), or beyond.

Also noteworthy is the fact, that the interaction energy cannot only be written as a sum of two-body interactions in terms of atoms or molecules, but also involves higher-body contributions. Thus it is commonly expanded in the many-body expansion [12, 13],

$$E_{\text{int}} = \underbrace{\sum_{i>j} E_{ij}}_{E_{2\text{body}}} + \underbrace{\sum_{i>j>k} E_{ijk}}_{E_{3\text{body}}} + \underbrace{\sum_{i>j>k>l} E_{ijkl}}_{E_{4\text{body}}} + \dots \quad (1.1)$$

Three-body and higher terms often cannot be neglected, thus the induction energy inherently is a many-body effect and also the dispersion energy contains many-body effects. An example for that is the well-known Axilrod-Teller-Muto tripole-dipole dispersion [14, 15].

1.2 Experiment

From a molecular point of view, molecular clusters, i. e. isolated aggregates of one to many molecules (monomers) play a prominent role as test systems in the experimental investigation of intermolecular interactions [16–18]. In the absence of perturbations arising from environmental influences, solvent effects and collisions,

1 General introduction

structure and binding of the clusters is solely determined by their intermolecular behavior.

Experimentally, molecular clusters are produced in supersonic beam expansions. Here the monomer substances are mixed with a seed gas and are expanded under pressure (continuously or pulsed) through a tiny nozzle into high vacuum. The evaporating seed gas cools the produced clusters down to very low temperatures of approximately 15 to 30 Kelvin (vibrational temperature). By varying the experimental parameters, such as pulse length, mixing ratios or pressure, the cluster formation can be influenced.

The beam can then be characterized by various spectroscopic methods [19]. Direct indicators for intermolecular forces within the clusters are the intermolecular vibrational modes, which lie in the far infrared region. With far infrared vibrational rotational-tunneling spectroscopy (FIR-VRT) [20, 21] it is possible to measure these transitions directly and with a high resolution. But transitions in the far infrared region are generally not easily accessible. Their measurement is possible indirectly via electronically excited states, or via the intramolecular vibrational modes of the monomers. By using resonant two-photon ionization (R2PI) it is possible to measure intermolecular modes size selectively. This can also be combined with laser induced dispersed fluorescence emission and hole burning techniques. Via mass analyzed threshold ionization (MATI) spectroscopy it is in some cases also possible to determine binding energies with high precision [22]. All these methods have in common, that an ultraviolet chromophore has to be contained in the cluster system, which acts as an antenna and makes the electronically excited states due to its high transition strength accessible. Therefore these methods are limited to clusters with at least one aromatic molecule.

Another way of characterization is the infrared cluster spectroscopy. Here the intramolecular modes are regarded as indicators for the acting intermolecular forces in the clusters [23–25]. Especially for H bonded clusters the OH or NH stretch modes are meaningful, because the spectral shift of these bands with respect to the signal in the lone monomer directly allows conclusions on the cluster topology [26–28] and structure. Since no chromophore is needed, these measurements can be applied to a larger variety of systems, e.g. homogenous solvent clusters.

In many cases the obtained spectra are complicated, so that without a complementary analysis by theoretical methods their interpretation can only be done on a speculative footing. Fortunately the clusters are not extended systems and thus in the scope of high-level *ab initio* methods.

1.3 Theory

1.3.1 Synopsis

Ab initio electronic structure theory describes chemical systems by solving the stationary form of the Schrödinger’s equation ”from the beginning”, i.e. without the usage of empirical data.

$$\hat{H}\psi = E\psi \quad (1.2)$$

A hierarchical system of approximations allows accuracy up to the limit of available computational resources (also see figure 1.2). Therefore, the ongoing development of computational resources and algorithms gradually lifts the limitations on accuracy and system size, hence enabling the application of these methods to a wider range of systems. In contrast to the empirical description of chemistry, theory offers a systematic and insightful access to interpret existing data, but also the ability to generate interesting challenges for experimental investigations.

The Born-Oppenheimer approximation [29] is the most basic and almost universally used simplification. It practically defines the chemists’ picture of a molecule and enables drawing structural formulae. It adiabatically decouples the motion of the electrons from the movements of the nuclei. The electronic wavefunction then depends parametrically on the spatial coordinates of the nuclei. Then, solving the electronic Schrödinger equation gives the electronic energy for a certain molecular geometry. The electronic energies of all geometries possible are represented by the potential energy surface (PES), which is a function of that space. Using the PES as the potential energy, the remaining nuclear Schrödinger equation can be solved to investigate e.g. vibrations or reactions. At near-degeneracies or crossings of electronic states the approximation fails, because the non-adiabatic coupling becomes non zero.

Relativistic effects are of importance for heavy elements mainly. For light elements up to the second period they are very small and usually neglected. These effects can be partially accounted for by substituting the heavy nuclei and their inner electrons by pseudopotentials [30]. Nevertheless, to describe relativistic effects directly, different theoretical approaches need to be employed [31].

For solving the electronic Schrödinger equation numerically, a finite basis set is used for representing the wavefunction. Usually, this basis consists of Gaussian type functions, which offer computational advantages by virtue of the Gaussian product theorem. Gaussian functions as a basis have the drawback, that a linear combination of many functions is required to properly describe the Coulomb hole, i.e. the situation when two electrons of opposite spins come spatially close. Hence, the truncation of the full infinite basis is an approximation. Since the computa-

1 General introduction

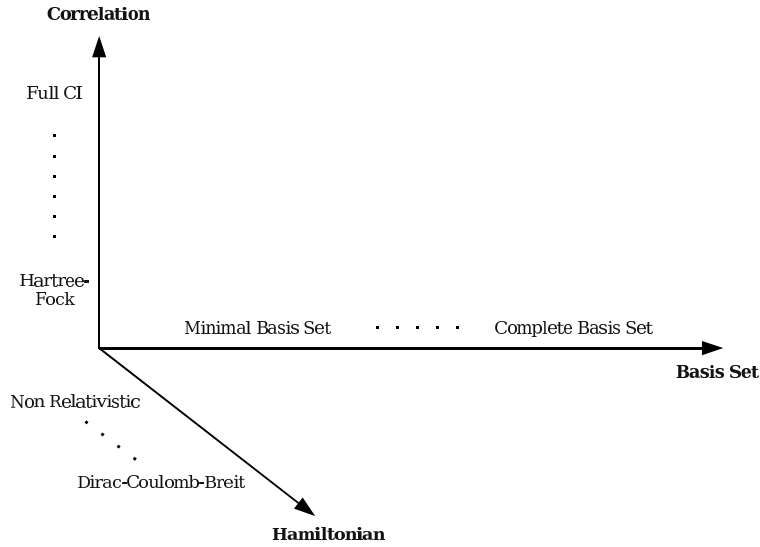


Figure 1.2: Schematic overview of the three axes of hierarchical approximations in the *ab initio* electron structure theory. Since the computational resources are limited, an appropriate level of accuracy has to be chosen. The choices are the truncation of the basis set, treating the electron correlation approximately and accounting for relativistic effects by using different hamilton operators.

tional problem sizes of the methods used scale with a power law to the basis set size, the selection of the actual basis set is therefore a compromise. There are hierarchical series of basis sets, such as the correlation-consistent sets of Dunning [32–34], which allow systematic convergency towards the basis set limit and furthermore allow the usage of extrapolation techniques [35].

The basic step in solving the Schrödinger equation for the electrons, alias their many-body problem, is the self-consistent field procedure. Here the approximation is that the electrons are treated as if they move in the average field of themselves (excluding their own respective field), i.e. they are uncorrelated. The wavefunction is a product of molecular orbitals (MOs), antisymmetrized by the Slater determinant approach. MOs are a linear combination of atomic orbitals (AOs) with variationally determined coefficients. Usually a single Slater determinant is used in the first place, which is known as Hartree-Fock (HF) [36, 37]. To treat the correlation of the electrons on top of the HF wavefunction, a linear combination of the obtained non excited determinant and all possible excited determinant is required. This is known as full configuration interaction (Full CI), and practically only solvable for the smallest systems. In order to approximatively treat the missing correlation a wide range of methods exist which truncate this expansion. The

restriction to certain determinants in terms of excitation classes is known as CI with single excitations (CIS), single and double excitations (CISD), ... A more clever way of addressing the expansion coefficients by an exponential approach is known as coupled cluster (*vide infra*) [38]. Also perturbation theoretical approaches exist. A prominent example is the Møller-Plesset perturbation theory in second order (MP2) [39]. All methods have in common that the computational complexity increases by their accuracy, so again here a tradeoff has to be done. A remedy to this problem is to use local methods, which exploit the spatially short-ranged nature of the correlation and try to achieve low-order scaling behavior with respect to the system size (*vide infra*).

1.3.2 Supermolecule method

Besides the perturbative approach by means of the above discussed SAPT, another prominent way to calculate the interaction between molecules is the so-called supermolecule ansatz. Basically, the interaction energy is calculated as the difference between the total energies of the complete cluster and the single monomers,

$$E_{\text{int}} = E^{\text{cluster}} - \sum_i E_i^{\text{monomer}}. \quad (1.3)$$

The so obtained interaction energy can be further decomposed into the many-body terms by a gradual, systematic subtraction of the interaction energies of the contained subclusters [13]. So the three-body interaction energy of a trimer is obtained by subtracting the interaction energies of the three possible dimer subclusters from the total interaction energy.

This approach is problematic, in the sense that the interaction energies are usually very small as compared to the total energies. Therefore, the accuracy of the calculations needs to be high. Sufficiently sized basis sets as well as post-HF methods to describe the dispersion are hence mandatory. Furthermore each calculation has to be done not only with the same basis set quality but also in exactly the same basis set size. Thus, dummy functions on ghost atoms which substitute the lacking other monomers, are used in the monomer or subcluster calculations. The reason for this is the correction of the basis set superposition error (BSSE). If no ghost centers were used, the tails of the lacking basis set functions positioned on these centers could not improve the wavefunction of monomers, as they do in the full cluster calculation. This procedure is known as the counterpoise correction (CPC) [40]. The usage of local correlation methods is beneficial in this context, since they avoid a large fraction of the BSSE of the correlation energy by construction [41].

1 General introduction

The interaction energy is just a theoretical concept. The binding energy, obtained as the energy difference of the cluster and the monomers in infinite distance, also includes relaxational effects as well as the vibrational zero-point energy difference. The relaxation energy is calculated as the difference of the monomer in the cluster geometry and its relaxed geometry. Usually only the monomer basis without ghost functions is used, to avoid linear dependency problems of the basis. Obtaining the zero-point energy within the harmonic approximation is problematic in clusters, because the important intermolecular vibrational modes typically contain strong anharmonicity. The usage of methods to correct of the anharmonicity, such as multi-dimensional vibrational SCF (VSCF) or CI (VCI) [42–45], are often computationally too costly.

For the calculations of the single-point energies in this thesis the Møller-Plesset perturbation theory in second order and the time-dependent coupled cluster linear response theory based on the CC2 model [46, 47] and their spin component scaled (SCS) [48, 49] versions are prominently used. A brief overview is given in the following sections.

1.3.3 Coupled cluster model

In contrast to the CI expansion, which is a linear combination of the reference wavefunction $|0\rangle$ and its i -fold excited configuration state functions (CSFs), $|\mu_i\rangle$, the coupled cluster wavefunction is based on an exponential ansatz [38],

$$|\text{CC}\rangle = \exp(\hat{T})|0\rangle = \exp\left(\sum_{\mu} t_{\mu}\hat{\tau}_{\mu}\right)|0\rangle. \quad (1.4)$$

Here the cluster amplitudes t_{μ} are the equivalents of CI coefficients. The operator $\hat{\tau}_{\mu}$ is the plain excitation operator, which generates the excited configurations. Similar to CI, the coupled cluster expansion can be truncated in terms of excitation classes. This is done by truncating the cluster operator $\hat{T} = \hat{T}_1 + \hat{T}_2 + \dots$ (after \hat{T}_1 for CCS, after \hat{T}_2 for CCSD, \dots). The advantage of this ansatz is twofold: On one hand, the exponential ansatz guarantees a multiplicative separability, which leads to size-consistent energies. On the other hand, it can be seen by expressing the exponential cluster operator in a Taylor expansion, that not only the sole \hat{T}_{μ} describes the excitation μ , but also product terms of the same total excitation class μ contribute. In other words, coupled cluster achieves a more efficient mapping of the information with the same amount of numbers.

The CC problem is then to solve the amplitude equation system 1.6 and the energy equation 1.5,

$$\langle 0 | \exp(-\hat{T}) \hat{H} \exp(\hat{T}) | 0 \rangle = \langle 0 | \hat{H} \exp(\hat{T}) | 0 \rangle = E_{CC}, \quad (1.5)$$

$$\langle \mu | \exp(-\hat{T}) \hat{H} \exp(\hat{T}) | 0 \rangle = 0. \quad (1.6)$$

The use of the projected equations is beneficial, because the variational approach to the amplitudes requires the solution of a nonlinear equation system with the full set of full CI determinants and high-order products of the amplitudes. The formulae above are the linked coupled cluster equations, which use the similarity-transformed Hamiltonian $\bar{H} = \exp(-T) \hat{H} \exp(T)$. It can be shown that these are equivalent to the unlinked equations, which omit the $\exp(-T)$. By using the Baker-Campbell-Hausdorff expansion,

$$\exp(-\hat{T}) \hat{H} \exp(\hat{T}) = \hat{H} + [\hat{H}, \hat{T}] + \frac{1}{2!} [[\hat{H}, \hat{T}], \hat{T}] + \frac{1}{3!} [[[\hat{H}, \hat{T}], \hat{T}], \hat{T}] + \dots, \quad (1.7)$$

polynomial commutator expressions are obtained. These can be written in terms of amplitudes and integrals by using diagrammatic techniques [50, 51], which can be then evaluated numerically.

1.3.4 MP2 and CC2

The Møller-Plesset perturbation theory [39] bases on the Fock operator \hat{F} and fluctuation potential as the perturbation. The sum of the energies zeroth and first order energy are equivalent to the Hartree-Fock energy. In coupled cluster formulation the amplitudes of the second order (MP2) can be obtained by equation 1.9 and the energy from equation 1.8.

$$\langle 0 | \hat{H} + [\hat{H}, \hat{T}_2] | 0 \rangle = E_{MP2} \quad (1.8)$$

$$\langle \mu_2 | [\hat{F}, \hat{T}_2] + \hat{H} | 0 \rangle = 0, \quad (1.9)$$

The CC2 method [46, 47] is very similar to MP2. Yet it treats the single excitations in zeroth order. With the T_1 -similarity-transformed Hamilton operator, $\bar{H} = \exp(-\hat{T}_1) \hat{H} \exp(\hat{T}_1)$, the energy equation,

$$\langle 0 | \bar{H} + [\bar{H}, \hat{T}_2] | 0 \rangle = E_{CC2}, \quad (1.10)$$

and the amplitude equations,

$$\langle \mu_1 | \bar{H} + [\bar{H}, \hat{T}_2] | 0 \rangle = 0, \quad (1.11)$$

$$\langle \mu_2 | [\hat{F}, \hat{T}_2] + \bar{H} | 0 \rangle = 0, \quad (1.12)$$

1 General introduction

can be derived. It can be shown that the MP2 case is obtained by setting the singles amplitudes to zero. The accuracy of CC2 is comparable to MP2, since the inclusion of the singles has only little effect on the ground state energy.

The real advantage of including the singles in zeroth order is, that they describe an approximal orbital relaxation, which is particularly important when ground and excited state properties are treated via the response theory. Thus, the excitation energies and transition moments can be identified as the poles and residuals of the CC2 linear response function. This function is based on the time-dependent CC2 Lagrangian, which is the time-dependent quasi energy with the time-dependent CC2 amplitude equations in the presence of external perturbations as additional constraints and therefore includes corrections for the non-fulfillment of the Hellmann-Feynman theorem. The poles are correct up to second order.

1.3.5 Spin component scaled methods

The spin component scaling introduces two empirical determined scaling factors. So the spin component scaled methods can be considered as semiempirical methods. These scaling factors $p_{\sigma\sigma'}$ are $\frac{1}{3}$ for even spin combinations, and $\frac{6}{5}$ for uneven spin combinations. They are introduced in the respective energy equations of MP2 (see equation 1.8, $\tilde{H} \Rightarrow \hat{H}$) and CC2 (see equation 1.10, $\tilde{H} \Rightarrow \bar{H}$),

$$\langle 0 | \tilde{H} + \sum_{\sigma\sigma'} p_{\sigma\sigma'} [\tilde{H}, \hat{T}_2^{\sigma\sigma'}] | 0 \rangle = E_{\text{SCS}}, \quad (1.13)$$

and additionally in the singles amplitude equation in the case of CC2 (see equation 1.11),

$$\langle \mu_1 | \bar{H} + \sum_{\sigma\sigma'} p_{\sigma\sigma'} [\bar{H}, \hat{T}_2^{\sigma\sigma'}] | 0 \rangle = 0. \quad (1.14)$$

This numerical trick is attractive, since with virtually no higher computational costs, the systematic errors of the underlying methods are partially damped [48, 49]. SCS-MP2 describes, in contrast to MP2, π stacking interactions sufficiently well. In the case of H bonds the situation is inverse and MP2 is superior to SCS-MP2 [52]. Also other choices of the scaling factors are used, so employs e.g. the scaled opposite spin (SOS) approach [53] the value 1.3 for uneven spin combinations, but sets the other scaling factor to zero. This leads to improved scaling in the algorithm under usage of the Laplace transform [54] in the implementation.

1.3.6 Local approximation

The correlation is a short-range effect. E.g. the dispersion, which is a pure correlation effect, decays by the distance to the minus sixth. Since canonical orbitals tend to be delocalized over the whole system, their usage is not beneficial from a computational point of view. A solution to this problem is an unitary transform of the canonical orbitals into spatially localized orbitals. The effect is, that the integral and amplitude matrices in MO basis become sparse in the local basis. This can be exploited numerically [55–61].

There are multiple ways to obtain localized orbitals from canonical ones. Prominently used is the procedure by Pipek and Mezey [62]. Here the Mulliken charge is tried to be maximized on an atom by a localized MO. According to the approach of Pulay [56], the occupied local orbitals (LMOs) still have to be orthogonal with respect to each other. The virtual space then is spanned by projected AOs (PAOs), which are obtained by projecting out the LMOs from the AO space.

Based on spatial criteria, e.g. atomar distances in the system, the correlation problem can be truncated. So restricted LMO tuple lists can be specified, from which distinct excitation subspaces of PAOs (domains) are defined. The space of the problem which is not included in these lists and domains either is completely neglected or treated computationally cheaper. This so-called local approximation allows up to a linear scaling behavior of the computational costs with respect to the system size.

However, the price to pay are more difficult algorithms to be implemented. The Fock matrix is not diagonal anymore in case of local orbitals, the PAOs are no longer orthogonal and the virtual space is overcomplete.

1.3.7 Density fitting approximation

The integrals can be seen as a four dimensional object. By using the density fitting (DF) approximation [63–67] it is decomposed to objects of smaller dimensionality. This is done in expressing the orbital product in the integral as an orbital density,

$$(ai|bj) = \int \frac{\phi_a(\mathbf{r}_1)\phi_i(\mathbf{r}_1)\phi_b(\mathbf{r}_2)\phi_j(\mathbf{r}_2)}{r_{12}} d\mathbf{r}_1 d\mathbf{r}_2 = \int \frac{\rho_{ai}(\mathbf{r}_1)\rho_{bj}(\mathbf{r}_2)}{r_{12}} d\mathbf{r}_1 d\mathbf{r}_2. \quad (1.15)$$

Then, the orbital density is fitted to an auxiliary basis set Ξ_A ,

$$\rho_{ai}(\mathbf{r}) \approx \bar{\rho}_{ai}(\mathbf{r}) = \sum_A d_A^{ai} \Xi_A(\mathbf{r}). \quad (1.16)$$

1 General introduction

The fitting coefficients d_A^{ai} can be determined by minimizing for instance the given error functional,

$$f(d_A^{ai}) = \int (\rho_{ai}(\mathbf{r}_1) - \bar{\rho}_{ai}(\mathbf{r}_1)) r_{12}^{-1} (\rho_{bj}(\mathbf{r}_2) - \bar{\rho}_{bj}(\mathbf{r}_2)) d\mathbf{r}_1 d\mathbf{r}_2, \quad (1.17)$$

which is equivalent of solving the set of linear equations,

$$\sum_B (A|B) d_B^{ai} = (ai|A). \quad (1.18)$$

Then, the integrals can be approximated as

$$(ai|bj) \approx \sum_A d_A^{ai} (A|bj) + \sum_B (ai|B) d_B^{bj} + \sum_{AB} d_A^{ai} (A|B) d_B^{bj}, \quad (1.19)$$

which is known as robust fitting. By selecting the error functional based on the coulomb metric as it is shown above in equation 1.17, the fitting is correct up to second order and the integrals can be approximated to two and three dimensional quantities,

$$(ai|bj) \approx \sum_A d_A^{ai} (A|bj) = \sum_{AB} (ai|A) (A|B)^{-1} (B|bj). \quad (1.20)$$

The use of the DF approximation does not reduce the scaling in MP2 and CC2, but significantly reduces the prefactor of the scaling law. On the other hand the loss in accuracy almost is negligible.

1.4 Overview

This thesis is structured in the following way: In chapter 2 the phenol-water_{1≤n≤3} clusters are investigated in their ground and lower excited states, and are compared to the existing experimental data. Subsequently in chapter 3 the related 2-naphthol-water₂ systems are explored in a similar way. Then, in chapter 4, the low lying minima of the aniline di- and trimer cluster potential energy surfaces are located, in order to set up the stage for the investigation of the important structures in the excited states within chapter 5. Finally, the subject of chapter 6 is the structure and binding of adduct compounds of tantalum chlorides and phosphorus sulfide cage molecules.

2 Phenol-water $_{1\leq n\leq 3}$ clusters

2.1 Introduction

Phenol (Ph) as the simplest aryl alcohol serves as a prototype molecule for structurally related subunits of larger aromatic biomolecules (e.g., tyrosine residues in proteins). Therefore the photophysics of this molecule is of particular interest. Furthermore, clusters of phenol with simple solvent molecules, especially with water, can be used to study hydrogen bonding, solvation effects, and their influence on the photophysical behavior of the solute, with the phenol again mimicking structurally related chromophores of larger biomolecules. Phenol-water clusters therefore have been extensively investigated by many groups during the last two decades, both experimentally and theoretically. In the context of this work we want to focus on the $\text{Ph}(\text{H}_2\text{O})_n$ clusters with $1 \leq n \leq 3$. Mass-selective absorption spectra obtained by one or two-color resonance enhanced multiphoton ionization have been measured by several groups [68–78] in the vicinity of the electronic origin of Ph. It turns out that the absorption spectrum of the $n = 2$ cluster is strikingly different from those obtained for the $n = 1$, $n = 3$, and $n = 4$ clusters. While on the one hand for all the latter rather narrow line spectra with intense origins have been obtained, the $n = 2$ cluster, on the other hand, exhibits only a weak, broad, and congested band structure (see Fig. 2.1). Whereas for $n = 1$ and $n = 3$ it was readily possible to measure well resolved dispersed fluorescence emission [74, 76, 77] or ion dip spectra [73], this has not been possible for $n = 2$ due to the low quantum yield and anomalously short lifetime of the S_1 state. Jacoby *et al.* postulated in Ref. 77 that a linear geometry might become more stable in the excited state than the cyclic structure corresponding to the ground state *vide infra*. Due to the high vibrational mode density provided by this linear geometry at the Franck-Condon point, strong vibrational coupling between the modes of the cyclic and the linear structure might occur, explaining the broadening of the band structure. In the same work the authors also stated that the $n = 2$ cluster may be less stable in the excited state than in the ground state. Yet since the $n = 2$ features are red-shifted with respect to the Ph origin, this statement appears to be in conflict with experimental evidence.

2 Phenol-water $_{1 \leq n \leq 3}$ clusters

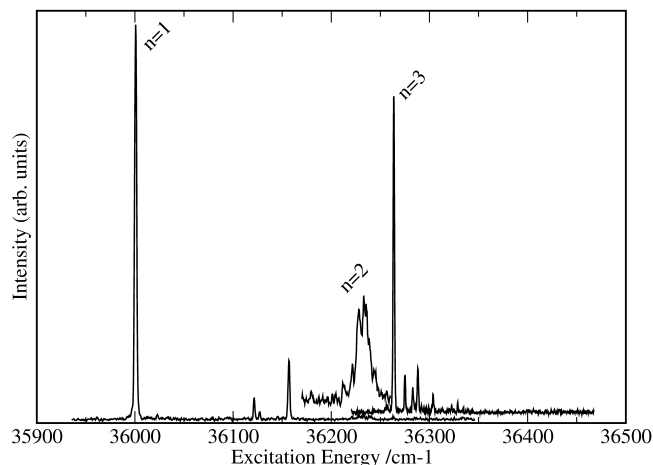


Figure 2.1: Mass specific absorption spectra of the $\text{Ph}(\text{H}_2\text{O})_n$, $1 \leq n \leq 3$, clusters in the vicinity of the electronic origin of Ph, obtained with two-color resonant two photon ionization spectroscopy in a molecular beam experiment. For details see Refs. 74 and 76.

Ab initio electronic structure calculations on these clusters in the electronic ground state S_0 (primarily at the level of Hartree-Fock or second-order Møller-Plesset perturbation theory) have been performed by several groups [74, 76, 77, 79–85], in order to elucidate low-energy geometries and corresponding (harmonic) vibrational frequencies. Furthermore, diffusion quantum Monte Carlo studies investigating the vibrational ground states on the S_0 surfaces of these clusters are also available in the literature [86, 87]. The equilibrium geometry of the binary complex corresponds to a translinear hydrogen bonding arrangement reminiscent of water dimer, with the H_2O plane perpendicular to the phenol plane. For the $\text{Ph}(\text{H}_2\text{O})_2$ cluster three cyclic low-energy geometries exist, usually denoted as (Udu), (Uud), and (Udd), indicating, e.g., for the first minimum that the phenyl ring is in the Up, the first free hydrogen in the down, and the second free hydrogen again in the up position with respect to the plane given by the two hydrogen bonds involved (donor-acceptor indicates the direction). The (Udu) is the most stable conformer of $\text{Ph}(\text{H}_2\text{O})_2$ on the S_0 surface. The equilibrium geometry of the $\text{Ph}(\text{H}_2\text{O})_3$ cluster is also cyclic and can be described according to the notation above as (Udud).

Only a few calculations on the excited states of these clusters have been published so far. Energies, geometries, and (harmonic) vibrations of the $S_1(\pi^* \leftarrow \pi)$ state have been computed by Fang and Liu using the configuration interaction singles (CIS) and complete active space self-consistent field (CASSCF) methods [83, 84]. The equilibrium geometries on the $S_1(\pi^* \leftarrow \pi)$ surface turned out to be quite similar to those on the S_0 surface, i.e., a translinear (TL) hydrogen bond

and cyclic geometries were obtained for $\text{Ph}(\text{H}_2\text{O})$ and $\text{Ph}(\text{H}_2\text{O})_2$, respectively. In particular, the linear $\text{Ph}(\text{H}_2\text{O})_2$ geometry postulated by Jacoby *et al.* turned out to lie 5.3 kcal/mol (CASSCF) and 9.2 kcal/mol (single-point CASPT2) *above* the cyclic minimum-energy geometry on the $S_1(\pi^* \leftarrow \pi)$ surface. It has to be stressed at this point that neither CIS nor CASSCF (without subsequent treatment of dynamic correlation) is a reliable method for excited-state calculations, yet analytic energy gradients have not been available for other methods at that time. Recently, Sobolewski *et al.* explored the $S_1(\pi^* \leftarrow \pi)$ and $S_2(\sigma^* \leftarrow \pi)$ surfaces of Ph, $\text{Ph}(\text{H}_2\text{O})$, and $\text{Ph}(\text{H}_2\text{O})_3$ (enforcing C_s symmetry) in order to elucidate the mechanism of photoinduced electron and proton transfer in these systems [88, 89]. Geometry optimizations were performed again at the level of CASSCF with additional single-point energy calculations at the CASPT2 (perturbation theory of second order using a CASSCF reference wave function) level. A conical intersection (CI) between these two surfaces was found, which is responsible for predissociation of the $S_1(\pi^* \leftarrow \pi)$ and subsequent concerted electron- and protontransfer reactions from the chromophore to the solvent molecules. More recently, the authors also performed quantum-wave-packet dynamics for the case of phenol in order to get a more detailed picture of this predissociation of the $S_1(\pi^* \leftarrow \pi)$ state. In the light of these results a connection between the observed congested band structure of the absorption spectrum and the anomalously short lifetime of $\text{Ph}(\text{H}_2\text{O})_2$, on the one hand, and the $S_1(\pi^* \leftarrow \pi)$ / $S_2(\sigma^* \leftarrow \pi)$ conical intersection, on the other hand, appears to be plausible.

In this work we have explored the $S_1(\pi^* \leftarrow \pi)$ surface and its conical intersection with $S_2(\sigma^* \leftarrow \pi)$ at the level of coupled cluster response theory employing the CC2 model [46]. To the best of our knowledge these are the first excited-state geometry optimizations for these systems performed at a theoretical level which includes dynamical electron correlation effects. The $\text{Ph}(\text{H}_2\text{O})_2$ minimum-energy geometries so obtained are qualitatively different from those reported by Fang and Liu at the CASSCF level: Only one stable cyclic ring structure (similar to the one in the S_0 state) could be located, which lies about 3 kcal/mol above the global $S_1(\pi^* \leftarrow \pi)$ minimum. Instead, two distinct conformers were found with the second water molecule acting as a H donor to the aromatic ring system (one of these geometries constitutes the global minimum). Apparently, the oxygen atom and the π -ring system of phenol switch role in acting as H acceptors on going from the S_0 to the $S_1(\pi^* \leftarrow \pi)$ state. For $n = 3$ a stable cycle geometry similar to the one obtained for the S_0 state was found, yet energetically lower-lying minima featuring bonding to the π -ring system were also located. Additional CASPT2 geometry optimizations, performed for $n = 2$, confirm the existence of these global minimum structures.

2.2 Computational Methods

The minimum-energy geometries on the S_0 and the $S_1(\pi^* \leftarrow \pi)$ surfaces of Ph and the $\text{Ph}(\text{H}_2\text{O})_n$, $1 \leq n \leq 3$, clusters were optimized by applying time-dependent coupled cluster response theory at the level of the CC2 model. The analytic CC2 energy gradient implemented by Hättig and Köhn in the TURBOMOLE program package [90, 91] was used for that purpose. The minimum-energy geometries on the conical intersection seam between the $S_1(\pi^* \leftarrow \pi)$ and the $S_2(\sigma^* \leftarrow \pi)$ states were calculated by adopting the scheme proposed by Ragazos *et al.* [92]: The gradient \mathbf{g} used in the optimization is defined as

$$\mathbf{g} = \mathbf{P} \nabla E_2 + \frac{2|E_2 - E_1|}{|\mathbf{g}_{21}|} \mathbf{g}_{21}, \quad (2.1)$$

where E_2 and E_1 are the energies of the $S_2(\sigma^* \leftarrow \pi)$ and the $S_1(\pi^* \leftarrow \pi)$ states, respectively, \mathbf{g}_{21} is the difference gradient vector $\mathbf{g}_{21} = \nabla E_2 - \nabla E_1$, and \mathbf{P} is a projection operator projecting out the one-dimensional vector space given by the direction of \mathbf{g}_{21} , i.e., $\mathbf{P} = (\mathbf{1} - |\mathbf{g}_{21}\rangle\langle\mathbf{g}_{21}|)$. Here, \mathbf{P} deviates from the projector of Ref. 92 insofar that the interstate coupling vector, which presently is not available for CC2, has been neglected, assuming that it is small for the present two states, which are rather different in their character.

One should mention at this point that due to the non-Hermitian character of the coupled cluster ansatz, calculations on points on the conical intersection seam are in general not unproblematic (for a recent discussion see Ref. 93). However, in the particular case of the $S_1(\pi^* \leftarrow \pi)$ and $S_2(\sigma^* \leftarrow \pi)$ intersection of phenol and its water clusters these problems turned out to be rather small. The maximum imaginary component (right at the conical intersection) was less than 0.0004 eV, i.e., much less than in the examples presented in Ref. 93.

Additional single-point energies at the stationary points of the ground- and excited-state surfaces have been calculated within bigger atomic orbital (AO) basis sets (*vide infra*) by using both canonical and local CC2 linear response theory [94, 95]. The local calculations, which by construction avoid the basis set superposition error (BSSE) to a large extent [41], were performed with our local CC2 response program [94, 95] recently implemented in the MOLPRO [96] program package to have a means of comparison to the counterpoise (CP) corrected [40] canonical excitation energies and interaction energies in the excited state. For the local calculations, the Pipek-Mezey orbital localization was employed. The pair lists remained untruncated. For the ground state amplitudes, the pair domains were constructed from full monomer orbital domains. Redundancies in the pair domains were specified at large intermonomer distances, which is the proper prescription to avoid BSSE, as discussed in Ref. 41. Domains for the amplitude responses

were determined according to the scheme proposed in Ref. 94, using a criterion of $\kappa_e = 0.995$ to determine orbitals important for the related excited state.

In order to verify the stability of the new $S_1(\pi^* \leftarrow \pi)$ minimum-energy geometries of the $\text{Ph}(\text{H}_2\text{O})_2$ cluster predicted by the CC2 response theory, which are markedly different from related geometries on the S_0 surface and from minimum-energy geometries predicted previously at the level of CASSCF for the $S_1(\pi^* \leftarrow \pi)$ state (*vide infra*), additional geometry optimizations have been performed at the level of CASPT2. The analytic energy gradient by Celani and Werner [97], implemented recently in the MOLPRO package [96], has been used for that purpose. An active space of six electrons in the six valence π orbitals of the phenyl ring was chosen for the underlying CASSCF reference wave function. A level shift of 0.25 was used in the subsequent CASPT2 calculation due to the presence of an intruder state. Test calculations without and with level shift performed within the same active space for the clusters in the electronic ground state show that the level shift causes an *underestimation* of the interaction energy by 10%–15%. Since the CASPT2 gradient so far uses internal contraction only for the doubly external configuration space, these geometry optimizations turned out to be very time consuming.

As AO basis sets, the aug-cc-pVDZ sets [34, 98] together with the related fitting basis sets optimized for DF-MP2 (Ref. 99) were employed in all geometry optimizations. For the canonical and local CC2 single-point energy calculations at the stationary points, the bigger aug-cc-pVTZ AOs with related fitting sets were utilized.

2.3 Results and Discussion

Figure 2.1 shows the mass specific absorption spectra of the $\text{Ph}(\text{H}_2\text{O})_n$, $1 \leq n \leq 3$, clusters in the vicinity of the electronic origin of Ph, measured by one of us 15 years ago (for experimental details, see Refs. 74 and 76). Evidently, both the $n = 1$ and $n = 3$ clusters exhibit narrow line spectra with the individual intermolecular modes being clearly visible (for an interpretation of the spectra, again see Refs. 74 and 76). The spectrum of $n = 3$ shows apart from a very weak band at 186.9 cm^{-1} (intermolecular stretching mode) no further features higher 90 cm^{-1} above the origin. Similar observations were made also for the deuterated species which all indicates that efficient intramolecular vibrational redistribution (for the stretch mode) and vibrational predissociation at rather small excess energies play a role in the $n = 3$ cluster (see also discussion in Ref. 76).

2 Phenol-water_{1≤n≤3} clusters

In contrast to $n = 1$ and $n = 3$, merely a broad, weak, and congested band structure is observed for $n = 2$. This indicates, together with the short lifetime and the low quantum yield, that no stable minimum, able to support the lowest vibrationally excited modes or even the vibrational ground state, does exist on the $S_1(\pi^* \leftarrow \pi)$ potential energy surface in the vicinity of the Franck-Condon point and that efficient nonradiative channels are available at virtually no excess energies.

2.3.1 Minimum energy geometries

In Figs. 2.2–2.5 the CC2 minimum-energy geometries of the clusters on the S_0 and the $S_1(\pi^* \leftarrow \pi)$ surfaces are displayed. A compilation of the counterpoise corrected [40] interaction energies for the individual minima and other stationary points on the S_0 and the $S_1(\pi^* \leftarrow \pi)$ surfaces is given in Tables 2.1 and 2.2. For $n = 1$ and $n = 3$ the global minima in the S_0 state are represented by a translinear and a cyclic (Udud) configuration, respectively. The lowest S_0 energy minimum of the $n = 2$ cluster corresponds to the (Udu) conformer with an interaction energy of -16.59 kcal/mol (aug-cc-pVTZ basis), followed by the (Udd) and the (Uud) conformers, 0.42 and 0.58 kcal/mol above (Udu), respectively. Such an energy separation appears to be sufficient that at typical temperatures of a molecular beam experiment (vibrational temperature around 50 K) the absorption spectrum is dominated by the (Udu) conformer. This is also in agreement with the results obtained by hole-burning experiments reported by Lipert and Colson in Ref. 72.

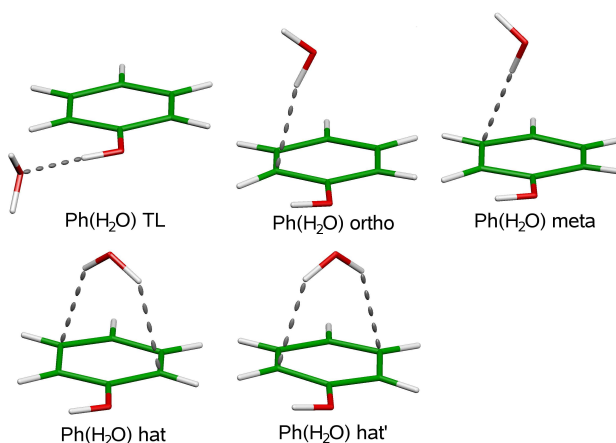


Figure 2.2: Ph(H₂O) structure minima on the S_1 surface.

Table 2.3 compiles the $S_1 \leftarrow S_0$ oscillator strength f (length gauge) and the relative size of the component of the transition dipole vector μ perpendicular to the

	DF-CC2		CASPT2		DF-CC2*		DF-CC2		DF-LCC2*	
	aug-cc-pVDZ						aug-cc-pVTZ			
	S ₀	S ₁	S ₀	S ₁	S ₀	S ₁	S ₀	S ₁	S ₀	S ₁
<i>n</i> = 1										
TL,S ₀	-6.34	-3.61	-5.50	-2.64	-7.51	-6.97	-6.75	-6.20	-6.67	-6.13
TL,S ₁		-7.57		-6.33		-8.92		-8.10		-8.03
CI		-3.10				-6.65		-5.57		-5.50
<i>n</i> = 2										
(Udu),S ₀	-15.45	-11.59	-13.68	-9.93	-18.57	-16.99	-16.59	-15.00	-16.44	-14.81
<i>hat</i>		-16.81		<i>a</i>		-20.66		-18.30		-18.06
CI		-11.03				-16.46		-14.34		-14.06
(Udd),S ₀	-15.03	-10.91	-13.38	-9.60	-18.00	-16.14	-16.17	-14.31	-16.01	-14.06
<i>ortho</i> (Udu)		-17.85		-14.23		-21.69		-19.39		-19.32
<i>ortho</i> (Udd)		-18.00		-14.45		-21.85		-19.55		-19.46
(Uud),S ₀	-14.85	-11.00	-13.17	-9.53	-17.79	-16.20	-16.01	-14.40	-15.86	-14.18
(Uud),S ₁		-15.35		-13.39		-18.37		-16.57		-16.35
<i>n</i> = 3										
(Udud),S ₀	-25.98	-21.74			-31.02	-29.07	-28.01	-26.05	-27.68	-25.61
(Udud),S ₁		-26.16				-31.23		-28.25		-27.85
(Udud) CI		-19.86				-26.84		-23.52		-23.12

a) Ph(H₂O)₂ *hat* collapses to *ortho*(Udd) on the CASPT2 S₁ potential energy surface.

Table 2.1: Interaction energies in kcal/mol. All columns except those denoted by an asterisk contain counterpoise corrected values.

2 Phenol-water_{1≤n≤3} clusters

DF-CC2, S ₁		
	aug-cc-pVDZ	aug-cc-pVTZ
<i>n</i> = 1		
TL	-7.57	-8.10
<i>meta</i>	-2.67	-3.20
<i>ortho</i>	-2.62	-3.11
<i>hat</i>	-3.86	-4.43
<i>hat'</i>	-3.82	-4.38
<i>n</i> = 2		
<i>hat</i>	-16.81	-18.30
TS <i>hat</i> ↔ <i>ortho</i> (Udu)	-16.36	-17.78
<i>ortho</i> (Udu)	-17.85	-19.39
<i>ortho</i> (Udd)	-18.00	-19.55
<i>ortho</i> (Uuu)	-17.17	-18.71
<i>ortho</i> (Uud)	-17.86	-19.40
TS <i>ortho</i> (Udu)	-17.52	-19.08
↔ <i>ortho</i> (Udd)		
(Uud)	-15.35	-16.57
<i>n</i> = 3		
(Udud)	-26.16	-28.25
<i>hat</i>	-28.59	-31.13
<i>meta</i> (Uddu)	-26.92	-29.19
<i>meta</i> (Uudu)	-26.76	-29.08
<i>ortho</i> (Udud)	-27.81	-30.22
<i>ortho</i> (Uudu)	-27.07	-29.40

Table 2.2: Counterpoise corrected interaction energies in kcal/mol for different stationary points on the S₁ surface.

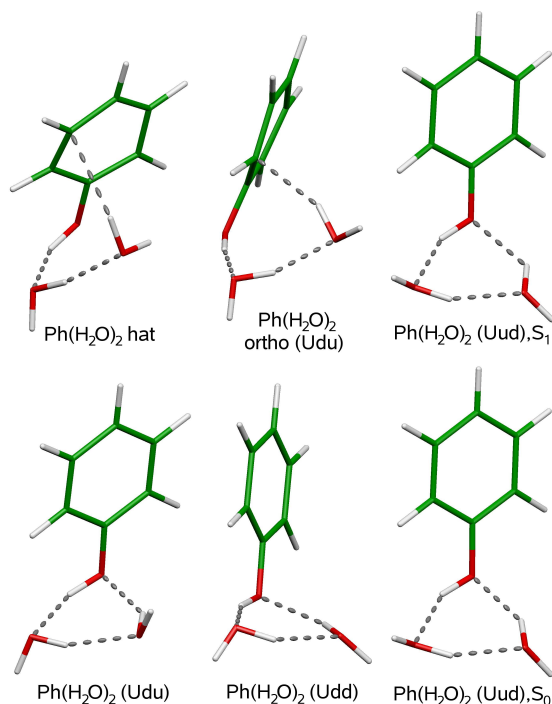


Figure 2.3: $\text{Ph(H}_2\text{O)}_2$ S_1 (first row) and S_0 (second row) minimum-energy geometries.

phenyl-ring plane (with respect to the norm of μ for the individual S_0 minimum-energy geometries of $n = 1$, $n = 2$, and $n = 3$). Evidently, the perpendicular component of μ increases from 0 to about 30% on going from $n = 1$ to $n = 2$ and $n = 3$, implying that also out-of-plane modes can couple with the $S_1 \leftarrow S_0$ excitation for $n \geq 2$. In Table 2.4 the local and CP corrected canonical adiabatic and 0–0 excitation energies are given for the excitations from the global S_0 minima to the relevant minima on the S_1 surface (*vide infra*). The 0–0 excitation energies are based on the harmonic zero-point energy correction calculated within the aug-cc-pVDZ basis. The resulting CC2 values for the 0–0 excitations agree quite well with the experiment with discrepancies of less than 0.1 eV. The CASPT2 results, on the other hand, do not agree so well. Already the adiabatic excitation energies are lower than the experimental values by about 0.3 eV, which presumably is being caused by the level shift (see Section 2.2). Furthermore, we note in passing that the local and the CP corrected canonical excitation energies deviate by less than 0.005 eV.

From Table 2.4 it is evident that the error in the excitation energies is very systematic (the CC2/aug-cc-pVTZ 0–0 excitation energies are blueshifted by 0.06–

2 Phenol-water_{1≤n≤3} clusters

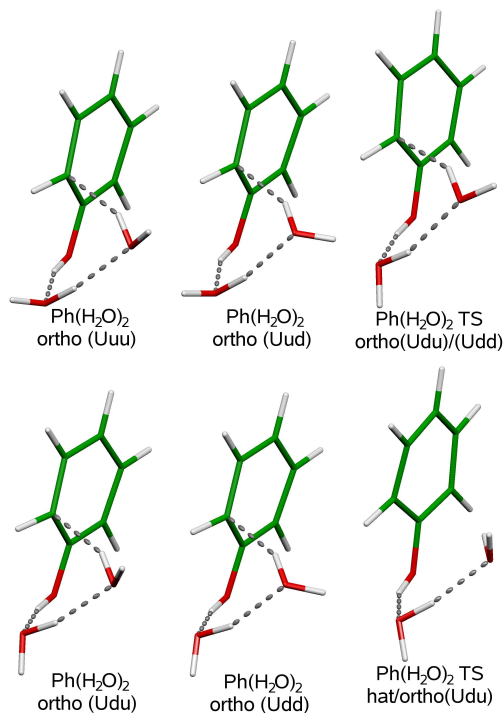


Figure 2.4: Manifold of $\text{Ph}(\text{H}_2\text{O})_2$ *ortho* conformers with transition state structures *ortho*(Udd) \leftrightarrow (Udu) and *hat* \leftrightarrow *ortho*(Udu).

0.07 eV relative to the experiment [73]). This implies that for the interaction energies of the individual clusters, and even more so for the relative energies of individual conformers of a given cluster size, the errors in the excitation energies are virtually identical and cancel. For CC2 we expect a methodical error similar to MP2 for ground state calculations, for which it is known that for hydrogen bonded systems close to equilibrium geometries, interaction energies very similar to CCSD(T) are obtained (see Ref. 100 and references therein). Of more concern than the methodical error is the error related to the basis set size. For that reason single-point calculations within the aug-cc-pVTZ basis set were performed at the individual CC2/aug-cc-pVDZ stationary points. The remaining error in the CC2/aug-cc-pVTZ interaction energies can be expected to be considerably smaller than the difference between CC2/aug-cc-pVTZ and CC2/aug-cc-pVDZ interaction energies.

Let us now turn to the stationary points on the $S_1(\pi^* \leftarrow \pi)$ surface. The global minimum of the binary complex again is translinear, structures with the water subunit acting as a donor to the π -ring system (see Fig. 2.2 and Table Table 2.2) are much less stable. The structural discrepancy between the two translinear S_0

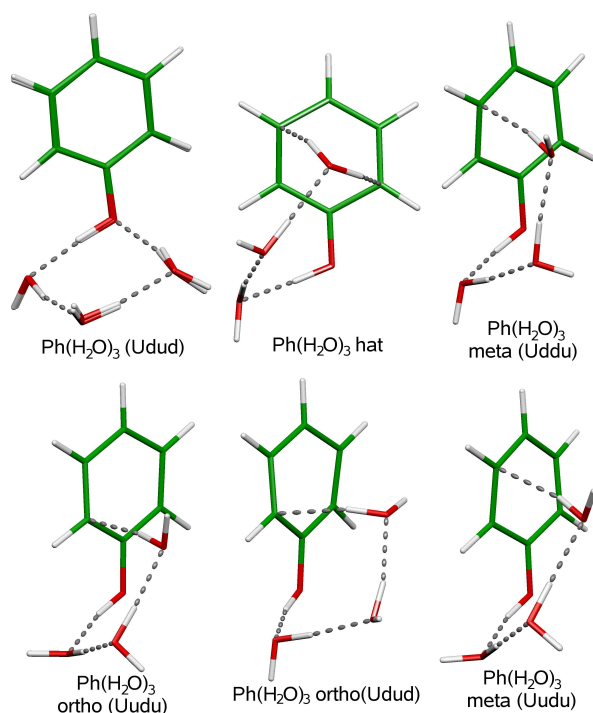


Figure 2.5: $\text{Ph}(\text{H}_2\text{O})_3$ (Udud) S_0 and S_1 geometries (superimposed) and several other minimum-energy geometries such as *hat*, *meta*, and *ortho* of $\text{Ph}(\text{H}_2\text{O})_3$.

and S_1 geometries of $n = 1$ is small, the root-mean-square (rms) deviation in the atomic positions (see Eq. (64) in Ref. 101) is only 0.06 Å. The primary effect of the $S_1 \leftarrow S_0$ excitation on the $n = 1$ geometry manifests in an elongation of the C–C distances within the phenyl ring (by about 0.03 Å, see Table 2.5), a shortening of the C–O distance (≈ 0.02 Å), and a substantial shortening of the hydrogen bond (≈ 0.08 Å), reflecting the enhanced acidity of Ph in the $S_1(\pi^* \leftarrow \pi)$ state. The interaction energy increases by 1.35 kcal/mol due to excitation to the S_1 state, which corresponds to a shift of the origin relative to that of bare phenol by 472 cm^{-1} (experimentally observed: 354 cm^{-1})

For $n = 3$ a cyclic (Udud) structure, very similar to the global minimum of the ground state, represents also a minimum on the ${}_1(\pi^* \leftarrow \pi)$ surface (not the global minimum though, *vide infra*). The rms deviations in the atomic positions between the S_0 and S_1 (Udud) geometries are again small, i.e., 0.09 Å, with similar changes in the phenyl ring, the C–O distance, and contractions of the hydrogen bonds as obtained for $n = 1$. The interaction energy increases only slightly by 0.25 kcal/mol on excitation to the S_1 state.

2 Phenol-water_{1≤n≤3} clusters

	f	$\mu_{\perp}/ \boldsymbol{\mu} $	f	$\mu_{\perp}/ \boldsymbol{\mu} $
	aug-cc-pVDZ		aug-cc-pVTZ	
Ph(H ₂ O) TL	0.0305	0.21%	0.0287	0.21%
Ph(H ₂ O) ₂ (Udu)	0.0240	27.17%	0.0226	27.20%
Ph(H ₂ O) ₂ (Udd)	0.0236	33.79%	0.0222	33.76%
Ph(H ₂ O) ₂ (Uud)	0.0253	27.50%	0.0238	27.46%
Ph(H ₂ O) ₃ (Udud)	0.0225	31.65%	0.0212	31.76%

Table 2.3: CC2 oscillator strengths f (length gauge) and ratios of the components perpendicular to the plane of the phenyl ring of $\boldsymbol{\mu}$, $\mu_{\perp}/|\boldsymbol{\mu}|$, for the $S_1 \leftarrow S_0$ excitations of the individual clusters.

For the $n = 2$ cluster, on the other hand, the situation turned out to be different: while for the cyclic (Uud) S_0 conformer a corresponding stable S_1 geometry with a rms deviation of 0.09 Å could be located, no corresponding cyclic S_1 geometries were found for the more stable S_0 conformers (Udu) and (Udd). In the S_1 state the oxygen atom and the phenyl ring switch roles in acting as H acceptors for the second water molecule. Starting from the cyclic (Udu) geometry, i.e., the global minimum on the S_0 surface, in a geometry optimization on the S_1 surface, an S_1 conformer was found with the second water subunit acting as a double H donor to a π system (see Fig. 2.3). This *hat* conformer is 1.73 kcal/mol more stable than the cyclic (Uud) S_1 conformer. Similarly, starting from the (Udd) geometry another even more stable S_1 conformer was found with the second water subunit acting as a H donor to a C atom in *ortho* position. The rms deviations of the *hat* and *ortho*(Udu) conformers with respect to the related parental starting geometries are much larger and amount to 0.63 and 0.88 Å, respectively. The increase in the interaction energies on going from the cyclic (Udu) geometry in the S_0 state to the *hat* or *ortho*(Udu) conformers in the S_1 state is rather large and amount to 1.71 and 2.96 kcal/mol, respectively, implying that the related origins in the absorption spectrum would appear on the red side of the origin of the $n = 1$ cluster. Furthermore, the shortenings of the C–O distance and the first (phenolic) hydrogen bond on going from the cyclic (Udu) S_0 to *ortho*(Udu) S_1 geometry are substantially larger than for $n = 1$ and $n = 3$, i.e., 0.04 and 0.17 Å, respectively (see Table 2.5). This again reflects the much increased stabilization of the cluster due to the $S_1 \leftarrow S_0$ excitation compared to $n = 1$ and $n = 3$. As a particular feature of both the *hat* and *ortho*(Udu) geometries, a distinct puckering of the phenyl ring is noticed. *hat* and *ortho* geometries are separated by a transition state (TS) structure 0.52 kcal/mol above the *hat* minimum. For the *ortho* geometry four different conformers do exist, which (similar to the cyclic ground state) differ in the positions of the free

	DF-CC2	CASPT2	DF-CC2	DF-LCC2	Experiment
	aug-cc-pVDZ		aug-cc-pVTZ		
Ph	37700.38 (36361.12)	33992.15	38280.68 (36941.42)	38280.69	36352 (-589)
Ph(H ₂ O) TL	37269.79 (35963.43)	33733.03	37808.51 (36502.15)	37804.93	35998 (-504)
Ph(H ₂ O) ₂ <i>hat</i> ←(Udu)	37226.20 (36029.80)	^a	37682.94 (36486.54)	37715.26	36231
Ph(H ₂ O) ₂ <i>ortho</i> (Udu)←(Udu)	36863.27 (35615.38)	33829.79	37300.83 (36052.94)	37276.06	
Ph(H ₂ O) ₃ (Udud)	37483.30 (36039.40)		38197.60 (36753.70)	38222.16	36261 (-493)

a) Not available since Ph(H₂O)₂ *hat* is no minimum geometry on the CASPT2 S₁ surface.

Table 2.4: Adiabatic excitation energies in cm⁻¹ calculated with DF-CC2, CASPT2 and DF-LCC2. 0–0 excitation energies are also given (in parentheses). All energies are counterpoise corrected, except those of DF-LCC2. Harmonic zero-point energy corrections were calculated within the aug-cc-pVDZ basis set. Experimental values (Ref. 73) are given in the right column, together with the difference to the DF-CC2 0-0 excitation energies within aug-cc-pVTZ basis-set (in parentheses).

	$n = 1$			$n = 2$			$n = 3$		
	TL,S ₀	TL,S ₁	CI	(Udu),S ₀	<i>ortho</i> ,S ₁	CI	(Udud),S ₀	(Udud),S ₁	CI
$d(\text{C} - \text{O})$	1.366	1.358	1.323	1.384	1.349	1.327	1.387	1.363	1.330
$d(\text{O} - \text{H})$	0.980	0.990	1.031	0.987	1.010	1.051	0.996	1.010	1.031
$d(\text{H} \cdots \text{OH})^a$	1.851	1.775	1.554	1.824	1.655	1.468	1.708	1.634	1.537
$d(\text{H} \cdots \text{OH})^b$				1.883	1.783	1.680	1.740	1.725	1.669
$d(\text{H} \cdots \text{OH})^c$							1.767	1.779	1.792

- a) H-bond length between Ph and 1st H₂O
b) H-bond length between 1st and 2nd H₂O
c) H-bond length between 2nd and 3rd H₂O

Table 2.5: Distances (in Å) for some key parameters of the stationary point geometries of the Ph(H₂O)_n clusters with $1 \leq n \leq 3$. All geometries were optimized with the CC2 (response) method and the aug-cc-pVDZ AO basis set.

hydrogen atoms relative to the planes defined by the related two hydrogen bonds and which, ordered from most to least stable conformer, can be denoted according to our notation introduced above as *ortho*(Udd), *ortho*(Uud), *ortho*(Udu), and *ortho*(Uuu) (see Fig. 2.4 and Table 2.2). The TS structure between *ortho*(Udd) and *ortho*(Udu) was also located (see Fig. 2.4) and a barrier of 0.47 kcal/mol for isomerization was obtained. For the less stable *hat* form, only one geometry was found. Any optimization starting from an alternative geometry with flipped free hydrogen atoms collapsed to one of the *ortho* geometries.

In order to verify these findings, additional geometry optimizations by a method complementary to CC2, i.e., CASPT2, were performed. The related interaction energies, compiled in Table 2.1, are smaller than the related CC2 values, yet one should again keep in mind that for the CASPT2 calculations, due to an intruder state problem, a level shift had to be used, which leads to an underestimation of the interaction energies by 10%–15% (see Sec. 2.2). In any case, the CASPT2 results provide more or less the same picture as those of CC2, in particular, they confirm (i) that no stable cyclic structure exists on the $S_1(\pi^* \leftarrow \pi)$ surface in the vicinity of the (Udu) Franck-Condon point and (ii) that the *ortho* geometries are indeed the most stable structures for the $n = 2$ cluster. In contrast to the CC2 results, the *hat* geometry was not stable and collapsed to the *ortho*(Udd) configuration.

Table 2.1 furthermore compares local CC2 interaction energies for ground and excited states with the corresponding canonical CC2 values without and with CP correction (aug-cc-pVTZ basis only). It is evident that (i) the BSSE of the aug-cc-pVTZ basis still amounts to more than 10% of the interaction energy and (ii) that uncorrected local and CP corrected canonical interaction energies closely agree, notably, also for the excited states.

Accepting the fact that for $n = 2$ the oxygen atom and the phenyl-ring switch roles in acting as H acceptors, the immediate next question is if this also applies for $n = 3$ with the less strained cyclic structure including three water units. Indeed, also for $n = 3$, analogous *ortho*, *meta*, and *hat* geometries could be located on the $S_1(\pi^* \leftarrow \pi)$ surface, which are more stable than the cyclic (Udud) with the phenol-oxygen acting as the H acceptor (see Table 2.2). However, in contrast to $n = 2$, the latter still constitutes a stable local minimum close to the Franck-Condon point. Several transition structures between the metastable cyclic (Udud) conformer and the energetically lower-lying structures were located with the lowest one corresponding to a barrier of 0.18 kcal/mol (63 cm^{-1} , CP corrected CC2/aug-cc-pVDZ result). We can conclude that the H acceptor switching in phenol from the oxygen atom to the π system of the ring in the $S_1(\pi^* \leftarrow \pi)$ state already explains qualitatively the different absorption spectra measured for the $n = 1$, $n = 2$, and $n = 3$ clusters.

2 Phenol-water_{1≤n≤3} clusters

For $n = 1$ the minima in the S_0 and the $S_1(\pi^* \leftarrow \pi)$ state both correspond to a translinear hydrogen bond arrangement with a rms deviation in the atomic positions of 0.06 Å. Reasonably large Franck-Condon factors therefore can be expected, leading to absorption spectra featuring bands related to the relevant intermolecular modes as observed experimentally. For $n = 3$, which has a stable cyclic (Udud) S_1 minimum close to the Franck-Condon point (0.09 Å rms), the situation is similar. However, this minimum is metastable and can only support intermolecular modes up to a certain energy. Beyond that, predissociation occurs. The redshift of the origin of the cyclic (Udud) local minimum is, according to the calculations (see Table 2.4), considerably smaller than for $n = 1$, which is in agreement with the experiment.

For $n = 2$ on the other hand, due to the large deviation between the cyclic (Udu) S_0 and the S_1 *ortho* geometries (0.75 Å rms), only a very small Franck-Condon factor for the 0_0^0 transition of this most stable conformer of the $n = 2$ cluster and therefore a very weak electronic origin with a *larger* redshift than $n = 1$ are expected. The observed $n = 2$ band structure in Fig. 2.1 on the blue side of the $n = 1$ origin may then correspond to some intramolecular mode of phenol and not to the origin. This intramolecular mode of phenol could possibly be of out-of-plane type considering the puckered ring in the $S_1(\pi^* \leftarrow \pi)$ *ortho* conformers. Note that the component of the oscillator strength vector perpendicular to the phenyl ring plane increases from 0 to 25%–30% of its norm on going from $n = 1$ to $n = 2$ or $n = 3$ (see Table 2.3). Alternatively, the existence of a very shallow minimum close to the Franck-Condon point corresponding to the cyclic S_0 (Udu) conformer also cannot entirely be ruled out, even though it is not found in the present calculations. Coupling between low-frequency intermolecular modes of this minimum and vibrational states of the more stable *ortho/hat* minima (with high density of modes at that energy) may give rise to the extremely low-frequency progression and the broad shape of the band. In both cases, the $n = 2$ cluster, either being vibrationally excited in an intramolecular out-of-plane mode of Ph or due to vibrational coupling between modes of the cyclic local minimum and the *ortho/hat* conformers, may carry enough energy in the relevant degrees of freedom to cross the conical intersection seam and to access the energetically much lower-lying configuration space of S_1 with $\sigma^* \leftarrow \pi$ character, where the proton has been transferred from Ph to the solute molecules.

2.3.2 Conical Intersection and Proton Transfer

As just mentioned, there exists a conical intersection seam between the $S_1(\pi^* \leftarrow \pi)$ and the $S_2(\sigma^* \leftarrow \pi)$ surfaces. Beyond the conical intersection seam, proton trans-

fer from Ph to the solvent molecules takes place. The corresponding dissociated structures are energetically more favorable than the minima on the $S_1(\pi^* \leftarrow \pi)$ surface discussed so far. In order to investigate if the conical intersection seam is of any relevance for the low-energy configuration space considered in the present work, geometry optimizations on the seams of the individual clusters have been performed employing the scheme outlined in Sec. 2.2. The resulting geometries are displayed in Fig. 2.6 and the related interaction energies are compiled in Table 2.1. For $n = 1$ again a translinear geometry is found featuring even larger contractions of the C–O distance and the hydrogen bond relative to the ground state minimum than the S_1 minimum-energy geometry, i.e., by ≈ 0.05 and 0.30 Å, respectively (see Table 2.5). The CI geometries of both the $n = 2$ and $n = 3$ clusters feature open chain conformers with the last water subunit no longer acting as a H donor (see Fig. 2.6).

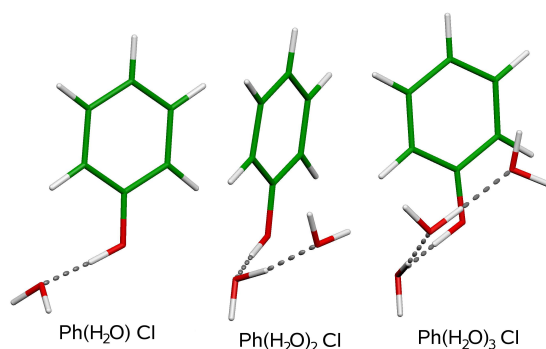


Figure 2.6: Conical intersection seam geometries of the lowest energy of $\text{Ph}(\text{H}_2\text{O})_n$, $1 \leq n \leq 3$.

For $n = 2$ the C–O distance and the first H bond again contract dramatically by 0.06 and 0.36 Å, respectively, compared to the cyclic S_0 (Udu) conformer. Also the second H bond contracts by 0.20 Å. For $n = 3$ the C–O distance shortens by a similar amount (0.06 Å) relative to the cyclic S_0 (Udud) conformer, however, the H-bond contractions are less pronounced, i.e., by 0.17 and 0.06 Å for the first and second H bonds, respectively. These strong H-bond contractions are forestalling the H transfer from Ph to the solvent cluster beyond the conical intersection. The CI geometries lie energetically 0.63 , 0.66 , and 2.53 kcal/mol above the corresponding Franck-Condon points on the $S_1(\pi^* \leftarrow \pi)$ surface for $n = 1$, $n = 2$, and $n = 3$, respectively (see Table 2.1), which corresponds to 8% , 3% , and 9% of the corresponding interaction energy of the clusters in the S_1 state. Since the $n = 2$ cluster has the highest excess energy for the reasons discussed above, we anticipate that $n = 2$ more easily reaches the seam and undergoes proton transfer to the solvent than $n = 1$ or $n = 3$. This would then explain the much shorter lifetime and the

low quantum yield of $n = 2$ in comparison to $n = 1$ and $n = 3$ as observed in the experiments.

2.4 Conclusions

In this work the $S_1(\pi^* \leftarrow \pi)$ state surfaces of the phenol-water_{1≤n≤3} clusters were reexplored at the level of coupled cluster (CC2) response theory, aiming at a better understanding of the anomalous behavior of $n = 2$ (broad congested absorption band structure, low quantum yield, short lifetime) in comparison to $n = 1$ and $n = 3$. Minima and other stationary points were located – to our knowledge for the first time – at a level of theory which includes dynamical electron correlation. As a consequence, global minimum structures were found for $n = 2$ and $n = 3$, which are qualitatively different from those obtained so far using methods such as CIS or CASSCF. Evidently, the oxygen atom and the π -ring system of phenol switch roles as H acceptors on going from the S_0 to the S_1 state. The global minima on the S_1 surface for $n = 2$ and $n = 3$ correspond to cyclic structures where the second (third) water subunit acts as a donor to the π ring. These structures deviate substantially from those corresponding to the global S_0 minima. The Franck-Condon factors related to the corresponding 0–0 transitions therefore are expected to be very small. For $n = 2$ no local minimum close to the Franck-Condon point could be located, while for $n = 3$ such a minimum exists. Furthermore, the $n = 2$ cluster, having a rather high excess energy possibly in an out-of-plane mode driving it toward the conical intersection seam, is more likely to cross the conical intersection and to undergo proton transfer to the solvent molecules than the $n = 1$ and $n = 3$ clusters. These results now offer a qualitative explanation of the anomalous behavior of $n = 2$ and the predissociation of $n = 3$ at excess energies beyond $\approx 100 \text{ cm}^{-1}$ apparent in the absorption spectrum. We can conclude that the interpretation given almost a decade ago by Jacoby *et al.* in Ref. 77 for the broad congested absorption band structure observed for $n = 2$ is basically correct, provided that the anticipated linear hydrogen arrangement is replaced by a cyclic structure where the π -ring system acts as H acceptor for the second water subunit.

3 2-Naphthol-water₂ clusters

3.1 Introduction

The photophysics of hydrogen-bonded clusters formed between aryl alcohols and water or ammonia have been investigated extensively within the last two decades. They mimic intermolecular interactions ubiquitous in biochemical systems, but are also interesting by themselves. Experimentally, such clusters can be synthesized in molecular beam expansions at very low (vibrational) temperatures. Furthermore, due to the aromatic chromophore they are spectroscopically easily accessible by various laser spectroscopic techniques, including the mass-selective resonant two-photon ionization (R2PI) spectroscopy. Theoretically, the description of the relevant excited states and, in particular, the determination of the related minimum-energy geometries still is a challenging task, since long-range dynamical correlation effects, i.e., van der Waals forces, play a nonnegligible role in these systems. Analytical gradients of energy functionals fulfilling these requirements still are scarce.

Recently, we re-explored the $S_1(\pi^* \leftarrow \pi)$ state surfaces of the phenol-water_{*n*}, $n \in \{1, 2, 3\}$ clusters at the level of time-dependent coupled cluster (CC2) response theory [102]. Based on these calculations it became possible to elucidate the photophysics of these systems and, in particular, to resolve the anomalous behavior of the $n = 2$ cluster featuring a broad congested absorption band structure, low quantum yield, and a short lifetime, in stark contrast to the other $n = 1$ and $n = 3$ clusters. A disturbing disagreement between experiment and theory persisting for almost a decade so was finally settled. In the present work we applied the same methodology in a study on the S_0 and $S_1(\pi^* \leftarrow \pi)$ state surfaces of the 2-naphthol-water_{*n*}, $n \in \{1, 2\}$ clusters. 2-naphthol (2-NpOH) exists in a *cis* and a *trans* isomeric form due to the two possible rotational orientations of the OH group relative to the naphthyl ring system. There is experimental evidence that the *cis* isomer is more stable in the S_0 state, whereas the *trans* isomer becomes more stable in the S_1 state [103–105]. Different experiments have been carried out by Ebata *et al.* to photoinduce the isomerization in the S_1 state with the result that (i) the isomerization yield is only high for *cis* \longrightarrow *trans* isomerization and (ii) hydrogen-bonding strongly enhances the isomerization yield [106, 107]. Mass-

3 2-Naphthol-water₂ clusters

selective R2PI absorption and fluorescence emission spectra of 2-NpOH clustered with water, ammonia, and other solvent molecules were measured by several groups [75, 108, 109], especially also in the context of photoinduced proton transfer for bigger clusters [108] (2-NpOH is known to be a weak acid in the S_0 state but a strong acid in the S_1 state with pK_a values of 9.8 and 2.8, respectively [110]). Experimental information on the geometries of some of the binary complexes, based on rotationally resolved fluorescence excitation spectra, is also available in the literature [111]. Furthermore, geometrical assignments were deduced by Matsumoto *et al.* [112] for the 2-NpOH(H_2O)_{*n*} clusters up to $n = 5$ in the S_0 state, based on comparisons of experimental OH stretch vibrational frequencies [measured by infrared (IR)-ultraviolet double-resonance spectroscopy] with corresponding harmonic Hartree-Fock values obtained at the related minimum-energy geometries. The proposed geometries coincide closely to those of phenol(H_2O)_{*n*} or (H_2O)_{*n*+1} with a translinear (TL) C_s arrangement for $n = 1$, cyclic structures for $n \in \{2, 3\}$, and a cage structure for $n = 5$. By applying photofragment-detected IR spectroscopy the same group also provided an upper bound of 7.6 kcal/mol for the S_0 binding energy of 2-NpOH· H_2O [113].

Theoretically, the 2-NpOH(H_2O)_{*n*} clusters were not yet studied with more sophisticated *ab initio* electronic structure methods. So far, the S_0 potential energy surfaces (PESs) were investigated at the level of Hartree-Fock theory with rather modest atomic orbital (AO) basis sets, focusing mainly on the relevant, i.e., energetically low-lying minimum-energy structures, and calculating the related normal modes and (harmonic) vibrational frequencies [109, 112]. The S_1 PES of these clusters, to our knowledge, remained unexplored so far. The S_1 state of the 2-NpOH· NH_3 complex was recently studied by using the (semiempirical) time-dependent density functional tight binding method [114].

The R2PI spectrum of 2-NpOH(H_2O)₂, similarly to the phenol(H_2O)₂ case, features some peculiarities distinguishing it from those of the $n = 1$ and $n = 3$ clusters. The two band structures assigned to the *cis* and *trans* isomers are broad and congested for $n = 2$, whereas sharp progressions are observed for $n = 1$ and $n = 3$ (cf. Fig. 3.1). This is in close analogy to the situation encountered for the phenol-water clusters. However, the R2PI spectrum of 2-NpOH(H_2O)₂ features also a third band structure, namely, two rather long progressions of sharp lines shifted quite far to the red. No analogous band shape is seen, neither in the spectrum of phenol(H_2O)₂ nor in the spectra of 2-NpOH(H_2O)_{1,3}. Also in the spectrum of the deuterated 2-NpOD(D_2O)₂ such a feature is absent (cf. Fig. 6 in Ref. 75). This implies that for the 2-NpOH(H_2O)₂ cluster at least a third stable conformer, responsible for these line progressions, has to exist in the S_0 state, which, on the other hand, is not stable for the deuterated cluster.

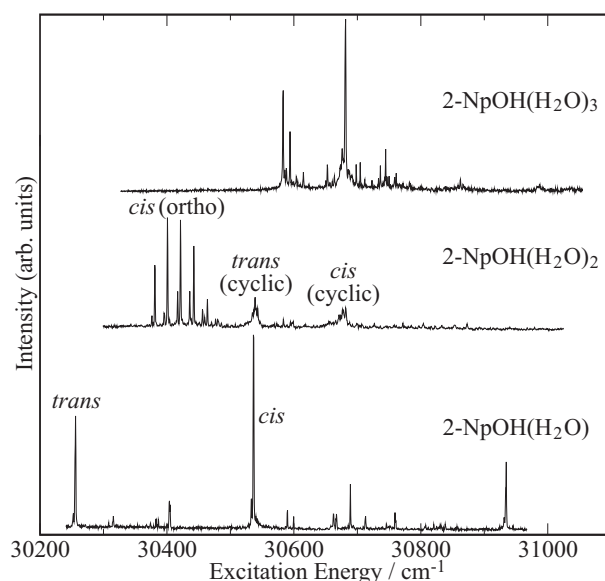


Figure 3.1: Mass-selective resonant two-photon ionization (R2PI) spectra of 2-NpOH(H₂O)_n, $n \in \{1, 2, 3\}$.

In this work we have explored the relevant regions of the S_0 and S_1 state PESs of the 2-NpOH(H₂O)_{1,2} clusters at the level of coupled cluster response theory employing the CC2 model [46]. Various low-energy stationary points were located and harmonic vibrational frequencies were calculated at these points in order to get an estimate for the corresponding zero-point energy (ZPE) corrections. The main impetus for the present work was again to obtain at least a qualitative explanation for the anomalous behavior of the $n = 2$ cluster and, in particular, to identify the third stable conformer responsible for the sharp line progressions in its R2PI spectrum.

3.2 Computational methods

The minimum-energy and first-order saddle point geometries on the S_0 and $S_1(\pi^* \leftarrow \pi)$ PES of the two 2-NpOH isomers and their water clusters 2-NpOH(H₂O)_n, $n \in \{1, 2\}$ were optimized by applying time-dependent coupled cluster response theory at the level of the CC2 model. The analytic CC2 energy gradient program implemented by Hättig and Köhn in the TURBOMOLE program package [90, 91], which employs the density fitting (DF) approximation to factorize the electron repulsion integrals, was used for that purpose. For the individual stationary points the harmonic ZPE corrections were computed based on the nuclear Hessians ob-

tained by numerical differentiation of the analytic CC2 gradients. Furthermore, for the individual minima on the S_0 surface the one-photon transition strength vectors were calculated from the residues of the CC2 linear response functions. These calculations were carried out by using both canonical [115] and local [94, 95] CC2 response theory, the later being implemented in the **MOLPRO** program package [96]. In the present context the local method has the major advantage of avoiding basis set superposition error (BSSE) effects to large extent [41, 102]. For the local calculations Pipek-Mezey orbital localization was used. The pair list remained untruncated. Domains were constructed by natural population analysis (NPA) [116] and extended by all next nearest neighbor atoms (relative to those of the NPA core domains). Redundancies in the pair domains were determined at large intermonomer distances and kept fixed. The domains for the amplitude responses were obtained via NPA analysis of density matrices calculated from semilocal CC2 response singles eigenvectors of the excited state and also extended by all next nearest neighbor atoms. Important orbitals (for the excitation) were determined according to the scheme discussed in Ref. 94, using the default criterion of $\kappa_e = 0.995$.

As AO basis sets the aug-cc-pVXZ sets [34, 98] together with the related fitting basis sets optimized for DF-MP2 (Ref. 99) were employed in all calculations. For the geometry optimizations and the calculations of the geometric relaxation energies, transition strengths, and ZPE corrections, X=D was used. In order to obtain better converged (with respect to the AO basis) interaction and excitation energies additional single-point calculations within the X=T basis were performed at the stationary points of the S_0 and S_1 state surfaces corresponding to the X=D basis (*vide infra*). Interaction energies obtained from canonical calculations were counterpoise corrected [40] to correct for BSSE effects. The transition strength vectors were also computed with the X=T basis (with the local method only).

3.3 Results and discussion

Figure 3.1 displays the mass-selective absorption spectra of the 2-NpOH(H₂O)_{*n*}, $n \in \{1, 2, 3\}$ clusters in the vicinity of the two electronic origins (related to the *cis* and *trans* isomers) of 2-NpOH. These two-color R2PI spectra were measured by one of us about 15 years ago, for experimental details, we refer to Ref. 109. The two origins of $n = 1$ appearing at 30256 and 30535 cm⁻¹, which belong to the *trans* and *cis* isomers, respectively, are clearly visible. The absorption spectrum of $n = 1$ features a set of sharp bands corresponding to intermolecular modes of the complex, for example, the short progressions of the intermolecular stretch modes (≈ 150 cm⁻¹) are clearly recognizable for both isomers. There are also bands corresponding to intramolecular modes present in the spectrum, for a

detailed assignment, we again refer to Ref. 109. Also for the $n = 3$ cluster the two systems of bands corresponding to the two isomers are easily identified. Again, the spectrum consists of sharp bands. The two origins of $n = 3$ are much less redshifted (relative to the corresponding origins of the bare 2-NpOH monomer) than those of $n = 1$, i.e., 372 cm^{-1} ($n = 1$) versus 226 cm^{-1} ($n = 3$) for the *cis* isomer and 334 cm^{-1} ($n = 1$) versus 7 cm^{-1} for *trans*. The corresponding redshifts for phenol-H₂O and phenol(H₂O)₃ amount to 350 and 92 cm^{-1} , respectively [74, 76]. The redshifts of the electronic origins of the clusters relative to those of the bare monomer directly indicate the increase of their binding energies upon electronic excitation.

The R2PI spectrum of the 2-NpOH(H₂O)₂ cluster, on the other hand, is quite different. It exhibits two congested broad band structures, quite similar to the one observed for phenol(H₂O)₂. These two band structures at 30536 and 30676 cm^{-1} were assigned to the *trans* and *cis* isomers of a cyclic hydrogen-bonding arrangement, respectively [75]. Surprisingly, there is an additional third band structure consisting of two rather long progressions of sharp lines with the same fundamental frequency of 20 cm^{-1} , starting at 30376 and 30381 cm^{-1} . Such band shapes are entirely absent in the R2PI spectrum of the deuterated 2-NpOD(D₂O)₂ species, as well as in the spectra of phenol(H₂O)₂ or its deuterated subspecies. In Ref. 75 these band shapes were assigned to open-chain hydrogen-bonding arrangements. Based on these experimental facts and on the results of our theoretical study on the phenol-water clusters [102] we conjecture that (i) the two broad band shapes of 2-NpOH(H₂O)₂ indeed correspond to cyclic hydrogen-bonding arrangements of the *trans* and *cis* forms of 2-NpOH, (ii) the cyclic hydrogen-bonding arrangements are either unstable (or metastable with very low barriers) in the excited S₁ state, (iii) at least a third, energetically competitive conformer coexists in the S₀ state, corresponding to a hydrogen-bonding arrangement where the π system of the naphthyl ring rather than the oxygen atom acts as the H acceptor of 2-NpOH, (iv) the corresponding geometries, in analogy to the phenol(H₂O)₂ case, are stable in the S₁ state (which is a prerequisite for the observed line progressions), and (v) the lower ZPE of the deuterated species preferentially stabilizes the cyclic hydrogen-bonding arrangements. In the following we want to test this hypothesis at the level of time-dependent CC2 response theory.

3.3.1 S₀ minimum-energy geometries

The energy relevant S₀ minimum-energy geometries of the *cis*- and *trans*-2-NpOH-(H₂O)_{*n*}, $n \in \{1, 2\}$ clusters are displayed in Figs. 3.2 and 3.3, respectively, and the related binding energies are compiled in Table 3.1. The final binding energies

3 2-Naphthol-water₂ clusters

in Table 3.1 are BSSE corrected and include the geometric relaxation energies of the related monomers. Supplementary binding energies including harmonic ZPE corrections of the undeuterated or the deuterated species are also given, even though the harmonic approximation is bound to fail for some of the intermolecular modes. This is especially true for the low-energy isomerization coordinates of the $n = 2$ cluster *vide infra*. Therefore, the ZPE uncorrected binding energies are used in the discussion of the relative stability of the individual $n = 2$ conformers. A further problem is the BSSE, which can deviate by more than a kcal/mol between different conformers of the same cluster (cf. Table 3.1). Since BSSE free geometry optimizations are too expensive with canonical methods and analytical local CC2 nuclear energy gradients not yet available, we have to rely on the assumption that the effect of BSSE on geometries is much less severe than on the interaction energies.

The binary $n = 1$ complexes show the usual TL hydrogen-bonding arrangement as known from the water dimer and from phenol·H₂O. The binding energies are slightly larger than those obtained for phenol·H₂O, i.e., -4.79/-4.82 versus -4.59 and -5.24/-5.27 versus -5.04 kcal/mol for the X=D and the X=T bases, respectively (relaxation energies and ZPE corrections always are calculated with the X=D basis).

For the $n = 2$ clusters, evidently, there are two groups of relevant S₀ minimum-energy geometries, namely, those forming a cyclic hydrogen-bonding arrangement involving the 2-NpOH OH group as H donor and acceptor and those forming a hydrogen-bonding network where the NpOH π system acts as the H acceptor instead. For the cyclic *cis* and *trans* geometries the usual three conformers exist, denoted as (Udu), (Uud), and (Udd), respectively. This nomenclature, introduced originally in Ref. 117 in the context of the water trimer, indicates, e.g., for the first minimum, that the aromatic ring is in Up, the first free hydrogen atom in down, and the second free hydrogen again in up position relative to the plane defined by the two hydrogen bonds involved (donor-acceptor indicates the direction of the axial vector of the plane). Analogous cyclic geometries were found for the water trimer and phenol(H₂O)₂. The most stable cyclic conformer for both isomers again is (Udu), the others are 0.4–0.7 kcal/mol above (Udu).

For the second group with the naphthyl π system acting as the H acceptor of 2-NpOH also numerous conformers coexist. The two ortho C atoms, either in *syn*- or *anti*-position relative to the hydrogen atom of the OH group, act as H acceptors of the naphthyl π system, again with several sub-conformers differing in the relative positions of the dangling H atoms. The notations *ortho* and *ortho'*, respectively, are used to distinguish these geometries from the cyclic ones, e.g., (*ortho*Udu) for the corresponding conformer. No geometries of that kind were

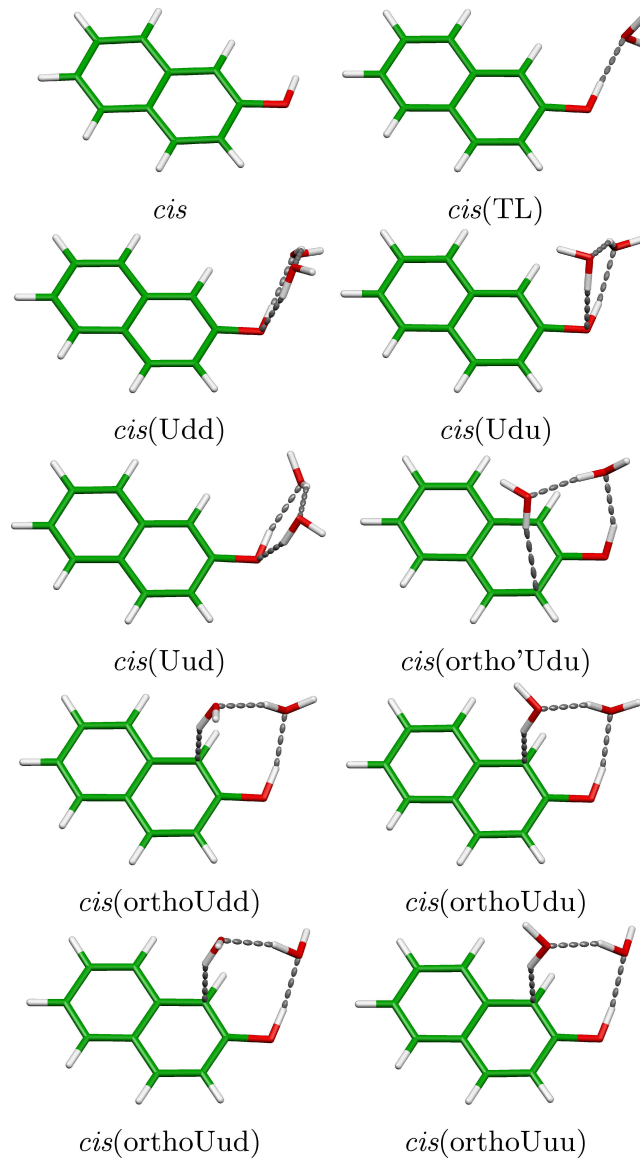


Figure 3.2: *cis*-2-naphthol(H_2O) $_n$, $n \in \{0, 1, 2\}$ geometries of the electronic ground state.

3 2-Naphthol-water₂ clusters

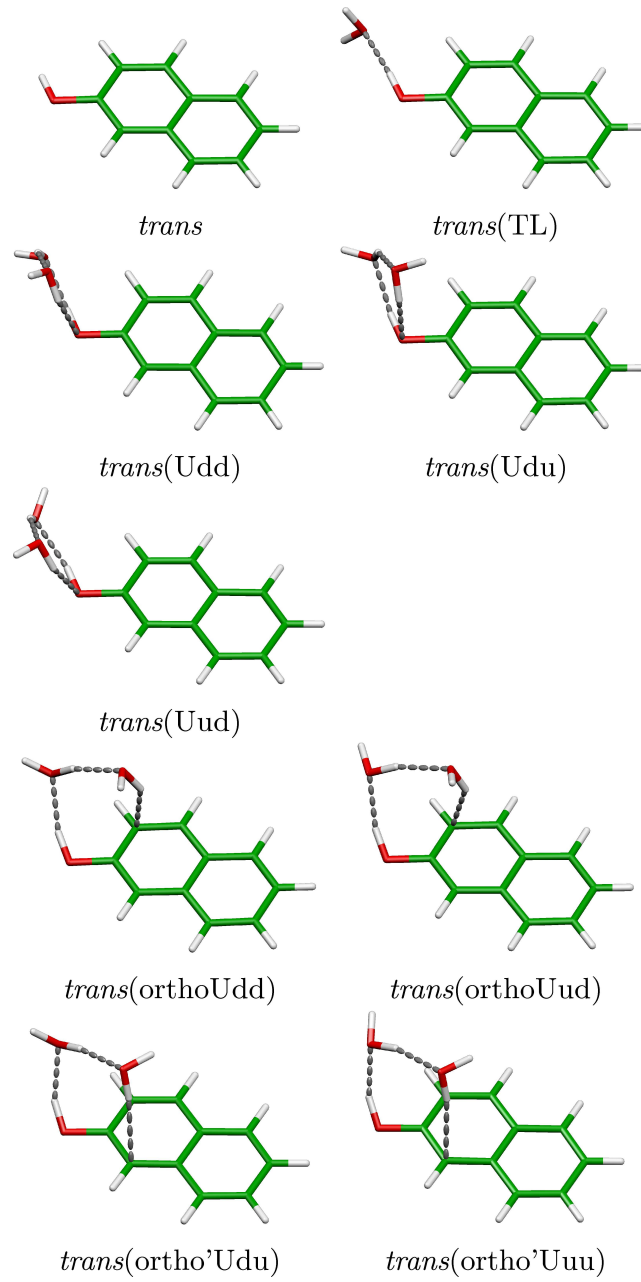


Figure 3.3: *trans*-2-naphthol(H₂O)_n, $n \in \{0, 1, 2\}$ geometries of the electronic ground state.

m -2-NpOH(H ₂ O) _{n}			X=D					X=T			
m	n	Conformer	δ_{BSSE}	δ_{rel}	ΔE	ΔE^{H}	ΔE^{D}	δ_{BSSE}	ΔE	ΔE^{H}	ΔE^{D}
<i>cis</i>	1	TL	1.60	-0.11	-6.55	-4.79	-5.15	0.78	-6.99	-5.24	-5.60
<i>cis</i>	2	Udd	3.77	-0.48	-15.08	-10.80	-11.73	1.86	-16.40	-12.13	-13.05
<i>cis</i>	2	Udu	4.16	-0.44	-15.54	-11.13	-12.08	2.05	-16.90	-12.50	-13.45
<i>cis</i>	2	Uud	3.63	-0.50	-14.86	-10.59	-11.54	1.81	-16.19	-11.92	-12.87
<i>cis</i>	2	<i>ortho</i> Udd	4.76	-0.93	-15.60	-11.33	-12.22	2.26	-17.08	-12.81	-13.70
<i>cis</i>	2	<i>ortho</i> Udu	4.81	-1.09	-15.60	-11.35	-12.24	2.28	-17.09	-12.84	-13.72
<i>cis</i>	2	<i>ortho</i> Uud	4.62	-1.07	-15.23	-11.15	-12.01	2.21	-16.72	-12.63	-13.49
<i>cis</i>	2	<i>ortho</i> Uuu	4.60	-1.13	-14.68	-10.91	-11.70	2.20	-16.14	-12.37	-13.16
<i>cis</i>	2	<i>ortho</i> Udu	5.15	-2.19	-14.68	-10.58	-11.42	2.43	-16.13	-12.03	-12.87
<i>trans</i>	1	TL	1.58	-0.11	-6.62	-4.82	-5.19	0.77	-7.07	-5.27	-5.64
<i>trans</i>	2	Udd	3.76	-0.49	-15.34	-10.99	-11.93	1.84	-16.90	-12.33	-13.26
<i>trans</i>	2	Udu	4.05	-0.44	-15.75	-11.25	-12.22	1.99	-17.12	-12.61	-13.59
<i>trans</i>	2	Uud	3.63	-0.50	-15.03	-10.70	-11.66	1.80	-16.37	-12.04	-13.00
<i>trans</i>	2	<i>ortho</i> Udd	4.71	-1.21	-15.42	-11.19	-12.06	2.25	-16.92	-12.68	-13.56
<i>trans</i>	2	<i>ortho</i> Uud	4.64	-1.43	-14.94	-10.97	-11.80	2.22	-16.44	-12.47	-13.30
<i>trans</i>	2	<i>ortho</i> Udu	5.05	-1.80	-15.15	-10.89	-11.76	2.38	-16.67	-12.41	-13.28
<i>trans</i>	2	<i>ortho</i> Uuu	4.91	-1.86	-14.13	-10.25	-11.03	2.33	-15.64	-11.76	-12.54
<i>cis</i>	2	[Udu \rightleftharpoons <i>ortho</i> Udd] ‡	4.31	-0.49	-15.37			2.09	-16.75		
<i>cis</i>	2	[Udu \rightleftharpoons <i>ortho</i> Udu] ‡	4.43	-0.65	-15.12			2.12	-16.50		
<i>cis</i>	2	<i>ortho</i> Ud[d \rightleftharpoons u] ‡	4.66	-0.99	-15.33			2.19	-16.79		
<i>cis</i>	2	[U \rightleftharpoons D]du ‡	3.30	-0.52	-14.90			1.68	-16.24		
<i>trans</i>	2	[Udu \rightleftharpoons <i>ortho</i> Udd] ‡	4.44	-0.70	-15.27			2.11	-16.66		

Table 3.1: Counterpoise corrected binding energies ΔE in kcal/mol of the individual low-energy minima and first-order saddle points on the S_0 PES, calculated with the aug-cc-pVXZ AO basis and corresponding fitting sets. δ_{BSSE} and δ_{rel} are the incremental BSSE and geometric relaxation energies, respectively. The harmonic ZPE corrected binding energies for both the undeuterated and the deuterated (H atoms on hydroxy group and water molecules) cluster are also given.

3 2-Naphthol-water₂ clusters

found for the phenol(H₂O)₂ cluster in the S₀ state. For the *cis* isomer the three conformers (*ortho*Udu), (*ortho*Udd), and (Udu) differ by the tiny amount of less than 0.06 kcal/mol (local CC2 single-point calculation without counterpoise correction yields 0.03 kcal/mol or 10 cm⁻¹). This difference certainly is below the accuracy of the present method. These three conformers hence are expected to be significantly populated at typical vibrational temperatures of a molecular beam expansion, confirming conjecture (iii) of our initial hypothesis. Interestingly, the barrier separating the cyclic (Udu) conformer from (*ortho*Udd) is very low (50–60 cm⁻¹). Only a slight tilting movement of the second water molecule is required to go from (Udu) to (*ortho*Udd) and vice versa. Its free and its H bonded hydrogen atoms change role in a concerted way along the interconversion pathway, in the transition state (TS) structure it acts as a double donor to both the hydroxy group and the π system of 2-NpOH. The barrier separating (Udu) from (*ortho*Udu), on the other hand, is almost three times as high. Here, the H bond of the second water molecule is broken and reformed and no switching of roles of its two H atoms occurs. The interconversion pathway linking *ortho*Udd with *ortho*Udu corresponds to a flip of the dangling H atom. Consequently no hydrogen bond is broken in the process and the related barrier amounts to 94 cm⁻¹.

For the *trans* isomer the situation is somewhat less subtle. The most stable *ortho* conformer, *trans*(*ortho*Udd), is about 0.3 kcal/mol less stable than the cyclic (Udu) structure. The TS between these two geometries lies 52 cm⁻¹ above the *ortho* conformer. Due to this low barrier and the lower energy of the cyclic (Udu) structure the latter is anticipated to be of primary relevance for the R2PI spectrum, quite similar to the situation encountered in phenol(H₂O)₂. Moreover, the CC2 method (such as MP2) treats dispersion at the uncoupled Hartree-Fock level. Consequently, CC2 may somewhat overestimate this component of the intermolecular interaction energy, then even being slightly biased in favor of those conformers where the π system is involved in the H bonding relative to the cyclic ones.

The difference in the (harmonic) ZPEs of undeuterated and deuterated cluster species reveals no hint on why the related R2PI spectra are so different. Deuteration apparently leads to a slight destabilization of the *ortho* relative to the cyclic cluster geometries (cf. binding energies with harmonic ZPE corrections in Table 3.1), yet the effect at the level of the harmonic approximation is tiny. Hence, conjecture (v) cannot be verified at the present stage. On the other hand, the harmonic approximation is bound to fail entirely for those modes corresponding to the interconversion pathways connecting the individual low-energy minima of the *cis* isomer.

Finally, the barrier corresponding to the up and down flip of the naphthyl ring system was determined. This barrier connects the three cyclic minima with their

enantiomeric counterparts, i.e., (Udu) with (Ddu) = (Uud). A value of 224 cm^{-1} was obtained, which is more than three times higher than the barrier for interconversion to the ortho conformer.

3.3.2 S_1 minimum-energy geometries

The relevant minimum-energy geometries on the $S_1(\pi^* \leftarrow \pi)$ state surfaces are depicted in Figs. 3.4 and 3.5 for *cis* and *trans*, respectively. Table 3.2 compiles the corresponding binding energies, which again are counterpoise corrected and include geometric relaxation of the monomers. Additionally, as for the S_0 minima, binding energies corrected for the harmonic ZPE are also given. Table 3.3 shows the relations between the individual minima on the S_0 and S_1 surfaces, i.e., to which S_1 geometry an initial S_0 geometry converges in the geometry optimizations. The discrepancies between related S_0 and S_1 geometries are also given in Table 3.3 as the root-mean-square (rms) deviation of their atomic positions [see Eq. (64) in Ref. 101 for the definition of d^{rms}].

For the binary $n = 1$ complexes again the usual TL hydrogen-bonding arrangement is found. The length of the hydrogen bond shrinks by 0.07 \AA (*cis*) and 0.08 \AA (*trans*) on going from the S_0 to the S_1 state (cf. Table 3.4). The geometric discrepancy between these two geometries is only $d^{\text{RMS}} = 0.04\text{ \AA}$ (*cis*) and $d^{\text{RMS}} = 0.06\text{ \AA}$ (*trans*). Thus, sizable Franck-Condon factors are anticipated, reflected in the absorption spectrum as rather short progressions of sharp bands related to the individual inter- and intramolecular modes. This is exactly what is observed experimentally. The binding energies of the complex increase by about 30% and 25% from the S_0 to the S_1 state, for *cis* and *trans*, respectively. This is very similar to the values obtained for the phenol·H₂O case.

For the $n = 2$ clusters the situation is much more complicated. The cyclic cluster geometries with the hydroxy group of 2-NpOH acting as H acceptor are no longer competitive to those cluster geometries where the naphthyl π system is taking up this role. Analogously to the phenol(H₂O)₂ case [102] the π system becomes the preferred H acceptor in the S_1 state. Of the three cyclic conformers in the S_0 state only the (Uud) conformer constitutes a local minimum on the S_1 surface at rather high energies, about 2 kcal/mol (*cis*) and 2.9 kcal/mol (*trans*) above the corresponding global minimum. The other conformers all collapse to various distinct cluster geometries involving the π system, as displayed in Figs. 3.4 and 3.5. In particular, the *cis*(Udu) conformer collapses to *cis*(*hat*Ud-) geometry about 0.8 kcal/mol above the global minimum, where the second water acts as a double donor to the π system (the two water molecules arrange as a TL water dimer alike geometry). The *trans*(Udu) conformer, on the other hand, collapses to the

3 2-Naphthol-water₂ clusters

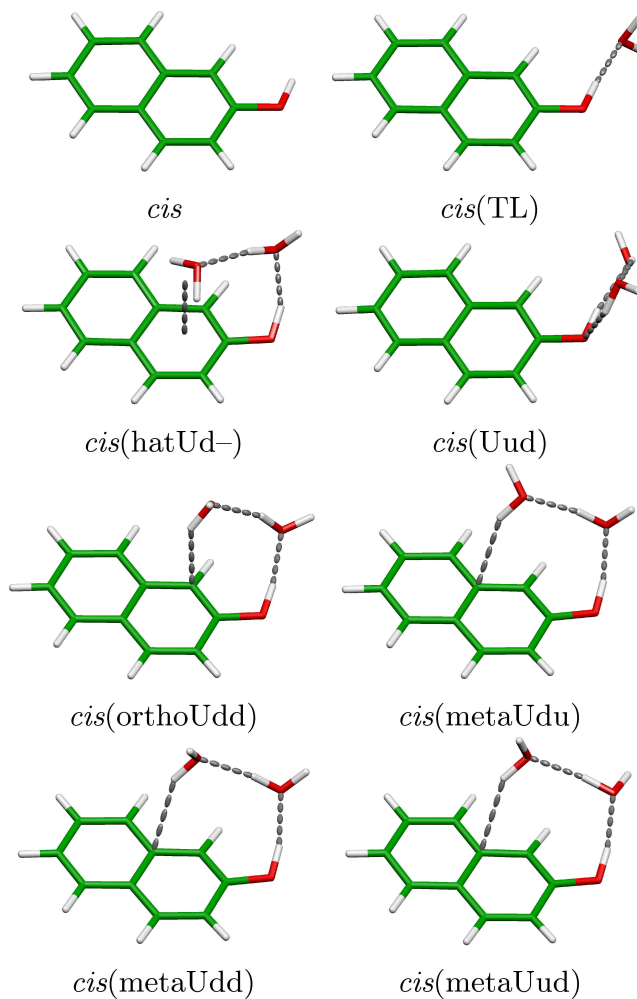


Figure 3.4: *cis*-2-naphthol(H₂O)_{*n*}, *n* ∈ {0, 1, 2} geometries of the S₁ electronically excited state.

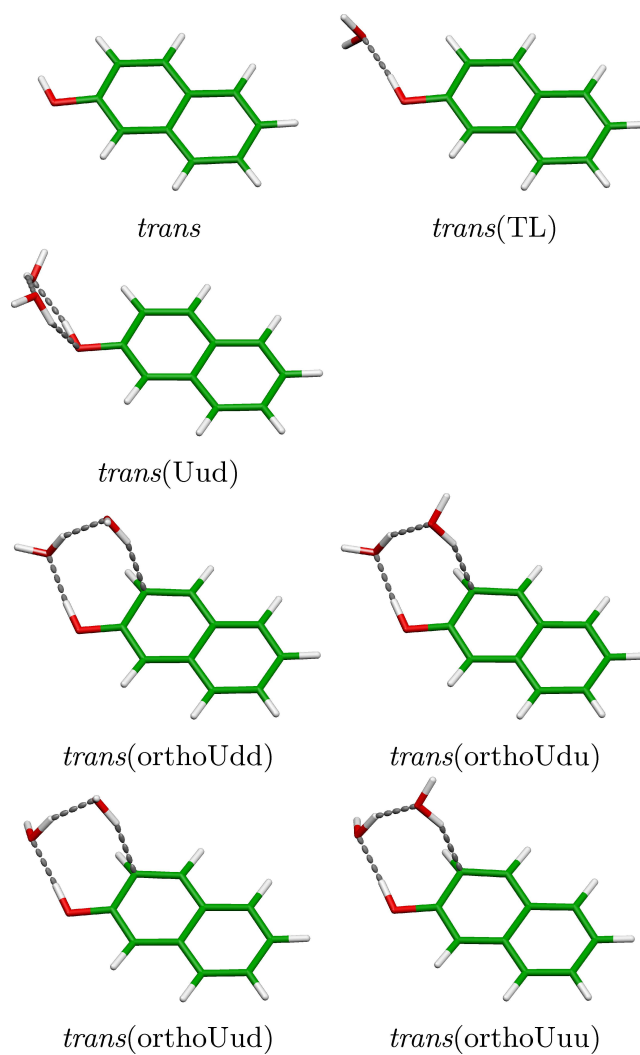


Figure 3.5: *trans*-2-naphthol(H₂O)_{*n*}, *n* ∈ {0, 1, 2} geometries of the S₁ electronically excited state.

m -2-NpOH(H ₂ O) _{n}			X=D					X=T			
m	n	Conformer	δ_{BSSE}	δ_{rel}	ΔE	ΔE^{H}	ΔE^{D}	δ_{BSSE}	ΔE	ΔE^{H}	ΔE^{D}
<i>cis</i>	1	TL	1.77	-0.22	-8.04	-6.23	-6.57	0.84	-8.55	-6.75	-7.09
<i>cis</i>	2	hatUd–	5.47	-2.40	-16.93	-12.63	-13.48	2.54	-18.51	-14.21	-15.06
<i>cis</i>	2	Uud	3.67	-0.70	-15.72	-11.75	-12.60	1.79	-17.06	-13.09	-13.94
<i>cis</i>	2	orthoUdd	4.95	-1.49	-17.52	-13.45	-14.26	2.34	-19.15	-15.08	-15.89
<i>cis</i>	2	metaUdd	5.04	-2.31	-17.57	-13.46	-14.25	2.34	-19.24	-15.13	-15.92
<i>cis</i>	2	metaUdu	5.09	-2.30	-17.71	-13.44	-14.27	2.34	-19.39	-15.12	-15.95
<i>cis</i>	2	metaUud	4.87	-2.15	-17.40	-13.34	-14.13	2.29	-19.06	-15.00	-15.78
<i>trans</i>	1	TL	1.72	-0.23	-7.81	-6.03	-6.36	0.83	-8.34	-6.57	-6.90
<i>trans</i>	2	Uud	3.69	-0.72	-15.38	-11.39	-12.24	1.79	-16.75	-12.77	-13.61
<i>trans</i>	2	orthoUdd	4.87	-2.09	-18.29	-13.67	-14.53	2.30	-20.15	-15.53	-16.39
<i>trans</i>	2	orthoUdu	4.91	-2.21	-18.18	-13.55	-14.41	2.30	-20.01	-15.39	-16.25
<i>trans</i>	2	orthoUud	4.72	-2.28	-18.23	-13.71	-14.55	2.27	-20.07	-15.55	-16.39
<i>trans</i>	2	orthoUuu	4.79	-2.31	-17.54	-13.14	-13.96	2.26	-19.36	-14.96	-15.77
<i>cis</i>	2	[ortho \rightleftharpoons meta]Udd [‡]	^a								
<i>cis</i>	2	metaUd[d \rightleftharpoons u] [‡]	5.04	-2.16	-17.57			2.31	-19.26		

a) PES too shallow, could not be located.

Table 3.2: Counterpoise corrected binding energies ΔE in kcal/mol of the individual low-energy minima and first-order saddle points on the S₁ PES, calculated with the aug-cc-pVXZ AO basis and corresponding fitting sets. δ_{BSSE} and δ_{rel} are the incremental BSSE and geometric relaxation energies, respectively. The harmonic ZPE corrected binding energies for both the undeuterated and the deuterated (H atoms on hydroxy group and water molecules) cluster are also given.

<i>m</i>	<i>n</i>	Conf. $S_0 \rightarrow$ Conf. S_1	d^{RMS}	$m\text{-}2\text{-NpOH}(\text{H}_2\text{O})_n$			Exp.	$m\text{-}2\text{-NpOD}(\text{D}_2\text{O})_n$		
				X=D	X=T			X=D	X=T	Exp.
<i>cis</i>	0		0.0379	30952.74 (31929.56)	31352.41 (32329.23)		30903	30948.46	31348.13	
<i>cis</i>	1	TL TL	0.0415	30449.89 (31408.31)	30805.41 (31763.84)		30535	30450.46	30805.98	30547
<i>cis</i>	2	Udd hatUd–	1.0808	30313.46 (31279.87)	30583.43 (31549.84)			30333.85	30603.81	
<i>cis</i>	2	Udu hatUd–	0.6744	30429.84 (31440.41)	30702.80 (31713.37)			30458.96	30731.93	
<i>cis</i>	2	Uud Uud	0.0853	30547.65 (31630.40)	30927.84 (32010.59)			30577.47	30957.66	
<i>cis</i>	2	orthoUdd orthoUdd	0.1358	30209.41 (31257.38)	30702.96 (31750.93)	30376,30381		30234.52	30728.07	
<i>cis</i>	2	orthoUdu metaUdu	0.3494	30222.35 (31192.93)	30509.82 (31480.40)	30376,30381		30238.04	30525.51	
<i>cis</i>	2	orthoUud metaUud	0.4126	30185.41 (31169.71)	30478.09 (31462.39)			30206.69	30499.38	
<i>cis</i>	2	orthoUuu metaUud	0.8608	30101.85 (30977.36)	30397.80 (31273.31)			30098.34	30394.29	
<i>cis</i>	2	ortho'Udu hatUd–	0.1282	30235.76 (31139.67)	30550.92 (31454.82)			30227.27	30542.42	
<i>trans</i>	0		0.0346	30466.49 (31431.34)	30857.26 (31822.11)		30586	30459.22	30849.99	
<i>trans</i>	1	TL TL	0.0582	30041.38 (31015.82)	30433.98 (31408.43)		30256	30048.01	30440.61	30273
<i>trans</i>	2	Udd orthoUdd	0.8832	29528.72 (30398.06)	29775.33 (30644.67)			29548.51	29795.12	
<i>trans</i>	2	Udu orthoUdd	0.6413	29618.78 (30541.85)	30040.37 (30963.44)			29650.28	30071.87	
<i>trans</i>	2	Uud Uud	0.0820	30223.07 (31309.36)	30592.42 (31678.71)			30254.98	30624.33	
<i>trans</i>	2	orthoUdd orthoUdd	0.3739	29597.58 (30428.40)	30074.54 (30905.36)			29596.81	30073.77	
<i>trans</i>	2	orthoUud orthoUud	0.4723	29506.93 (30281.81)	29820.92 (30595.80)			29495.14	29809.14	
<i>trans</i>	2	ortho'Udu orthoUdd	0.7216	29492.66 (30331.60)	29974.61 (30813.56)			29490.40	29972.35	
<i>trans</i>	2	ortho'Uuu orthoUuu	0.7491	29453.39 (30235.64)	29768.11 (30550.36)			29436.05	29750.77	

Table 3.3: rms geometry differences d^{RMS} (see text) and 0–0 excitation energies (harmonic ZPE correction) in cm^{-1} . Adiabatic excitation energies are given in parentheses. The aug-cc-pVXZ AO basis, together with the corresponding fitting sets, were used. All energies are counterpoise corrected. Experimental values according to Ref. 105 and Fig. 3.1 are also given.

trans(*ortho*Udd) cluster geometry in the S₁ state, i.e., the global minimum. The structural discrepancies between the energetically relevant cyclic (Udu) conformers in the S₀ state and the related structures on the S₁ state surface therefore are rather large (d^{rms} values of 0.67 and 0.64 Å, cf. Table 3.3). This is exactly the situation encountered for the phenol(H₂O)₂ case [102] and confirms conjecture (i) and (ii) of our hypothesis. Accordingly, the two weak, broad, and congested bands in the absorption spectrum are assigned to the cyclic *cis*- and *trans*(Udu) conformers, respectively.

For the *cis*(*ortho*Udd) and *cis*(*ortho*Udu) conformers, on the other hand, which are energetically competitive to *cis*(Udu) in the S₀ state, closely related geometries do exist as minima on the S₁ state surface, i.e., the *cis*(*ortho*Udd) and *cis*(*meta*Udu) minima, respectively (cf. Fig. 3.4). The latter constitutes the global minimum. The structural discrepancy between the related S₀ and S₁ geometries is rather small, in particular, for *cis*(*ortho*Udd) with $d^{\text{rms}} = 0.14$ Å (cf. Table 3.3). Further energetically low-lying *cis* conformers are the *cis*(*meta*Udd) and the *cis*(*meta*Udu) geometries. The barriers along the pathway leading from *cis*(*ortho*Udd) via *cis*(*meta*Udd) to *cis*(*meta*Udu) are negligibly small (cf. Table 3.2), i.e., virtually nonexistent. Apparently, the π system provides a rather isotropic electron density for hydrogen bonding. Judging from the X=T single-point energies it could as well be that the three minima just collapse to the single *cis*(*meta*Udu) geometry if a more extended basis set is employed. In any case, the PES along these coordinates is highly anharmonic and the related harmonic frequencies are entirely untrustworthy.

The related S₁ structure to the *trans*(*ortho*Udd) S₀ geometry, which, according to the ground state calculation, is significantly less stable than the cyclic counterpart, is the S₁ *trans*(*ortho*Udd) minimum, virtually isoenergetic to the *trans*(*ortho*Udu) geometry for the X=D basis. One of these constitutes the global minimum on the S₁ PES for the *trans* isomer.

Based on the results presented in this and the previous section we assign the two long progressions of sharp bands emerging at 30375 cm⁻¹ in the R2PI spectrum to the *cis*(*ortho*Udd) and the *cis*(*ortho*Udu) S₀ minima (or a superposition thereof), i.e., not to the *trans* isomer as in previous assignments [112]. Indeed, there is further data ruling out an assignment to the *trans* isomer (*vide infra*). In contrast to the case of phenol(H₂O)₂, we noticed no indications of a nearby conical intersection during the various optimizations on the S₁ PES.

3.3.3 Excitation energies and transition moments

In Table 3.3 the counterpoise corrected adiabatic and (harmonic) 0–0 excitation energies are collected for the excitations originating from the individual S₀ to the

m -2-NpOH(H ₂ O) _{n}				$d(\text{C-O})$	$d(\text{O-H})$	$d(\text{H}\cdots\text{OH})^a$	$d(\text{H}\cdots\text{OH})^b$	$\beta(\text{H-O-C-C})^c$	$\gamma(\text{H})^d$	$d(\text{O-H})^e$	$\alpha(\text{H-O-H})^f$
<i>cis</i>	0		S ₀	1.383	0.971			0.000	0.000		
<i>cis</i>	0		S ₁	1.365	0.975			0.000	0.000		
<i>cis</i>	1	TL	S ₀	1.376	0.981	1.849		0.000	0.000		
<i>cis</i>	1	TL	S ₁	1.355	0.989	1.779		0.000	0.000		
<i>cis</i>	2	Udu	S ₀	1.382	0.988	1.819	1.876	-0.348	-0.336		
<i>cis</i>	2	hatUd-	S ₁	1.351	0.997	1.784	1.855	22.321	2.171		
<i>cis</i>	2	orthoUdd	S ₀	1.370	0.988	1.805	1.854	15.172	-0.812	0.977	104.075
<i>cis</i>	2	orthoUdd	S ₁	1.349	1.001	1.704	1.827	14.214	-1.401	0.977	104.213
<i>cis</i>	2	orthoUdu	S ₀	1.369	0.988	1.809	1.852	18.323	-0.355	0.977	104.025
<i>cis</i>	2	metaUdu	S ₁	1.347	1.002	1.713	1.830	18.464	0.751	0.977	104.354
<i>trans</i>	0		S ₀	1.384	0.971			0.000	0.001		
<i>trans</i>	0		S ₁	1.364	0.975			0.000	0.000		
<i>trans</i>	1	TL	S ₀	1.377	0.980	1.850		0.002	0.000		
<i>trans</i>	1	TL	S ₁	1.354	0.990	1.768		0.000	0.000		
<i>trans</i>	2	Udu	S ₀	1.384	0.987	1.821	1.882	2.962	-0.112		
<i>trans</i>	2	orthoUdd	S ₀	1.372	0.987	1.811	1.857	25.394	0.058	0.976	103.482
<i>trans</i>	2	orthoUdd	S ₁	1.345	1.007	1.661	1.798	10.019	-12.496	0.987	104.580

a) H bond length between 2-NpOH and 1st H₂O

b) H bond length between 1st and 2nd H₂O

c) Out-of-plane torsion of the hydroxy group of 2-NpOH

d) Out-of-plane angle of the ortho hydrogen atom

e) O-H bond length of the bond of the 2nd H₂O pointing to 2Np-OH aromatic system

f) Bend angle of the 2nd H₂O molecule

Table 3.4: Some selected structural parameters of energetically low-lying conformers in the S₀ and S₁ states. Bond lengths are given in Å and angles in degrees.

3 2-Naphthol-water₂ clusters

related S_1 minima. The aug-cc-pVTZ 0–0 excitation energies of the *cis* and *trans* monomers are overestimated by 0.06 and 0.03 eV, respectively, which is well within the expected error bars of the CC2 model. For the smaller aug-cc-pVDZ basis set the agreement with experiment is fortuitously even better. The spectral shifts of the origins of the binary complexes relative to those of the monomers are somewhat overestimated, i.e., -503 cm^{-1} (X=D) or -547 cm^{-1} (X=T) versus -368 cm^{-1} (exp.) for the *cis* and -425 cm^{-1} (X=D) or -423 cm^{-1} (X=T) versus -330 cm^{-1} (exp.) for the *trans* isomer. Since the geometries represent true stationary points on the aug-cc-pVDZ surfaces only we restrict the following discussion about spectral shifts to that basis.

For the $n = 2$ cluster the origins of the cyclic (Udu) conformers are anticipated to appear on the *red* sides of the corresponding $n = 1$ origins, shifted by -20 cm^{-1} and by -423 cm^{-1} for *cis*(Udu) and *trans*(Udu), respectively. The large difference in these shifts between *cis* and *trans* is due to the fact that the related S_1 geometry to *cis*(Udu), *cis*(*hat*Ud–), is a metastable local minimum on the X=D S_1 state surface, 273 cm^{-1} above the global minimum. In the R2PI spectrum, on the other hand, the diffuse congested bands ascribed to the cyclic conformers occur on the *blue* sides of the corresponding $n = 1$ origins. Therefore it is plausible that the two diffuse bands do not constitute the origins but are related to some intramolecular mode of 2-NpOH. Due to the high density of states in the vicinity of such an intramolecular level diffuse congested bands are likely to appear. The true origin was probably not detected due to small Franck-Condon factors (cf. Sec. 3.3.2). A similar interpretation was recently proposed by us for the R2PI spectrum of the phenol(H₂O)₂ cluster [102].

The spectral origins of the *cis*(*ortho*Udd) and *cis*(*ortho*Udu) minima are computed to appear 240 and 228 cm^{-1} , respectively, to the red of the $n = 1$ *cis* origin, whereas for the *trans*(*ortho*Udd) conformer a redshift relative to $n = 1$ *trans* of 444 cm^{-1} is calculated. These shifts clearly rule out an assignment of the two long progressions in the R2PI spectrum, emerging 160 cm^{-1} to the red of the $n = 1$ *cis* origin, to any of the *trans*(*ortho*) geometries [which anyway are energetically less stable than the cyclic *trans*(Udu) structure].

Table 3.5 presents the $S_1 \leftarrow S_0$ transition strength vectors obtained by canonical and local CC2 response methods, respectively. For the latter, BSSE effects are expected to be small. The discrepancies between canonical and local transition strength vectors turn out to be quite small. Strikingly, for the *cis*(*ortho*) structures the transition strength vectors exhibit a sizable component perpendicular to the naphthyl ring plane, while for the corresponding *trans* conformers the transition strength vectors remain essentially parallel to this plane. Considering the planar symmetry of the solute molecule as still only slightly perturbed by the wa-

m -2-NpOH(H ₂ O) _{n}			DF-CC2, X=D				DF-LCC2, X=D				DF-LCC2, X=T			
m	n	Conformer	$S_{\parallel}^{\text{short}}$	$S_{\parallel}^{\text{long}}$	S_{\perp}	f	$S_{\parallel}^{\text{short}}$	$S_{\parallel}^{\text{long}}$	S_{\perp}	f	$S_{\parallel}^{\text{short}}$	$S_{\parallel}^{\text{long}}$	S_{\perp}	f
<i>cis</i>	0		-0.2426	-0.0130	0.0000	0.0294	-0.2405	-0.0117	0.0000	0.0291	-0.2271	-0.0078	0.0000	0.0270
<i>cis</i>	1	TL	-0.3008	0.1742	0.0000	0.0348	-0.2988	0.1736	0.0000	0.0346	-0.2814	0.1642	0.0000	0.0325
<i>cis</i>	2	Udd	-0.2385	0.1335	-0.0155	0.0276	-0.2380	0.1332	-0.0155	0.0276				
<i>cis</i>	2	Udu	-0.2322	0.1417	-0.0411	0.0281	-0.2295	0.1403	-0.0408	0.0278	-0.2200	0.1348	-0.0391	0.0265
<i>cis</i>	2	Uud	-0.2563	0.1174	-0.0130	0.0289	-0.2547	0.1172	-0.0129	0.0288				
<i>cis</i>	2	orthoUdd	-0.2441	0.1753	-0.1275	0.0349	-0.2413	0.1739	-0.1265	0.0345	-0.2316	0.1675	-0.1215	0.0330
<i>cis</i>	2	orthoUdu	-0.2352	0.1666	-0.1389	0.0349	-0.2330	0.1658	-0.1381	0.0347	-0.2247	0.1609	-0.1334	0.0332
<i>cis</i>	2	orthoUud	-0.2408	0.1751	-0.1469	0.0363	-0.2381	0.1740	-0.1459	0.0360				
<i>cis</i>	2	orthoUuu	-0.2358	0.1662	-0.1512	0.0362	-0.2338	0.1659	-0.1505	0.0360				
<i>cis</i>	2	ortho'Udu	-0.1675	0.1102	-0.1445	0.0292	-0.1672	0.1101	-0.1447	0.0292				
<i>trans</i>	0		-0.3048	0.0269	0.0000	0.0330	-0.3031	0.0277	0.0000	0.0328	-0.2877	0.0288	0.0000	0.0308
<i>trans</i>	1	TL	-0.2976	-0.0794	0.0000	0.0380	-0.2956	-0.0759	0.0000	0.0376	-0.2853	-0.0688	0.0000	0.0357
<i>trans</i>	2	Udd	-0.2455	-0.0229	-0.0595	0.0310	-0.2444	-0.0215	-0.0590	0.0308				
<i>trans</i>	2	Udu	-0.2524	-0.0328	-0.0475	0.0315	-0.2523	-0.0320	-0.0474	0.0314	-0.2424	-0.0274	-0.0450	0.0297
<i>trans</i>	2	Uud	-0.2706	0.0210	-0.0722	0.0324	-0.2705	0.0213	-0.0720	0.0324				
<i>trans</i>	2	orthoUdd	-0.2358	-0.0950	0.0061	0.0382	-0.2358	-0.0934	0.0061	0.0380	-0.2313	-0.0859	0.0087	0.0364
<i>trans</i>	2	orthoUud	-0.2307	-0.0759	0.0012	0.0373	-0.2313	-0.0745	0.0012	0.0372				
<i>trans</i>	2	ortho'Udu	-0.1704	-0.0729	0.0604	0.0283	-0.1719	-0.0727	0.0611	0.0285				
<i>trans</i>	2	ortho'Uuu	-0.1980	-0.0471	0.0416	0.0278	-0.2015	-0.0462	0.0426	0.0280				

Table 3.5: Transition strength vectors and oscillator strengths calculated with the aug-cc-pVXZ AO basis and corresponding fitting sets using both canonical and local CC2 response methods. The latter avoid BSSE effects to large extent by construction. $S_{\parallel}^{\text{short}}$, $S_{\parallel}^{\text{long}}$, and S_{\perp} denote the components of the transition strength vectors parallel to the short and long axis of, and perpendicular to the naphthyl frame, respectively.

ter solvent molecules of the cluster, then the $S_1 \leftarrow S_0$ transition can be regarded as electronically allowed for the *cis(ortho)*, and electronically forbidden for the *trans(ortho)* conformers, for light polarized in the direction perpendicular to the ring plane. This might be of use for an experimental distinction between *cis* and *trans* related band shapes.

3.3.4 Vibrational modes

Both the S_0 and S_1 PESs of the $n = 2$ cluster are very anharmonic along the various intermolecular degrees of freedom. This is reflected by the multiple low-energy minima separated by low barriers. To scrutinize the vibrational problem of the intermolecular modes of this cluster hence is an intricate task and beyond the scope of the present paper. Nevertheless, in order to get a first handle on possible modes in the S_1 state which might be related to the observed two long progressions in the R2PI spectrum, the projections of the geometric displacement vectors between the *cis(orthoUdu)*, *cis(orthoUdd)* S_0 minima, and the related S_1 minima onto the normal modes of the latter were computed. By far the largest component occurs along the translational mode of lowest harmonic frequency, involving in phase movement of the two water molecules. The second water molecule is skimming essentially parallel to the surface of the π system, in the direction of the C(1)–C(2) bond (enumeration according to the fixed numbering system for the naphthyl ring), trailing the first water molecule behind (cf. Fig. 3.6). The harmonic vibrational frequencies for these modes amount to 38 and 15 cm^{-1} for *cis(metaUdu)* and *cis(orthoUdd)*, respectively (the harmonic frequencies are just given here as a very rough estimate). Based on this analysis we tentatively assign the two long progressions featured by the R2PI spectrum to such low-frequency skimming modes.

3.4 Conclusions

In this work the S_0 and $S_1(\pi^* \leftarrow \pi)$ state surfaces of the 2-NpOH (H_2O)_{*n*}, $n \in \{1, 2\}$ clusters were studied at the level of coupled cluster (CC2) response theory. Low-energy minima and related first-order saddle points were located and characterized with the aim to interpret, on solid theoretical grounds, the rather peculiar R2PI spectrum of the $n = 2$ cluster, measured by one of us 15 years ago. For the $n = 1$ cluster, as expected, the usual TL hydrogen-bonding arrangement was found as the only relevant structure on both surfaces. The interpretation of the R2PI spectrum hence is straightforward and simple (cf. Ref. 109). For $n = 2$ the

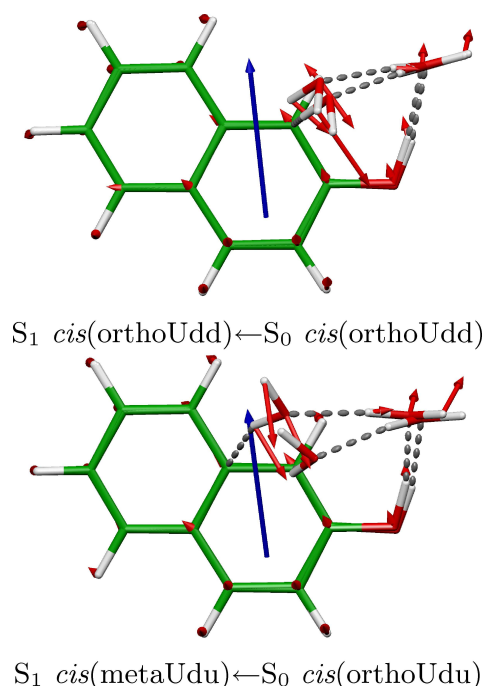


Figure 3.6: Normal coordinate of the lowest frequency mode at the S₁ minima *cis*(*orthoUdd*) and *cis*(*metaUdu*) (light color). The S₁ geometries are superimposed by those of the related S₀ conformers. The transition strength vector (calculated for the S₀ geometries) is also displayed (dark color).

situation is much more complicated. Already in the S₀ state two different types of hydrogen-bonding networks can coexist, a cyclic one [similar to (H₂O)₃ and phenol(H₂O)₂], where the hydroxy group of the 2-NpOH acts as H acceptor for the second water molecule, and an alternative one where the π system of 2-NpOH is taking over this role. While for the *trans* isomer the cyclic (Udu) conformer still is energetically preferred, these two forms become equivalent for the *cis* isomer. On the S₁ surface, on the other hand, the cyclic forms are no longer competitive, as it is the case for phenol(H₂O)₂ [102]. The cyclic S₀ conformers of *trans* and *cis* therefore have broad and congested band shapes in the R2PI spectrum [as that of phenol(H₂O)₂]. The alternative S₀ *cis* conformers with the π system acting as H acceptor for the second water molecule, due to much more modest structural changes between S₀ and related S₁ minima, are expected to have much more structured band shapes. This is exactly what is observed experimentally. Based on these calculations we assign the two long low-frequency progression to *cis* conformers of this type, in disagreement to previous assignments where these bands were related to the *trans* isomer. Furthermore, based on a simple vibrational analysis we ten-

3 2-Naphthol-water₂ clusters

tatively assign the related modes to a "skimming" movement of the second water molecule essentially parallel to the ring plane along the direction of the C(1)–C(2) bond. A more comprehensive study of the low-energy intermolecular vibrations in ground and excited states will be the subject of further work.

4 Aniline clusters in the electronic ground state

4.1 Introduction

Intermolecular forces are ubiquitous in nature, being of major importance for many different phenomena in physics, chemistry, and biology. Complex processes such as the self-assembly of molecular superstructures in nanoscience, the reproduction of biological information stored in DNA, or the catalytic activity of proteins are all based on and tuned by intermolecular forces. Molecular clusters, i.e., isolated aggregates of two to many molecules of interest are ideal systems to study such interactions in detail. Experimentally, such clusters can be synthesized in molecular beam expansions and analyzed subsequently. If (at least) one of the individual molecules of the cluster is an (aromatic) chromophore then the toolbox of spectroscopic methods to characterize such clusters is particularly rich: resonant two-photon ionization (R2PI) spectroscopy can be employed to obtain mass selective absorption spectra, the combination of that method with, e.g., infrared depletion spectroscopy provides information on the electronic ground state, hole burning experiments can be used to check if one or more distinct isomers coexist, etc [19].

Since molecular clusters are isolated systems of a well defined size (controlled in the experiment by the mass selective detection technique) a direct comparison of experiment and theory is possible. For a proper treatment of weak intermolecular forces however a level of electronic structure theory is required which includes dynamic electron correlation and long range van der Waals forces. Furthermore since (potentially many) different cluster minimum energy geometries and other stationary points on the potential energy surfaces (PES) have to be located the availability of analytical energy gradients (with respect to nuclear displacements) is indispensable. Efficient electronic structure methods fulfilling these requirements are Møller-Plesset perturbation theory of the second order (MP2) for electronic ground states. In our recent studies on phenol-water_{*n*} ($n \in \{1, 2, 3\}$) and 2-naphthol-water_{*n*} ($n \in \{1, 2\}$) CC2 response theory was successfully applied in order to understand the anomalous R2PI absorption spectra of the $n = 2$ clusters [102, 118].

4 Aniline clusters in the electronic ground state

In this contribution we present results from an *ab initio* study on the dimer and the trimer of aniline. Aniline (An) is the simplest member of the class of aromatic amines and an important precursor for the synthesis of more complex chemicals. Few experimental papers about the aniline dimer are in the literature. R2PI spectra on An₂ (both deuterated and nondeuterated) were measured by Yeh *et al.* [119]. The spectral shift of the S₁ ← S₀ origin of the dimer relative to that of the monomer is unusually large (a redshift of 678 cm⁻¹ was measured for the nondeuterated species), indicating a large increase in the binding energy of the complex on going from the electronic ground to the S₁ state. Furthermore, there is evidence for an An₂ excimer in the spectra. Hole burning experiments revealed that all the multiple bands in the vicinity of the origin belong to the same An₂ isomer [120]. IRDS measurements of the N–H stretch frequencies finally show that both of the amino groups of An₂ are equivalent [121], indicating that the minimum energy structure in the S₀ state is of sandwich type in a head-to-tail arrangement of the two amino groups (cf. Fig. 4.1), which is in agreement with the MP2 calculations of Yamamoto *et al.* [120]. This "symmetric" sandwich head-to-tail geometry of An₂ (labeled as An₂R33-1, according to our nomenclature, *vide infra*), where NH₂–π type H bonding appears to contribute significantly to the interaction energy, is entirely different to the known asymmetric structure of the phenol dimer. The latter structure is governed by hydrogen bonding involving the two hydroxy groups with one of the phenol monomers acting as the H donor and the other as the H acceptor.

In this work we determined the relevant low-energy minima on the ground state PES of An₂ and An₃ employing local MP2 (LMP2), and spin-component-scaled LMP2 (SCS-LMP2) [48]. Already for An₃, a large number of possible low energy conformers has to be screened. It is a well known problem that the number of possible minima on the PES increases exponentially with the cluster size [122, 123]. This problem is handled by a global optimization strategy [124], which has been successfully applied before in the context of small water clusters [125]. In order to systematically classify the various low energy cluster conformers, a general topological nomenclature is introduced, which is applicable also to other homoclusters (see Sec. 4.3). In order to gain more information about the trait of the intermolecular interactions DFT-SAPT (symmetry adapted intermolecular perturbation theory, based on DFT monomer properties) calculations were carried out for three typical dimer minimum energy geometries of the electronic ground state. Finally, harmonic vibrational frequency shifts of the N–H stretch modes were computed for the lowest S₀ minima of An₂ and An₃. In an upcoming publication we will present the results of a study on the lowest excited states of An₂ and An₃.

4.2 Computational methods

The search for energetically low lying minimum energy structures was performed by applying the following scheme: a set of global optimizations is carried out on an energy hypersurface described by a model potential. Each individual global optimization (with subsequent quenching to the next local minimum) yields a new candidate structure, which is added to a pool of possible low energy geometries. Its interaction energy is calculated with the chosen *ab initio* method. Before the next global optimization is carried out, the parameters of the model potential (or a subset thereof) are refitted to the *ab initio* interaction energies of the geometries in the pool, i.e., to the energies of the present and all previous geometries. Once the global optimizations no longer provide any new structural motifs, the collection of geometries with the lowest *ab initio* energies is considered as fully minimized on the *ab initio* energy hypersurface.

The global optimizations were performed with simulated annealing [126, 127] and threshold acceptance [128] methods (here using the OBA2_N algorithm [129]) with adaptive step length [130]. For the model potential, the electrostatic and induction energies were calculated with polarizable monopoles [131], for dispersion and exchange repulsion a Buckingham potential $E_{\text{Buck}} = f \exp(-gr) - \frac{d}{r^6}$ was used. The usage of higher-order multipoles and polarizabilities in the potential turned out to be computationally too expensive to be used within the global optimizations.

All *ab initio* calculations were carried out with the MOLPRO program package (Ref. 96). The energies needed in the context of the global optimization procedure outlined above, and the analytic energy gradients (with respect to nuclear displacements), required for the subsequent local optimizations on the *ab initio* energy hypersurface, were mainly calculated at the level of spin-component-scaled (SCS) [48], density fitted local Møller-Plesset perturbation theory of second-order (SCS DF-LMP2) [101, 132]. For comparison, local optimizations were also carried out at the (unscaled) DF-LMP2 level. At the optimized cluster geometries additional single point energy calculations at the level of density fitted local coupled cluster theory with single, double, and perturbative triple substitutions, DF-LCCSD(T) [59, 60, 133, 134], were performed, in order to compare DF-LMP2, SCS DF-LMP2, and DF-LCCSD(T). The local T0 approximation as described in Ref. 60 was used throughout for the triples correction in the DF-LCCSD(T) calculations, the postfix "0" is omitted in the following for brevity. Harmonic vibrational frequencies were calculated at the level of SCS DF-LMP2 by numerical differentiation of the corresponding analytic gradients [101].

Furthermore, for the three lowest ground state minima of the aniline dimer, as well as for the parallel-displaced geometry of the benzene dimer (for the pur-

pose of reference), density fitted DFT-SAPT (cf. Ref. 10 and references therein) calculations were carried out, which provide information on the individual physical components of the interaction energy. For these calculations the LPBE0AC exchange-correlation (xc) potential in combination with the ALDA kernel, as justified before in Ref. 10, was used. This potential involves an asymptotic correction based on the gradient-regulated connection of inner to outer parts of the xc potential (as described in detail in Ref. 135), adding, as a constant shift the difference between the negative ionization potential and the highest occupied molecular orbital (HOMO) energy of the underlying xc functional, to the asymptotic part of the potential. HOMO energies, as well as ionization potentials, were calculated for the individual monomers with the PBE0 functional in the respective AO basis sets; the resulting shift parameters amount to 0.0678 and 0.0719 hartree, for benzene and aniline, respectively (no relevant basis set dependence of these parameters was observed).

In the following, when referencing the individual methods used, the prefix "DF" is omitted altogether and it is implicitly understood that the density fitting approximation for the electron repulsion integrals is invoked.

In all calculations the augmented correlation consistent aug-cc-pVXZ AO basis sets [34] with $X \in \{D, T\}$, in conjunction with the corresponding fitting sets optimized for MP2 (Ref. 99) were used. For the methods based on a density fitted Hartree-Fock reference, i.e., the LMP2, SCS-LMP2, and LCCSD(T) calculations, the JK-fitting sets [136] related to the cc-pV(X+1)Z AO basis were used for the Hartree-Fock part of energies and gradients. The DFT-SAPT calculations were performed in the $X=T$ and $X=Q$ AO basis, employing related fitting sets, i.e., cc-pVXZ/JKFIT plus one additional even tempered diffuse function per primitive set (cf. MOLPRO basis set library) for Hartree-Fock and the generalized Coulomb and exchange matrices occurring in the first order and second-order induction terms of DFT-SAPT [10], and aug-cc-pVXZ/MP2FIT for the second-order dispersion terms.

The localized occupied MOs needed for the local methods were obtained with Pipek-Mezey localization [62], with the most diffuse functions being discarded in the localization procedure (option CPLDEL=1). Excitation domains were generated at large intermonomer distance (100 bohr) by using a completeness criterion of 0.980, 0.985, and 0.990 for $X=D$, $X=T$, and $X=Q$ AO basis sets, respectively. Additional calculations were performed with extended pair domains, which (i) include either all nearest atom centers within a distance of 3 bohr from the centers of the Boughton-Pulay core domains [137], or (ii) all centers on the aniline monomers. Geometry optimizations were carried out in force-constant weighted internal coordinates [138]. Finally, complete basis set (CBS) limits of the ground state inter-

action energies were estimated by extrapolating the correlation part according to the two-point formula [35] based on $X=T$ and $X = Q$ single point calculations at the optimized geometries.

In the following the term *binding energy* implies the inclusion of relaxational effects to the *interaction energy*, which in turn is understood to be calculated between rigid monomers.

4.3 Nomenclature

i	Edge type β_i	Directional?
0	$\pi \cdots \pi$ interaction	no
1	NH \dashrightarrow N hydrogen bond	yes
2	NH \dashrightarrow π hydrogen bond	yes
3	NH ₂ \dashrightarrow π hydrogen bond	yes

Table 4.1: Types of edges β_i (intermonomer bonding) in the nomenclature of the aniline clusters.

In order to entitle the cluster structures a nomenclature is introduced. It is required to give information about the cluster size, constitution, and conformation. Therefore each structure name consists of three parts. First An_M denotes the constitution of the monomer where M is the cluster size. Then information about the topology is given. After that different conformations of the same topology can be enumerated. One can clarify the topology as a graph. The vertices represent the monomers and the edges β_i bonds between them. Each edge β may be directional and is characterized by a number i , which defines the type of the bond, see Table 4.1. A graph is entitled by a number of topological elements Γ , which are defined in Table 4.2. These set up a pathway through the graph, passing every vertex at least once. Every symbol Γ is followed by the type of its edge or edges. A number of rules define the syntax:

- An edge can be substituted by a subgraph. This nesting can be given by putting the subgraph in round brackets at the position of the substituted edge. An edge which is substituted by only a linear series of edges can be written for convenience without round brackets and symbol L.
- If more than one edge belongs to a symbol, e.g., an branching with symbol B, the edges are separated by a dot and ordered by their length (if nested).

4 Aniline clusters in the electronic ground state

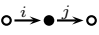
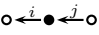
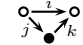
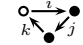
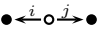
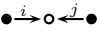

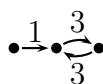
Γ	Topological symbol	Example	Comment
L	linear	$Li.j$ 	
I	inverse	$Ii.j$ 	Starting and terminal vertices change place.
C	closed	$Ci.jk$ 	
R	ring	$Ri.jk$ 	Starting and terminal vertices are the same.
B	branching point	$Bi.j$ 	No terminal vertex.
J	junction	$Ji.j$ 	No terminal vertex. Equivalent to $B(Ii).(Ij)$.
X	disconnected	X 	Starting and terminal vertices are the same.

Table 4.2: Topological symbols Γ of the nomenclature. The initial and terminal vertices are draw empty.

- To insert a side chain edge leaving the path after the last edge, it is written in square brackets. The terminal edge on the side chain is not continued.
- Every symbol has a defined initial vertex. Every symbol except B and J also has a defined terminal vertex. Therefore the symbols B and J can only be at the end of the path or a side chain. The symbol C has identical initial and terminal vertices.
- The symbol I inverts the direction of the following edge.
- It is possible to lead the path multiple times through a common edge. In this case, this common edge has to be designated by a defined number of primes.
- The path can go through nondirectional edges in both directions.
- Unconnected parts of a graph are separated by a diagonal slash. Single vertices are denoted by the symbol X.
- Since there are many possibilities to denote the topology, the simplest is to be preferred.

As an example the naming of the structure $An_3L1R33-1$ is reviewed. It consists of an aniline monomer which binds via an H bond between NH and N (type 1) to a stack of two monomers, which mutually bind their NH_2 group to the opposed π

system (in both cases type 3).



To describe this graph, we start from the left vertex with L1 to the cycle R33, which gives L1R33. Alternatively one could start at the two other vertices, but this will produce more complicated solutions. For other systems, one can redefine the edge types to also use this nomenclature.

4.4 Results and Discussion

4.4.1 Structures and interaction energies

The aniline dimer, An_2

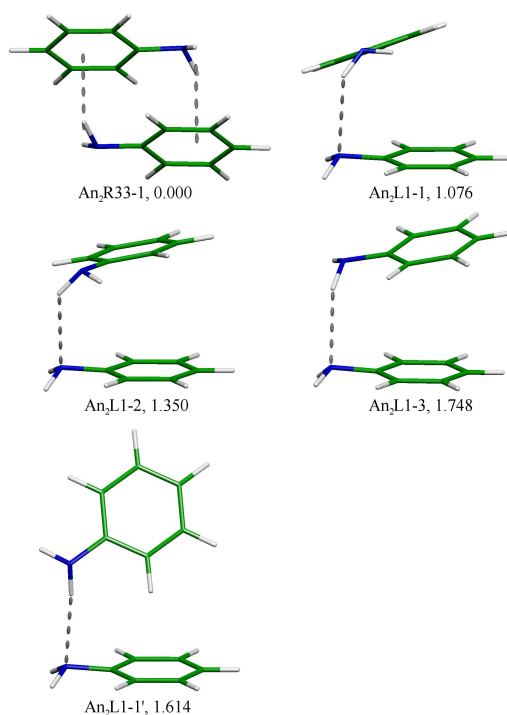


Figure 4.1: Aniline dimer geometries, together with binding energies ΔE^0 in kcal/mol relative to the most stable structure, calculated with SCS-LMP2 and by 3 bohr extended domains, extrapolated to the CBS limit (based on X=T and X=Q).

4 Aniline clusters in the electronic ground state

The five lowest energy geometries of the aniline dimer, located by the optimization scheme outlined in the previous section, are displayed in Fig. 4.1. The individual conformers are labeled according to a topological nomenclature, which is explained in detail in Section 4.3. In Table 4.3 the binding energies are given for different basis sets and extended/full monomer domains, along with the extrapolated CBS limits.

The most stable structure denoted as An₂R33-1 features a head-to-tail arrangement of the monomers. This is in agreement with the mass selective infrared depletion spectra measured by Sugawara *et al.* in molecular beam expansions [121]. The binding energy of An₂R33-1, calculated at the level of SCS-MP2 and extrapolated to the basis set limit, amounts to 7.6 kcal/mol (cf. Table 4.3). In contrast to earlier work by Yamamoto *et al.* [120], who performed MP2 geometry optimizations on An₂ in the rather smallish cc-pVDZ basis, both aniline monomers are slightly tilted with respect to each other (around their phenyl–N axes, each in the opposite direction), thus breaking the C_{2h} symmetry.

The C_{2h} conformer is only slightly higher in energy though, i.e., by 0.038 kcal/mol, at the level of SCS-LMP2/X=D with full monomer domains. A harmonic vibrational frequency analysis at that level yields a single imaginary frequency of 32.23i cm⁻¹ related to the coordinate linking C_{2h} with the two C₁ minima, which indicates that the C_{2h} geometry corresponds to a transition state. Due to the tiny barrier the level splitting caused by such a double minimum potential is too small to be resolved in the spectra, as already conjectured by Sugawara *et al.* [121].

The four other local minima of Fig. 4.1 ranging between 1.1 and 1.7 kcal/mol above An₂R33-1 are the displaced head-to-head (sandwich) conformers (An₂L1-{1,2,3}) and the T-shaped head-to-head geometry (An₂L1-1'). They all feature a single distinct NH–N hydrogen bond, rather than the two NH₂– π H bonding interactions of An₂R33-1. In Ref. 120 Yamamoto *et al.* also reported a head-to-head conformer with NH–N H bonding topology about 1.2 kcal/mol above their head-to-tail C_{2h} minimum. Anyway, since typical molecular beam temperatures are very low (vibrational temperature around 50 K) it is unlikely that any other geometry but An₂R33-1 plays a significant role in the measured spectra.

In Table 4.4 the individual components of the DFT-SAPT interaction energies of the three lowest An₂ dimer geometries An₂R33-1, An₂L1-1, and An₂L1-2 (all optimized for the SCS-LMP2 energy functional and the X=T basis) are compared to those of the benzene dimer Bz₂ (most stable parallel displaced geometry of Ref. 10). Evidently, neither An₂R33-1, nor Bz₂ are bound at the uncorrelated Hartree-Fock level, although, for the latter, the Hartree-Fock interaction energy is much more repulsive. The first order electrostatic plus exchange repulsion components, $E_{\text{pol}}^{(1)} + E_{\text{xc}}^{(1)}$, are repulsive (2.8 kcal/mol for An₂R33-1 versus 5.5 kcal/mol for

Geometry	X=D, Y=D			X=T, Y=T		X=Q, Y=T		X $\rightarrow \infty$, Y=T	
	normal	ext.	full	normal	ext.	normal	ext.	normal	ext.
An ₂ R33-1	-5.466	-6.078	-5.923	-6.134	-6.646	-6.459	-6.739	-7.467	-7.578
An ₂ L1-1	-4.866	-5.397	-5.335	-5.331	-5.708	-5.481	-5.710	-6.380	-6.502
An ₂ L1-2	-4.502	-5.091	-5.109	-4.954	-5.412	-5.128	-5.419	-6.060	-6.228
An ₂ L1-3	-4.130	-4.613	-4.629	-4.663	-5.040	-4.819	-5.056	-5.695	-5.830
An ₂ L1-1'	-4.383	-4.712	-4.459	-4.765	-5.143	-4.978	-5.171	-5.907	-5.964
An ₃ L11-1	-12.260	-13.327	-13.076	-12.993	-14.142	-13.474	-14.337	-14.992	-15.647
	-0.670	-0.718	-0.815	-0.744	-0.767	-0.728	-0.773	-0.717	-0.778
An ₃ R122-1	-11.517	-12.647	-12.536	-12.117	-13.171	-12.354	-13.259	-13.659	-14.455
	-0.354	-0.443	-0.511	-0.309	-0.330	-0.278	-0.320	-0.255	-0.313
An ₃ R122-2	-11.584	-12.630	-12.453	-12.438	-13.513	-12.922	-13.670	-14.434	-14.942
	-0.504	-0.585	-0.557	-0.495	-0.514	-0.492	-0.512	-0.491	-0.512
An ₃ L1R33-1	-10.683	-11.839	-11.756	-11.331	-12.355	-11.565	-12.410	-12.907	-13.621
	-0.032	-0.076	-0.117	-0.005	-0.019	0.024	-0.005	0.046	0.006

Table 4.3: Binding energies in kcal/mol, calculated with SCS-LMP2. X and Y refer to the basis sets during the single point calculations and the optimization, respectively. Ext. denotes by 3 bohr extended domains, full denotes extended domains over the whole particular monomer. In the second line of the trimers, the three-body interaction energy is given.

4 Aniline clusters in the electronic ground state

Geometry	Bz ₂		An ₂ R33-1		An ₂ L1-1	An ₂ L1-2
Basis set	$X = T$	$X = Q$	$X = T$	$X = Q$	$X = T$	$X = T$
$E_{\text{int}}(\text{HF})$	5.13	5.13	0.72	0.72	-0.37	1.43
$\delta(\text{HF})^a$	-0.62	-0.62	-0.72	-0.72	-0.69	-0.71
E_{rest}^b	4.72	4.72	1.32	1.32	0.53	2.07
$E_{\text{pol}}^{(1)}$	-2.05	-2.05	-5.64	-5.63	-5.62	-4.54
$E_{\text{xc}}^{(1)}$	7.58	7.57	8.42	8.41	7.54	8.03
$E_{\text{ind}}^{(2)} + E_{\text{xind}}^{(2)}$	-0.19	-0.19	-0.74	-0.73	-0.70	-0.70
$E_{\text{disp}}^{(2)} + E_{\text{xdisp}}^{(2)}$	-7.45	-7.58	-8.89	-9.04	-7.00	-8.20
E_{int}^c	-2.72	-2.86	-7.58	-7.71	-6.47	-6.12
a) $\delta(HF) = E_{\text{int}}(\text{HF}) - E_{\text{pol}}^{(1)}(HF) - E_{\text{xc}}^{(1)}(HF) - E_{\text{ind}}^{(2)}(HF) - E_{\text{xind}}^{(2)}(HF)$						
b) $E_{\text{rest}} = E_{\text{pol}}^{(1)} + E_{\text{xc}}^{(1)} + E_{\text{ind}}^{(2)} + E_{\text{xind}}^{(2)} + \delta(\text{HF})$						
c) $E_{\text{int}} = E_{\text{pol}}^{(1)} + E_{\text{xc}}^{(1)} + E_{\text{ind}}^{(2)} + E_{\text{xind}}^{(2)} + E_{\text{disp}}^{(2)} + E_{\text{xdisp}}^{(2)} + \delta(\text{HF})$						

Table 4.4: DFT-SAPT components of the interaction energies for the benzene dimer and the three lowest-energy geometries of the aniline dimer optimized using SCS-LMP2 and the X=T basis set. The LPBE0AC exchange correlation potential in combination with the ALDA kernel has been used for the DFT-SAPT calculations. All values are given in kcal/mol.

Bz₂; the smaller value for An₂ is primarily due to the more attractive electrostatic component). The corresponding second order induction plus exchange induction contributions, $E_{\text{ind}}^{(2)} + E_{\text{xind}}^{(2)}$, are slightly attractive (−0.7 kcal/mol for An₂ versus −0.2 kcal/mol for Bz₂). The total interaction energy is, in spite of the more attractive electrostatic and inductive components for An₂, dominated by van der Waals dispersion in both cases; the sums of the second order dispersion, $E_{\text{disp}}^{(2)}$, and its exchange counterpart, $E_{\text{xdisp}}^{(2)}$, are adding up to −9.0 kcal/mol for An₂R33-1 and −7.6 kcal/mol for Bz₂, respectively. For An₂R33-1, the overall DFT-SAPT interaction energy amounts to −7.7 kcal/mol, which compares well to the SCS-MP2 X=Q value of −7.2 kcal/mol (no geometry relaxation effects are included here, in contrast to Table 4.3), appreciating the fact that DFT-SAPT and SCS-MP2 are entirely complementary approaches to calculate intermolecular interaction energies. For Bz₂, on the other hand, the overall DFT-SAPT interaction energy amounts to only −2.9 kcal/mol. Thus, while for Bz₂ the total interaction energy is somewhat more than a third of the dispersive component; for An₂R33-1 it is of similar magnitude. We conclude that the cyclic NH₂− π H bonding situation is somewhere intermediate

between a (weak) H bond and an (almost) purely dispersive π - π interaction like that of the Bz₂ prototype.

The changes in the SAPT components on going from An₂R33-1 to An₂L1-1 and An₂L1-2 reflect the delicate balance between NH-N and NH- π H bonding, and π -stacking, at work in aniline clusters. For the An₂L1-1 geometry the dimer is already stable at the uncorrelated Hartree-Fock level, although the sum of the first order and second order induction components (evaluated for DFT monomers) is still repulsive. Comparison with An₂R33-1 reveals that the first order exchange repulsion is reduced by 1 kcal/mol, while electrostatics is hardly affected. However this comes at a price of losing almost 2 kcal/mol in van der Waals dispersion, rendering An₂L1-1 as less stable than An₂R33-1. An₂L1-2, on the other hand, with a more parallel arrangement of the two phenyl rings than An₂L1-1, again has a larger dispersive component, but loses in the electrostatic and the first order exchange component against the latter.

Table 4.5 compares SCS-LMP2, LMP2, and LCCSD versus LCCSD(T) interaction energies for the five energetically lowest An₂ structures. All calculations were carried out by using the X=D AO basis sets and standard domain sizes. The geometry optimizations were performed for both SCS-LMP2 and unscaled LMP2 for comparison. Evidently, SCS-LMP2, for the present case, indeed provides interaction energies much closer to LCCSD(T) than unscaled LMP2. Furthermore, larger (abs. value) LCCSD(T) interaction energies are obtained at SCS-LMP2 geometries than at unscaled LMP2 geometries. This justifies our decision to optimize the An₂ and An₃ geometries for the SCS-LMP2 energy functional. Comparison of LCCSD versus LCCSD(T) shows that the former consistently underestimates the interaction energies by (13%–24%), yet, in contrast to LMP2 the energetical order of the five An₂ structures is the same as that of LCCSD(T).

The aniline trimer, An₃

The four energetically lowest An₃ geometries are depicted in Fig. 4.2, along with the related SCS-LMP2 CBS limit binding energy differences relative to the most stable An₃L11-1 conformer. As for the dimer, the trimer structures are labeled according to the nomenclature defined in Sec. 4.3. Table 4.3 compiles the SCS-LMP2 binding energies of the four An₃ geometries computed in different AO basis sets and with extended/full monomer domains, along with the related extrapolated CBS limits (based on the X=T and X=Q correlation energies). Furthermore, the nonadditive three-body terms [12, 13] are given.

The An₃L11-1 conformer, with a binding energy of -15.6 kcal/mol (basis set limit estimate) clearly constitutes the most stable minimum found by our global

4 Aniline clusters in the electronic ground state

Geometry	LCCSD(T)	LCCSD	LMP2	SCS-LMP2
LMP2 dimer geometries				
An ₂ R33-1	-5.324	-4.152 (+22.0%)	-7.691 (-44.5%)	-5.401 (-1.4%)
An ₂ L1-1	-4.797	-3.765 (+21.5%)	-6.919 (-44.2%)	-4.867 (-1.5%)
An ₂ L1-2	-4.166	-2.809 (+32.6%)	-7.023 (-68.6%)	-4.463 (-7.1%)
An ₂ L1-3	-3.896	-2.658 (+31.8%)	-6.380 (-63.8%)	-4.092 (-5.0%)
An ₂ L1-1'	-4.560	-3.847 (+15.6%)	-5.833 (-27.9%)	-4.331 (+5.0%)
SCS-LMP2 dimer geometries				
An ₂ R33-1	-5.589	-4.573 (+18.2%)	-7.617 (-36.3%)	-5.646 (-1.0%)
An ₂ L1-1	-5.146	-4.294 (+16.6%)	-6.832 (-32.8%)	-5.142 (+0.1%)
An ₂ L1-2	-4.656	-3.546 (+23.8%)	-6.920 (-48.6%)	-4.838 (-3.9%)
An ₂ L1-3	-4.272	-3.232 (+24.3%)	-6.300 (-47.5%)	-4.391 (-2.8%)
An ₂ L1-1'	-4.702	-4.073 (+13.4%)	-5.785 (-23.0%)	-4.485 (+4.6%)
SCS-LMP2 trimer geometries				
An ₃ L11-1	-13.066	-11.344 (+13.2%)	-16.312 (-24.8%)	-12.681 (+2.9%)
	-0.547	-0.570 (+4.2%)	-0.675 (+23.4%)	-0.670 (+22.5%)
An ₃ R122-1	-12.135	-10.499 (+13.5%)	-15.676 (-29.2%)	-11.921 (+1.8%)
	-0.205	-0.245 (+19.5%)	-0.349 (+70.2%)	-0.354 (+72.7%)
An ₃ R122-2	-12.135	-10.612 (+12.6%)	-15.449 (-27.3%)	-11.890 (+2.0%)
	-0.364	-0.400 (+9.9%)	-0.506 (+39.0%)	-0.504 (+38.5%)
An ₃ L1R33-1	-11.107	-9.425 (+15.1%)	-15.009 (-35.1%)	-11.198 (-0.8%)
	-0.005	-0.022 (+340.0%)	-0.026 (+420.0%)	-0.032 (+540.0%)

Table 4.5: Counterpoise corrected interaction energies in kcal/mol, calculated within X=D basis sets and normal domains. In parentheses the deviations from the LCCSD(T) reference calculations are given. For the trimer structures the individual three-body interaction energies [and their deviations from the LCCSD(T) reference value] are given in the second line.

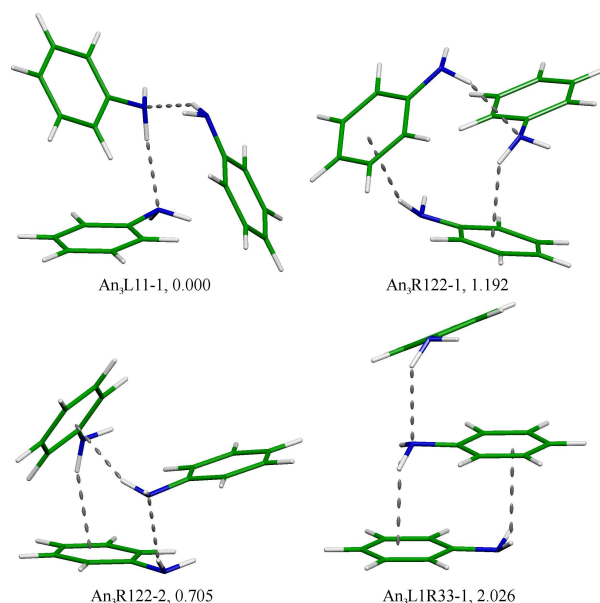


Figure 4.2: Aniline trimer geometries, together with binding energies ΔE^0 in kcal/mol relative to the most stable structure, calculated with SCS-LMP2 and by 3 bohr extended domains, extrapolated to the CBS limit (based on X=T and X=Q).

optimization scheme. It features two directional NH–N hydrogen bonds with one monomer acting as H donor, another as H acceptor, and the third simultaneously as H donor and H acceptor. It can be considered as an assembly of two T-shaped head-to-head geometries ($\text{An}_2\text{L1-1}'$), arranged such that they nearly form a ring. Yet the distance between the acceptor N atom and the phenyl ring of the donor is too long to form a third H bond of NH– π type (apparently, the ring strain is too large). $\text{An}_3\text{L11-1}$ also features the largest nonadditive three-body contribution, which amounts to about 5% of the binding energy. The next lowest geometries are the $\text{An}_3\text{R122-}\{1,2\}$ conformers, 0.7 and 1.2 kcal/mol above the most stable minimum. $\text{An}_3\text{R122-}\{1,2\}$ both feature a single NH–N and two NH– π type hydrogen bonds, so one of the two NH–N hydrogen bonds of $\text{An}_3\text{L11-1}$ is sacrificed to ease the ring strain and to form two NH– π H bonds instead. The two geometries $\text{An}_3\text{R122-1}$ and $\text{An}_3\text{R122-2}$ are quite similar; the root-mean-square deviation of the atomic positions amounts to only 0.2388 and 0.3037 Å, for the X=D and X=T structures, respectively. Already 2.0 kcal/mol above the most stable minimum is the $\text{An}_3\text{L1R33-1}$ conformer, which features a single NH–N hydrogen bond plus two NH_2 – π bonds as found in the dimer. It can be considered as a combination of the structural motifs $\text{An}_2\text{R33-1}$ and $\text{An}_2\text{L1-1}$, the two most stable dimer conformers. Apparently these most stable dimer motifs are not competitive as substructures in

the trimer, compared to other hydrogen bonding arrangements. In any case the (sole) An_3 conformer of relevance in molecular beam expansions is $\text{An}_3\text{L11-1}$.

In Table 4.5 again SCS-LMP2, LMP2, and LCCSD interaction energies are compared to the LCCSD(T) reference values, now for the trimer. Moreover, apart from the interaction energies also the nonadditive three-body contributions are considered. In the LCCSD and LCCSD(T) calculations, to save time, only the *intermolecular* pairs were treated at the local coupled cluster level, whereas the *intramolecular* pairs were described at the LMP2 level only. Since test calculations on the $\text{An}_2\text{R33-1}$ dimer gave for these both cases *exactly* the same result for the counterpoise corrected interaction energy, this approximation is well justified. Comparison of SCS-LMP2 and LCCSD(T) yields the same favorable picture as for the dimer with deviations of 2%–3%. Not surprisingly, the largest deviation occurs for the most stable $\text{An}_3\text{L11-1}$ conformer, featuring directional NH–N hydrogen bonds and hardly any π -stacking. LCCSD again consistently underestimates the LCCSD(T) interaction energy (by 13%–15%), yet in a much more regular way than LMP2 overestimates it.

When comparing the three-body contributions in Table 4.5 it is evident that the errors of the LMP2 and SCS-LMP2 methods, relative to LCCSD(T), are very similar, and quite large, while those of LCCSD are much smaller. This may be related to the absence of nonadditive three-body dispersion (Axilrod-Teller) terms in second-order perturbation theory. The lowest-order SAPT three-body dispersion term $E_{\text{disp,ABC}}^{(30)}$ (of third-order with respect to the inter- and of zeroth-order with respect to the intramolecular perturbation operator) appears in supermolecular calculations based on the Møller-Plesset partitioning in third-order (cf., e.g., Eqs. (8) and (9), and Fig. 1 in Ref. 139). This is not so much of a problem here, since the importance of the nonadditive three-body term overall, and the Axilrod-Teller term in particular relative to the total interaction energy is rather modest, and also π -stacking is of lesser importance for An_3 than for An_2 (certainly so for the most stable $\text{An}_3\text{L11-1}$ geometry). However, for systems where the relative importance of dispersion generally, and nonadditive three-body dispersion particularly, is larger, the SCS-LMP2 method should not be used blindly!

4.4.2 Vibrational frequencies of the N–H stretch modes

For the most stable geometry of An_2 and An_3 , i.e., $\text{An}_2\text{R33-1}$ and $\text{An}_3\text{L11-1}$, respectively, normal mode analysis based on the SCS-LMP2/X=D energy functional was carried out. Of interest here are the harmonic vibrational frequencies of the symmetric and antisymmetric N–H stretch modes, which are primarily affected by

Geometry	Vibration	harm.	rel. Int.	Exp.
An	ν_s	3541.7	5.10	3421.8
	ν_{as}	3651.0	5.86	3508.2
An ₂ R33-1	ν_s	3533.5 (-8.2)	0.01	
	ν_s	3533.9 (-7.8)	10.07	3394.0 (-27.8)
	ν_{as}	3632.4 (-18.6)	2.16	3465.9 (-42.3)
	ν_{as}	3632.5 (-18.6)	1.92	3465.9 (-42.3)
An ₃ L11-1	ν_s	3480.8 (-60.9)	44.69	
	ν_s	3501.7 (-40.0)	83.36	
	ν_s	3516.7 (-25.0)	5.36	
	ν_{as}	3607.5 (-43.5)	25.30	
	ν_{as}	3625.7 (-25.3)	13.51	
	ν_{as}	3626.4 (-24.7)	15.71	

Table 4.6: Calculated harmonic vibrational frequencies in cm^{-1} , their according shifts (in parentheses) and the relative intensities (arbitrary units), calculated with SCS-LMP2 and X=D basis sets. Experimental data are also given, cf. Refs. 119–121.

cluster formation. Table 4.6 compiles the frequencies, frequency shifts relative to the monomer, and the corresponding intensities of these modes. The SCS-LMP2 values are consistently too high, compared to the available experimental monomer and dimer values. The frequency shifts calculated for the dimer are correctly predicted as redshifts, but are far too small. It appears that a harmonic frequency analysis is insufficient for the present case. Unfortunately higher level calculations such as higher dimensional variational SCF and CI [42–45] turned out as too expensive for these systems.

4.5 Conclusions

In the present work the aniline dimer and trimer were studied by means of *ab initio* electronic structure theory. The ground state surfaces were thoroughly searched for energetically low lying minima by combining global optimizations on a model potential with *ab initio* energy calculations and adapting iteratively the model potential to the *ab initio* interaction energies for a growing set of relevant geometries. These calculations were performed at the level of local MP2 (LMP2) and SCS-LMP2. For the dimer, as well as for the trimer, a single ground state mini-

mum appears to be populated at typical molecular beam temperatures. For the dimer this minimum corresponds to head-to-tail arrangement of the two monomers, where each amino group acts as a double H donor to the π system of the phenyl rings. DFT-SAPT calculations reveal that the interaction energy is dominated by the component of van der Waals dispersion, which is of similar size as in the benzene dimer, yet in contrast to the latter, the component of first-order (polarization plus exchange repulsion) is much less repulsive. Overall the interaction energy of the aniline dimer is much larger than that of the benzene dimer (7.9 versus 2.9 kcal/mol, according to DFT-SAPT calculations in aug-cc-pVQZ basis).

The geometry of the relevant trimer ground state minimum exhibits two directional NH–N hydrogen bonds. Thus, in contrast to the dimer, the three monomers are non-equivalent, but can clearly be distinguished as an H donor, an H acceptor, and as an H donor and acceptor, respectively. This is of particular relevance for the absorption spectra, since in such a case three different electronic origins might be observed, related to the three individual chromophores in a different environment. This will be further discussed in chapter 5, where the lowest excited states of the aniline dimer and trimer are explored.

The nonadditive three-body terms of the trimer amount to 5% or less of the total interaction energy. The difference between MP2 (or SCS-MP2) and LCCSD, which we roughly relate to the three-body dispersion contribution, is repulsive and amounts to about 18% of the total three-body term for the most stable trimer geometry. From this angle, application of SCS-LMP2 to aniline clusters still appears to be justified.

5 The low-lying electronic excited states of aniline clusters

5.1 Introduction

Intermolecular forces between stable molecules are omnipresent in physics, chemistry, and biology. Moreover, electronic excitation of a chromophore can significantly influence the strength of such forces, with which it interacts with its environment, e.g., with the solvent molecules of a solvent shell, or with nearby amino acid residues in a binding pocket of a protein [140, 141]. Intermolecular interactions between molecules are therefore of great interest, particularly so, if one or multiple chromophores are involved. Molecular clusters, i.e., *isolated* aggregates of two to many molecules of interest are ideal systems to study such interactions in detail [142]. Experimentally, such clusters are synthesized in molecular beam expansions and detected/analyzed by using laser spectroscopy. If the cluster contains at least one (aromatic) chromophore, then the spectroscopic toolbox is particularly rich: mass selective absorption spectra can be obtained by applying resonant two-photon ionization (R2PI) spectroscopy, the combination of that method with, e.g., infrared depletion spectroscopy (IRDS) provides information on the electronic ground state, hole burning experiments can be used to check if one or more distinct isomers coexist, etc. [19]

In a previous study [143] the aniline (An) dimer and trimer were investigated in their electronic ground states. Using an *ab initio* global optimization approach, where the model potential used for the global optimization procedure is constantly recalibrated and thus improved on-the-fly by *ab initio* calculations (spin-component-scaled [48] local MP2) at relevant configurations, the lowest-energy configurations of these clusters could be determined. For the An₂ dimer this was a symmetric head-to-tail arrangement with two NH₂- π type interactions between amino groups and π systems of the two monomers (cf. Fig. 5.1). The Van der Waals dispersion is predominant in this system, as density functional theory-symmetry-adapted perturbation theory (DFT-SAPT) calculations show. The global minimum of the An₃ trimer, on the other hand, corresponds to an assembly of two head-to-head arrangements, grouped such that the three monomers nearly form a

ring. Two directional NH-N hydrogen bonds are formed, with one aniline subunit acting as a H donor, another as H acceptor, and the third simultaneously as H donor and acceptor (cf. Fig. 5.3). Therefore, each aniline monomer has a clearly distinct H-bonding environment, which is in strong contrast to the dimer. The distance between the acceptor N atom and the phenyl ring of the donor is too long to form a third H bond of NH- π type (apparently, the ring strain is too large). Non-additive three-body contributions amount to about 5%. Of these, only about 20% are related to dispersion (Axilrod-Teller contributions). A second-order treatment (which neglects Axilrod-Teller terms) therefore still is justified for this system.

To distinguish the multitude of individual geometries generated by the global optimization procedure, a topological nomenclature was introduced (cf. appendix in Ref. 143). According to this nomenclature the symmetric head-to-tail arrangement of the the An_2 dimer is denoted as An_2R33-1 , while the label An_3L11-1 is used for the global minimum of An_3 with the two directional NH-N hydrogen bonds.

For aniline clusters not much is presently known about their excited states. Few experimental papers on An_2 are available in literature. R2PI spectra (both deuterated and nondeuterated An_2) were measured by Yeh *et al.* [119]. The $S_1 \leftarrow S_0$ origin of the dimer is redshifted by 678 cm^{-1} relative to the monomer (nondeuterated species), which corresponds to an untypically large increase in the binding energy of the complex on going from the electronic ground to the S_1 state. Furthermore, there is a broad background feature in the spectrum hinting at the existence of an energetically lower lying excimer state. The multiple sharp bands of the spectra in the vicinity of the origin belong, as hole burning experiments reveal, all to the same (ground state) An_2 isomer. IRDS measurements of the N-H stretch frequencies finally ascertain the equivalence of both amino groups of An_2 , implying a sandwich type head-to-tail arrangement for the relevant S_0 state minimum, in agreement with *ab initio* calculations [120, 143].

Ab initio calculations investigating the excited states of An_2 have not yet been carried out so far, its S_1 state geometry is unknown. Also the aniline trimer is *terra incognita*. To our knowledge neither experimental nor theoretical studies on An_3 are available in literature, even though there have been measurements done on the dimer and trimer ions by Ohashi *et al.* [144, 145]

In the present work we have investigated the two/three lowest electronically excited states of An_2 and An_3 , respectively. Starting from the Franck-Condon point geometry optimizations were carried out on the individual excited state surfaces by employing time-dependent coupled cluster CC2 response theory (CC2 response) [46], as well as the spin-component-scaled variant of CC2 response [49]. CC2 response theory has already been applied successfully in our previous studies on phenol-water_n and 2-naphthol-water_n solvent clusters in order to understand the

anomalous R2PI absorption spectra of the $n = 2$ clusters [102, 118]. In the next section we provide details about the computational methods employed. The results of our study are presented and discussed in Sec. 5.3. Section 5.4 finally concludes this chapter.

5.2 Computational methods

Geometry optimizations on the excited state surfaces of An_2 and An_3 were studied with time-dependent coupled cluster response theory at the level of the second-order CC2 model [46]. Primarily, the spin-component-scaled (SCS) variant of CC2 (Ref. 49) was employed, though, also unscaled CC2 response calculations were performed for comparison. It turned out that the SCS-CC2 minima provide better (lower) interaction energies at the higher level of CCSD response theory than the CC2 minima (*vide infra*), which is due to the well known fact that the second-order CC2 model, such as MP2, describes van der Waals dispersion just at a level corresponding to the uncoupled Hartree-Fock representation of the underlying dynamical polarizabilities. This usually leads to a significant overestimation of the binding energy, particularly so, if the dispersive component is dominant as is the case, e.g., in the An_2 cluster. Spin-component scaling [48] alleviates this deficiency to some extent and was therefore used as the main tool in the present work. The geometry optimizations were carried out by using the density fitted, analytic CC2 response gradient implementation of Hättig and Köhn [90, 91, 115] available in the TURBOMOLE program package (Ref. 146). The CCSD response calculations were performed by using the equation-of-motion CCSD program [11] implemented in the MOLPRO program package [96].

For all calculations the augmented correlation consistent aug-cc-pVXZ AO basis sets [34] with $X \in \{\text{D}, \text{T}\}$, together with the related fitting sets [99], were used: $X=\text{D}$ for geometry optimizations and $X=\text{T}$ for single point energies. Also the An_2 and An_3 ground state geometries in Ref. 143 were reoptimized at the level of CC2 and SCS-CC2 response, respectively, in order to calculate adiabatic excitation energies, bathochromic shifts, and vertical density differences consistently.

In the following, the term "binding energy" implies the inclusion of relaxational effects to the "interaction energy", which is in turn understood to be calculated between rigid monomers. There is an ambiguity when calculating interaction energies, basis set superposition errors (BSSE, via the counterpoise correction), or relaxation energies of clusters involving excited states where the excitation is delocalized over individual monomers as, e.g., for the dimer (*vide infra*) due to the fact that the geometries of the noninteracting monomers taken as the reference are

unrelaxed and therefore different. Since only one of the noninteracting monomers is electronically excited it is ambiguous which one to choose. This problem does not appear for the dimer geometries obtained with the SCS-CC2 response method, which are virtually symmetric, yet it is present for the unscaled CC2 response geometries, which are not as symmetric. For the latter we provide both values. For the trimer, on the other hand, a clear assignment of the excitation to a particular monomer is possible since the excitations are localized on the individual monomers. For binding energies the ambiguity disappears in any case since here the reference is unambiguously represented by the *relaxed* geometries of the monomers in ground and excited states.

Concerning the numeration of the states we use the individual ground state geometries, i.e., the Franck-Condon points (FCPs) as reference. Thus S_1 is the lowest state, S_2 is the second lowest state, etc., *at the related FCP*, implying that, e.g., S_2 may become the lowest state for some other geometry, provided that S_1 and S_2 intersect. Furthermore, we use the term "minima" for stationary points obtained from a geometry optimization, even though only for structures $An\ S_0$, $An\ S_1$, $An_2R33-1\ S_0$, and $An_2R33\ S_2$, this was strictly verified by calculating the nuclear Hessian. However, since all other provided structures have no symmetry it can be quite safely assumed that the optimization procedure converges to a minimum and not a saddle point.

5.3 Results and Discussion

5.3.1 The aniline dimer, An_2

The $S_1 \leftarrow S_0$ excitation of the aniline monomer is of $\pi^* \leftarrow \pi$ type. Since An_2 comprises two monomers, two different excited states originating from this $\pi^* \leftarrow \pi$ excitation are expected. Furthermore since the two monomers are nearly equivalent (the $An_2R33-1\ S_0$ geometry almost has C_{2h} symmetry) the two excited states reflect this symmetry and are therefore delocalized. Analyzing the two excited states in the framework of C_{2h} symmetry, the energetically lower S_1 excited state of An_2 transforms as a basis function for the B_g irreducible representation (irrep) of the C_{2h} point group. The related transition is dipole-forbidden; the SCS-CC2 oscillator strength is therefore very weak, i.e., $f = 0.001$.

The energetically higher S_2 excited state, on the other hand, transforms as a basis function for the A_u irrep and the related transition is dipole-allowed (in the z -direction): The SCS-CC2 oscillator strength here amounts to $f = 0.035$. Figure 5.2 displays the SCS-CC2 density difference plots between the densities of

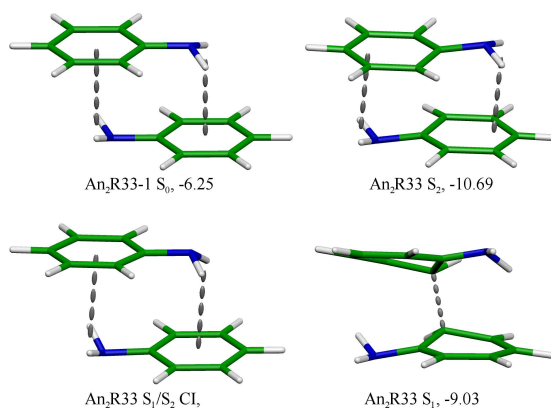


Figure 5.1: Aniline dimer minimum energy geometries in the ground and the excited state, calculated with SCS CC2 response in the X=D basis set, together with the respective binding energies ΔE^0 in kcal/mol.

$S_1(\pi_u^* \leftarrow \pi_u)$ and $S_2(\pi_g^* \leftarrow \pi_u/\pi_u^* \leftarrow \pi_g)$, respectively, and the density of the ground state, all calculated at the SCS-CC2 ground state minimum structure An₂R33-1 S₀. Obviously, for both transitions the excitation is delocalized on both aniline subunits. Furthermore, it is clearly seen that the $S_1 \leftarrow S_0$ excitation in An₂ *increases* the electron density between the two monomers, which is not the case for the optically stronger $S_2 \leftarrow S_0$ excitation. This buildup of density between the monomers in the S₁ state leads to the formation of an excimer: Geometry optimization on the S₁ state surface leads to the structure denoted as "An₂R33 S₁" in Fig. 5.1, where a bond of length 1.794 Å is formed between the two *ortho*-C atoms of the monomers. This structure and the related energies have to be taken with a grain of salt though, since a response method based on a closed-shell reference most likely is inappropriate. The newly formed "covalent" excimer bond is elongated and most likely leads to near degeneracy effects, such that a proper description of the ground state requires multiple determinants. Also calculating interaction energies is problematic since the excimer bond would need to be broken for the counterpoise correction. The BSSE uncorrected SCS-CC2 binding energy of the excimer amounts to -21.28 kcal/mol, which compares to -20.40 kcal/mol for the An₂R33 S₂ minimum (*vide infra*). The related values for unscaled CC2 are -33.49 kcal/mol versus -20.83 kcal/mol. Again, these energetics are highly unreliable, yet what can be postulated on the basis of these calculations is the existence of an excimer corresponding to the minimum on the S₁ state surface, which is *below* the An₂R33 S₂ minimum. This is in line with Fig. 4 in Ref. 119 and the conjecture made in that paper on the basis of the measured R2PI spectra (*vide supra*).

In order to obtain the minimum on the $S_2(\pi_g^* \leftarrow \pi_u/\pi_u^* \leftarrow \pi_g)$ state surface an initial geometry optimization within C_{2h} symmetry on the lowest A_u excited

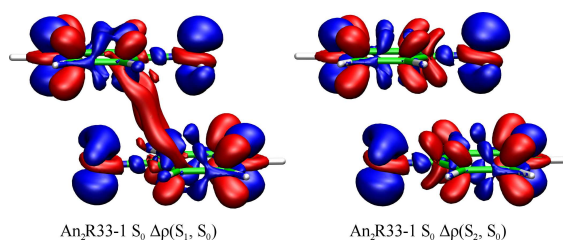


Figure 5.2: Density differences, calculated at the An₂R33-1 S₀ ground state geometry, between S₁ and S₀ (left) and S₂ and S₀ (right). The red iso-surface represents a value of 0.001, the blue one -0.001. (Upon excitation the electron density moves from blue to red regions)

state was carried out first [a direct relaxation in C₁ symmetry on the S₂ surface starting from the FCP again leads to the S₁($\pi_u^* \leftarrow \pi_u$) minimum of the excimer]. During this optimization the A_u state falls energetically below the B_g state. The resulting geometry was then fully relaxed in C₁ symmetry. The final geometry, denoted as "An₂R33 S₂", is depicted in Fig. 5.1. The geometry of this dimer minimum overall is similar to the An₂R33-1 S₀ head-to-tail arrangement, yet the vertical distance between the two phenyl rings decreases from 3.170 to 2.727 Å, while the horizontal displacement along the long axis decreases from 3.010 to 2.351 Å (cf. Table 5.1). The root-mean-square (rms) deviation in atomic positions d^{rms} between both structures is 1.977 Å (cf. Table 5.2). These rather large changes in the vertical distance and the horizontal displacement may be the origin for the low-frequency progressions and combination bands as seen in the absorption spectra of the dimer [119, 121].

A characteristic feature of the relevant $\pi^* \leftarrow \pi$ excitation is the flattening of the amino group; for the aniline monomer the dihedral angle β_{CHHN} decreases from 33.1° to essentially 0° on going from the S₀ to the S₁ state (the amino group is entirely planar in the S₁ state). For the dimer these angles decrease from 35.6° in the An₂R33-1 S₀ minimum to 27.4° in the An₂R33 S₂ minimum, as can be seen in Table 5.1. Furthermore, the *ipso* C atom, along with the adjacent amino group, is appreciably displaced by 8.5° out of the plane defined by the remaining C atoms, which compares to only 0.8° in the ground state structure.

The binding energy of the An₂R33 S₂ minimum is 4.44 kcal/mol larger than that of the An₂R33-1 S₀ minimum (cf. Table 5.3). This corresponds to a bathochromic shift of -1553 cm⁻¹ for the origin of the absorption spectrum, which is more than twice as large as the experimentally observed redshift of 678 cm⁻¹ (Ref. 119) (cf. Table 5.4). The calculation of such bathochromic shifts is a difficult task since it requires a well balanced description of the subtle intermolecular interactions in ground and excited states, and might be beyond the accuracy of a second-order

Geometry	$\Delta_{\parallel, \text{long}}^{\text{Ph}}$	$\Delta_{\parallel, \text{short}}^{\text{Ph}}$	$\Delta_{\perp}^{\text{Ph}}$	$d_{\text{NH-N}}$	β_{NCCN}	β_{CHHN}
An S ₀						33.1
An S ₁						0.0
An ₂ R33-1 S ₀	3.010	0.000	3.170		175.5	35.6, 35.6
An ₂ R33 S ₂	2.351	0.000	2.727		180.0	27.4, 27.4
An ₂ R33 S ₁ /S ₂ CI	3.253	0.000	3.004		180.0	26.6, 26.6
An ₃ L11-1 S ₀				2.193, 2.224		33.4, 32.6, 34.8
An ₃ L11 S ₁ (D)				2.058, 2.243		13.3, 33.3, 35.3
An ₃ R123 S ₂ (DA)				1.924		33.2, 9.5, 35.6
An ₃ R122 S ₃ (A)				2.218		32.6, 35.0, 8.4

Table 5.1: Selected geometry parameters of the individual SCS-CC2/X=D minima.

The Δ denote parallel and perpendicular components of the distance vector between the centers of the two phenyl rings of An₂. $d_{\text{NH-N}}$ denotes the individual NH-N H bonding distances. β_{NCCN} denotes the dihedral angle describing the displacement of the *ipso* C atom out of the plane defined by the five other C atoms of the individual monomers, and β_{CHHN} denotes the dihedral angle measuring the non-planarity of a NH₂ group. Distances are given in Å, angle in degrees.

method. Using CCSD (instead of SCS-CC2) response interaction energies, calculated at the SCS-CC2 An₂R33-1 S₀ and An₂R33 S₂ geometries (cf. Table 5.5) and combined with the corresponding SCS-CC2 relaxation energies of Table 5.3, yields a value of -710 cm⁻¹ for the bathochromic shift, which is much closer to experiment. Basis set extension, on the other hand, does not lead to an improvement of the bathochromic shifts, as the SCS-CC2 X=T results in Table 5.3 show.

In the context of the present work calculations based on unscaled CC2 response theory were also carried out, the resulting interaction and binding energies are compared to those of SCS-CC2 response in Table 5.5. CCSD response reference calculations, performed at the CC2 and SCS-CC2 An₂R33-1 S₀ and An₂R33 S₂ minimum structures, however, reveal that (i) the deviations from the CCSD interaction energies are much larger for CC2 than for SCS-CC2 at the related geometries, and (ii) the CCSD interaction energies are larger (absolute value) at the SCS-CC2 than at the unscaled CC2 geometries (cf. Table 5.5). This indicates that the CCSD minima most likely are closer to the SCS-CC2 minima than to the unscaled CC2 minima. Probably, even though spin-component scaling is not the ultimate answer for systems with a delicate balance between hydrogen bonding and π stacking [52], it seems to be more reliable than unscaled CC2. Thus, the

5 The low-lying electronic excited states of aniline clusters

An ₂	R33-1 S ₀	R33 S ₂	R33 S ₁ /S ₂ CI
R33 S ₂	1.9770		
R33 S ₁ /S ₂ CI	1.9446	0.4255	
R33 S ₁	0.5414	1.9579	2.0253
An ₃	L11-1 S ₀	L11 S ₁ (D)	R123 S ₂ (DA)
L11 S ₁ (D)	0.1087		
R123 S ₂ (DA)	1.1316	1.1968	
R122 S ₃ (A)	0.9328	0.9655	1.0582

Table 5.2: RMS geometry differences d^{RMS} between two individual aniline dimer and trimer geometries. All the geometries are calculated with SCS-CC2 response in the X=D AO basis set. The values are given in Å.

remaining discussion on the excited states of the An₂ and An₃ clusters is based on SCS-CC2 response calculations.

Between the S₂ and the S₁ state surfaces there is a conical intersection seam. We tried to locate a minimum energy point on the seam in the vicinity of the FCP by employing the same approach as in previous work [102], i.e., *without* the nonadiabatic coupling vector, which unfortunately is not yet available for the DF-SCS-CC2 implementation of TURBOMOLE [146]. The resulting geometry obtained from these tedious calculations is shown in Fig. 5.1, labeled as "An₂R33 S₁/S₂ CI". It is again similar to the S₀ head-to-tail arrangement An₂R33-1 S₀ of the ground state, and as for the An₂R33 S₂ minimum, there is quite a large change in the vertical distance and the horizontal long axis displacement of the two phenyl rings. The vertical distance decreases from 3.170 to 3.004 Å, while the horizontal displacement increases from 3.010 to 3.253 Å. The dihedral angles β_{CHHN} describing the "nonplanarity" of the amino groups, amount to 26.6°, i.e., a similar simultaneous flattening of both amino groups occurs as for the An₂R33 S₂ minimum. Overall, the geometry of the conical intersection minimum is close to both the An₂R33-1 S₀ and the An₂R33 S₂ minima; actually, the rms deviation in atomic positions d^{rms} between the An₂R33 S₂ minimum and the conical intersection is, with only 0.43 Å, rather small (cf. Table 5.2). It is therefore not surprising that the optimization of the An₂R33 S₂ minimum turned out to be difficult and tedious (*vide supra*).

Geometry	X=D				X=T		
	$\Delta E_{\text{int}}^{\text{CP}}$	δ_{BSSE}	δ_{rel}	$\Delta E_{\text{bind}}^{\text{CP}}$	$\Delta E_{\text{int}}^{\text{CP}}$	δ_{BSSE}	$\Delta E_{\text{bind}}^{\text{CP}}$
An ₂ R33-1 S ₀	-6.59	6.37	-0.35	-6.25	-7.23	2.68	-6.89
An ₂ R33 S ₂	-15.50	9.71	-4.80	-10.69	-16.87	3.96	-12.07
An ₂ R33 S ₁ /S ₂ CI	-8.41	7.09	-3.28	-5.14	-9.25	2.97	-5.97
An ₃ L11-1 S ₀	-14.27	12.70	-0.55	-13.72	-15.62	5.67	-15.07
An ₃ L11 S ₁ (D)	-17.79	13.37	-0.91	-16.88	-19.23	5.97	-18.32
An ₃ R123 S ₂ (DA)	-18.73	13.41	-1.37	-17.36	-20.20	5.94	-18.83
An ₃ R122 S ₃ (A)	-16.70	12.50	-0.87	-15.83	-18.10	5.59	-17.23

Table 5.3: Counterpoise corrected interaction energies $\Delta E_{\text{int}}^{\text{CP}}$, BSSE δ_{BSSE} , relaxation energies δ_{rel} (calculated within monomer basis) and binding energies $\Delta E_{\text{bind}}^{\text{CP}}$. The calculations were performed with SCS-CC2 response in the X=D and X=T AO basis sets at the X=D geometries. For the X=T binding energies the X=D relaxational energies were used. All values are given in kcal/mol.

5.3.2 The aniline trimer, An₃

In contrast to the dimer the three individual monomers of the trimer are not equivalent (or nearly equivalent) at the An₃L11-1 S₀ minimum, but clearly distinguishable as a NH-N donor (D), an acceptor (A), and a monomer acting simultaneously as donor and acceptor (DA) (cf. Fig. 5.3). Therefore, it can be anticipated that, in principle, three distinct electronic origins should be visible in the absorption spectrum, where the $\pi^* \leftarrow \pi$ excitation is localized either on the D, the A, or the DA monomer. This can be seen clearly in Fig. 5.4 displaying the density differences of the lowest excited states S₁(D), S₂(DA), and S₃(A) versus ground state at the FCP. The oscillator strengths for these three excitations amount to 0.0186, 0.0261, and 0.0119, respectively. For each of these three individual excited states geometry optimizations were carried out, which turned out to be even more tedious than for the dimer [at least for S₂(DA) and S₃(A)] due to the presence of conical intersection seams. Minimizing the energy on the S₁(D) surface, i.e., where the $\pi^* \leftarrow \pi$ excitation is located on the donor, leads to a geometry denoted in Fig. 5.3 (according to the nomenclature specified in Ref. 143) as "An₃L11 S₁(D)". It is quite similar to the S₀ minimum, and as the latter, has two directional NH-N hydrogen bonds. The rms deviation in atomic positions between the two geometries is quite small and amounts to a value of $d^{\text{rms}} = 0.109$ Å. On going from the S₀ to the S₁(D) minimum, the NH-N distance between D and DA decreases from 2.193 to 2.058 Å, while the NH-N distance between DA and A increases somewhat from 2.224 to

5 The low-lying electronic excited states of aniline clusters

Conformer	GS \rightarrow Conformer	XS	SCS-CC2	Exp.
An	S ₀	An S ₁	4.327	4.219
An ₂ R33-1	S ₀	R33 S ₁	(4.395)	
		R33 S ₂	4.134 (4.534)	4.135
An ₃ L11-1	S ₀	L11 S ₁ (D)	4.190 (4.430)	
		R123 S ₂ (DA)	4.169 (4.582)	
		R122 S ₃ (A)	4.235 (4.621)	

Table 5.4: Adiabatic excitation energies in eV, calculated with SCS-CC2 response in the X=D AO basis set, between ground state (GS) and excited state (XS). In parentheses the vertical excitation energies at the Frank-Condon point of the respective state are given. Experimental values according to Ref. 119 are also included, for comparison.

2.243 Å (cf. Table 5.1). Furthermore, there is a distinct flattening of the amino group on the D monomer from $\beta_{\text{CHHN}} = 33.4^\circ$ to $\beta_{\text{CHHN}} = 13.3^\circ$, whereas the amino groups of the DA and A monomers remain unaffected. This is indicative of the fact that the $\pi^* \leftarrow \pi$ excitation remains localized on the D monomer. Figure 5.4 depicts the density difference between the S₁(D) and S₀ states at the An₃L11 S₁(D) minimum. Evidently, the density difference is indeed entirely localized on the D monomer.

The binding energy of the An₃L11 S₁(D) minimum is 3.16 kcal/mol larger than that of the ground state minimum (cf. Table 5.3). This corresponds to a bathochromic shift of -1105 cm⁻¹, which is 448 cm⁻¹ less (absolute value) than that obtained for the dimer (*vide supra*). Unfortunately, there is no experimental value available for comparison.

The minimum geometry obtained on the initial S₂(DA) state surface is denoted as "An₃R123 S₂(DA)" in Fig. 5.3 and corresponds to the lowest root. The three monomers are arranged in a ringlike fashion. Just one directional NH-N hydrogen bond between the almost planar DA monomer carrying the electronic excitation and the A monomer occurs. The NH-N distance is quite short (1.924 Å, cf. Table 5.1), which is indicative of quite a strong H bond. The D monomer now acts as a donor to the DA molecule in a NH₂- π type interaction, while the A monomer now is also a donor to the D subunit via a NH- π type interaction.

Again, only the amino group of a single molecule, the DA monomer here, is affected by the excitation. The dihedral angle β_{CHHN} decreases from 32.6° to 9.5°, whereas for the other monomers the ground state value is preserved (cf. Table 5.1). Evidently, the $\pi^* \leftarrow \pi$ excitation remains localized on the DA monomer also for

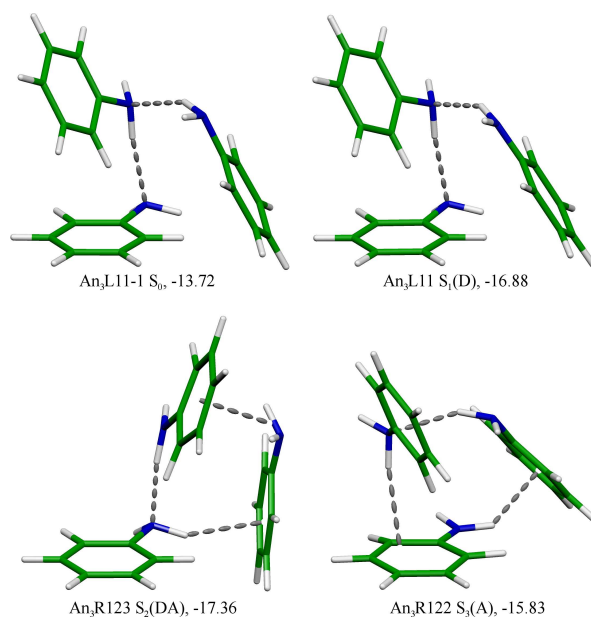


Figure 5.3: Aniline trimer minimum energy geometries in the ground and the excited state, calculated with SCS CC2 response in the X=D basis set, together with the respective binding energies ΔE^0 in kcal/mol.

the relaxed structure. This is also illustrated by the density difference plot between the S_2 and S_0 states at the $\text{An}_3\text{R123 } S_2(\text{DA})$ geometry in Fig. 5.4.

The $\text{An}_3\text{R123 } S_2(\text{DA})$ geometry constitutes the most stable excited trimer minimum found in the course of the present work. The binding energy increases by 3.64 kcal/mol relative to the ground state minimum, which corresponds to a bathochromic shift of -1273 cm^{-1} . Its electronic origin thus is predicted to be shifted to the red relative to that of the $\text{An}_3\text{L11 } S_1(\text{D})$ minimum. On the other hand, the structural changes relative to the $\text{An}_3\text{L11-1 } S_0$ geometry are much larger ($d^{\text{rms}} = 1.132 \text{ \AA}$) than for the $\text{An}_3\text{L11 } S_1(\text{D})$ conformer. Consequently, the related Franck-Condon factors are anticipated to be much smaller. This implies a much weaker electronic origin for the $\text{An}_3\text{R123 } S_2(\text{DA})$ compared to that of the $\text{An}_3\text{L11 } S_1(\text{D})$ conformer.

Finally, the minimum geometry optimized on the initial $S_3(\text{A})$ state surface is denoted as " $\text{An}_3\text{R122 } S_3(\text{A})$ " in Fig. 5.3. It also corresponds to the lowest root, and, as before, the three monomers are cyclically arranged, and a single directional NH-N hydrogen bond occurs. Yet here, this directional H bond is formed between the D and the DA monomers, and its length is with 2.218 \AA , not significantly shorter than in the ground state (the A monomer carrying the excitation is not involved in this hydrogen bond). Two NH- π type interactions, between DA and A, and A and D, respectively, close the cycle. This structure is reminiscent of the

5 The low-lying electronic excited states of aniline clusters

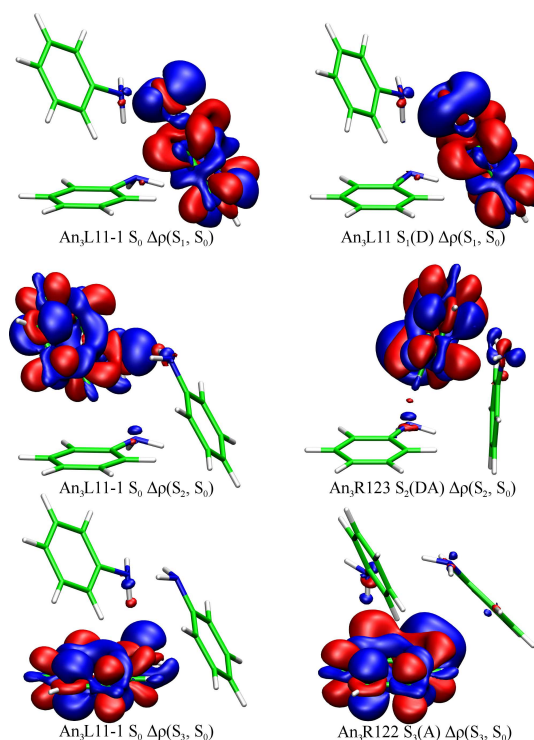


Figure 5.4: Density differences of An_3 geometries between excited and ground state. Left column: at ground state minimum; right column: at respective excited state minima. The red iso-surface represents a value of 0.001, the blue one -0.001. (Upon excitation electron density moves from blue to red regions)

$\text{An}_2\text{R122-1}$ ground state structure, as depicted in Fig. 2 of Ref. 143.

Here, the dihedral angle β_{CHHN} of the A monomer decreases from 34.8° to 8.4° , while the amino groups of the D and DA monomers remain unaffected. The excitation thus remains localized on the A monomer, which again is illustrated by the corresponding density difference plot in Fig. 5.4.

The binding energy of the $\text{An}_3\text{R122 S}_3(\text{A})$ minimum is 2.11 kcal/mol larger than that of the ground state minimum, which corresponds to a bathochromic shift of -738 cm^{-1} . The electronic origin related to the $\text{An}_3\text{R122 S}_3(\text{A})$ conformer is thus predicted to be blueshifted relative to that of $\text{An}_3\text{L11 S}_1(\text{D})$, yet, again due to small Franck-Condon factors (the geometric deviation from the ground state geometry is with a d^{rms} value of 0.923 \AA rather large) it probably would not constitute a prominent feature in the absorption spectrum neither.

Geometry	CCSD	CC2	SCS-CC2
An ₂ R33-1 S ₀ /CC2	-3.61	-9.58	-5.71
An ₂ R33-1 S ₀ /SCS-CC2	-4.82	-9.94	-6.59
An ₂ R33 S ₂ /CC2	-6.14/-4.28*	-17.79/-15.79*	-9.36/-7.46*
An ₂ R33 S ₂ /SCS-CC2	-11.30	-25.05	-15.49

* Two values provided, *cf.* text at the end of section 5.2.

Table 5.5: Counterpoise corrected interaction energies, calculated at the individual dimer geometries optimized by using the SCS –, and the unscaled CC2 response method, in the X=D AO basis set. All values are given in kcal/mol.

5.4 Conclusions

In the present work the excited state surfaces of the aniline dimer and trimer, related to the $S_1(\pi^* \leftarrow \pi)$ excitation of the monomer, were investigated at the level of spin-component-scaled CC2 response theory. For the case of the dimer, due to the near equivalence of the two monomers by symmetry, the two resulting excited states are delocalized over the two monomers. The one, which at the FCP is energetically lower, features an accretion of density between the two phenyl rings; geometry minimization on the related surface leads to an excimer structure. The existence of an excimer was also conjectured in previous experimental work [119]. Minimization of the second state leads to a head-to-tail geometry, where, relative to the ground state minimum the two phenyl rings exhibit a substantial displacement along two well defined coordinates, i.e., along the vertical and long horizontal axes. This offers an explanation for the occurrence of the low-frequency overtone and combination bands observed in the mass selective absorption spectra. In the vicinity of this geometry the second state corresponds to the lowest root, thus there is a conical intersection seam between the two states. A low-energy point of the seam was located in the course of this work, which also corresponds to a head-to-tail arrangement of the two monomers with a vertical displacement of the two phenyl rings somewhat smaller than that of the excited minimum energy structure, but with larger horizontal displacement.

The SCS-CC2 response calculations overestimate by far the measured bathochromic shift of the dimer. On the other hand, CCSD response single point calculations at the SCS-CC2 geometries provide a value for the bathochromic shift which is in quite good agreement with experiment. Possibly, a second-order method cannot achieve sufficient accuracy for this particular property. However, this needs to be investigated more thoroughly, separately in a systematic study involving several different systems.

5 *The low-lying electronic excited states of aniline clusters*

In contrast to the dimer the three aniline subunits of the trimer are clearly nonequivalent, each in a distinct hydrogen-bonding arrangement. The three excitations related to the $S_1(\pi^* \leftarrow \pi)$ excitation of the monomer thus are localized on the individual monomers, both at the FCP, as well as at the relaxed geometries. One of these relaxed geometries closely resembles the trimer ground state structure, with two directional NH-N hydrogen bonds and a donor (D), a donor/acceptor (DA), and an acceptor (A) monomer. For this geometry the excitation is localized on the D subunit. The other two relaxed trimer geometries, with the excitation either being localized on the DA or the A monomer, respectively, both considerably deviate from the ground state structure and involve just a single directional NH-N hydrogen bond plus $\text{NH}_2\text{-}\pi$ and/or $\text{NH-}\pi$ type interactions. One of them is more stable than the first conformer. Each of the three geometries corresponds to the lowest root in their respective geometrical environment.

Because of the large geometrical deviations from the ground state structure, small Franck-Condon factors are anticipated for the two geometries with the excitation either localized on the DA or the A monomer. The related electronic origins therefore are not expected to be visible in the absorption spectrum. Consequently, only the origin related to the first (metastable) minimum with the excitation localized on the D monomer might prominently appear in the spectrum. However, this depends on the barriers shielding this minimum from energetically lower lying configurations. If they are too small, then its vibrational states will dissolve in the continuum of those from the lower lying minimum, leading to extensive broadening. Based on these calculations, one may anticipate that the detection of the aniline trimer in a R2PI absorption spectrum is rather difficult.

6 Adducts of tantalum chlorides and phosphorus sulfide cages

6.1 Introduction

Neutral molecules, such as Ph_3P or CO , are frequently used as ligands for metal complexes. Among the more uncommon species of this group are cage-like non-metal molecules that can act as electron pair donors towards the metal. This research topic has been of wide interest over recent years [147–162]. With restriction to transition-metal halides such as TiX_4 or NbX_5 ($\text{X} = \text{halogen}$), adducts such as $(\text{NbCl}_5)_2(\beta\text{-P}_4\text{S}_4)$ and $(\text{NbCl}_5)(\text{P}_4\text{Se}_3)$ [163] or $(\text{TiX}_4)_2(\text{S}_4\text{N}_4)_2$ ($\text{X} = \text{Cl, Br, I}$) [148, 151, 154] were reported. We are now interested whether other cages, especially phosphorus chalcogenide cages, can be used for such purposes.

Screening with different phosphorus sulfides was carried out. They show a broader structural variety than the selenides and are easier to prepare and handle, since phosphorus selenides tend to glass formation and are much less soluble in any solvent.

In addition to the co-crystals $(\text{M}_2\text{Cl}_{10})(\text{P}_4\text{S}_{10})_2$ [164] and the $(\text{MCl}_5)_2(\beta\text{-P}_4\text{Ch}_4)$ adducts [165] isotopic with $(\text{NbCl}_5)_2(\beta\text{-P}_4\text{S}_4)$ [163] ($\text{M} = \text{Nb, Ta}$; $\text{Ch} = \text{S, Se}$), new adduct compounds of different phosphorus sulfide cages could now be obtained: $(\text{TaCl}_5)(\alpha\text{-P}_4\text{S}_4)$, $(\text{TaCl}_5)(\alpha\text{-P}_4\text{S}_5)$, $(\text{TaCl}_5)(\beta\text{-P}_4\text{S}_5)$, $(\text{NbCl}_5)(\beta\text{-P}_4\text{S}_5)$, and $(\text{TaCl}_5)(\beta\text{-P}_4\text{S}_6)$.

To understand the nature of the binding between metal center and cage, electronic structure calculations were performed employing density functional theory (DFT) as well as ab initio wavefunction-based methods. DFT yields exceedingly low binding energies and distances considerably too long for the coordinative bond between metal center and cage (in comparison to the experimental results). This result suggests that a major fraction of the binding energy may come from long-range van der Waals dispersion, which is not described at all by DFT in conjunction with common functionals. Therefore, the individual adducts were studied also at the level of Møller Plesset perturbation theory of second order (MP2), the computationally cheapest method capturing dynamical correlation effects (and thus van

der Waals dispersion). In the present study, we employed the local MP2 (LMP2) method [58], which apart from higher computational efficiency, also offers some additional benefits over the canonical MP2 method [41]. Of course, MP2 can only be applied if near degeneracy effects are absent. Indeed, the adducts investigated in the present study are not multireference cases, as we could verify by initially performing complete active space self-consistent field (CASSCF) test calculations. Hence, LMP2 appears to be a suitable method for the present case.

6.2 Computational methods

Minimum energy geometries and relative energies of different isomers of the individual compounds were calculated by employing DFT, as well as second-order Møller-Plesset perturbation theory. For the DFT calculations, the Becke-Perdew BP86 [166] and the B3-LYP [167] exchange correlation functionals were used. The MP2 calculations were performed because van der Waals forces, which are not included in a DFT treatment with present functionals, are likely to play a significant role in the bonding between the cage and the TaCl₅ subunits. Initial complete active space self-consistent field test calculations, also performed in the context of this work, indicate that a multireference treatment is not required for a proper description of the binding between the TaCl₅ subunit and the individual cages.

For the MP2 calculations, the local MP2 method [58, 132] as implemented in the MOLPRO [96] program package was used. The density fitting (DF) approximation for the electron repulsion integrals was invoked, which allows for much more efficient algorithms to be used (in particular also for computing analytic energy gradients [101] as required for geometry optimizations) at virtually no loss in accuracy.

It was demonstrated previously that local correlation methods avoid basis set superposition error (BSSE) effects to large extent by construction [41]. Hence, as a further bonus of local MP2, quasi-BSSE-free geometry optimizations can be carried out in a convenient way, that is, without any need for counterpoise correction [40] of the individual energy gradients involved.

For the tantalum atoms, the Stuttgart/Cologne ECP60MWB quasi-relativistic energy-adjusted pseudopotential, which substitutes the Ta¹³⁺ core orbitals, together with the related (8s7p6d2f1g)/[6s5p3d2f1g] AO basis set was employed [168, 169]. For the remaining atoms, the augmented correlation consistent AO basis sets aug-cc-pVXZ of Dunning [33, 34] were used (X=D for geometry optimizations, X=T for single-point energies). As fitting basis sets for the DF approximation, the auxiliary basis related to the aug-cc-pVXZ AO sets optimized for DF-MP2 [99]

were taken for the MP2 component of energy and gradient, while for the Hartree-Fock part the JK fitting basis sets of Weigend [136] related to the cc-pV(X+1)Z AO basis were used. For the tantalum/ECP60MWB AO basis no optimized fitting basis set is yet available. Therefore, the fitting basis set related to the QZVPP AO basis [170] was used, which should be sufficiently large to guarantee accurate fitting of the individual orbital product densities.

The localized molecular orbitals spanning the occupied orbital space of the Hartree-Fock reference were generated by using the Pipek-Mezey localization procedure [62]. Pair domains were constructed by using a completeness criterion [137] of 0.98 and 0.985 for the X=D and X=T AO basis sets, respectively. For all calculations the pair domains were further extended by all next nearest-neighbor centers.

For the DFT calculations (carried out by utilizing the **TURBOMOLE** program package [146, 171, 172]), the same AO and auxiliary basis sets and the same pseudopotential as for the local MP2 calculations were used. For both geometry optimizations and single-point energy calculations X=T was used. The final interaction energies, obtained at DFT and MP2 levels, were all counterpoise-corrected (in the case of local MP2 to remove the BSSE of the Hartree-Fock energy) and also include the relaxation energies of the individual fragments [173].

The experimental work is explained in detail in refs. 174 and 175.

6.3 Results and Discussion

6.3.1 Constitution and packing

Crystal-structure analysis showed that the title compounds are small adduct molecules consisting of one TaCl₅ or NbCl₅ unit linked with a phosphorus sulfide cage (Figures 6.1–6.4). The constitution of the respective phosphorus sulfide part does not change upon coordination. In contrast to the starting materials, tantalum and niobium pentachloride are monomeric in all analyzed adducts. A distorted octahedron was found as the coordination sphere around the metal atom for each adduct. The coordinative bond towards the metal atoms is formed by a terminal sulfur atom, if present, or otherwise by a phosphorus atom of the cages.

The dumbbell-shaped molecules are arranged in distorted hexagonal layers with the layers oriented parallel to the crystallographic (001) planes in all cases (Figure 6.5).

6 Adducts of tantalum chlorides and phosphorus sulfide cages

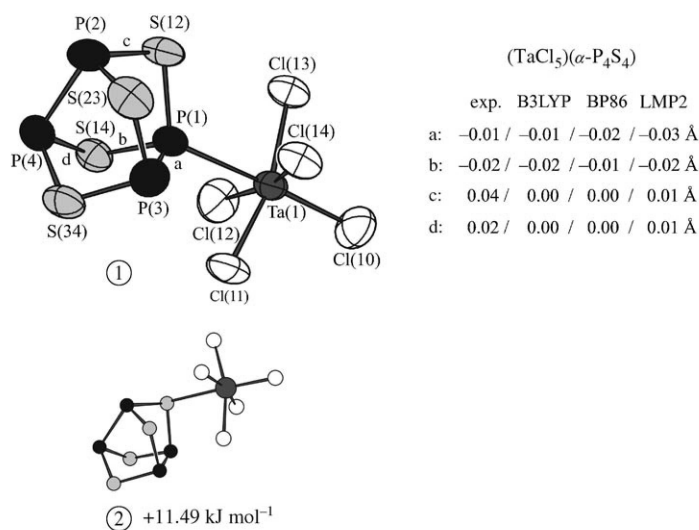


Figure 6.1: Experimental and calculated structures of (TaCl₅)(α-P₄S₄). Phosphorus: black, sulfur: light gray, tantalum: dark gray, chlorine: white. Left: Crystal structure; ellipsoids enclose 70 % probability for atomic displacement. Right: The four largest changes (labeled a, b, c, d) in bond lengths from experimental results and calculations with DFT (using B3LYP and BP86 xc functional, aug-cc-pVTZ AO basis set) and LMP2 (by one-nearest-neighbor extended domains, aug-cc-pVDZ AO basis set) level of theory. Bottom: coordination alternatives with relative energies relative to coordination modes found. See Table 6.2.

In (TaCl₅)(α-P₄S₄), one of the four equivalent phosphorus atoms of the D_{2d} -symmetrical α-P₄S₄ molecule is connected to one metal chloride unit. The C_s symmetry of the resulting adduct is almost preserved in the crystal structure.

In the closely related adducts (NbCl₅)(β-P₄S₅) and (TaCl₅)(β-P₄S₅), one phosphorus atom of the remaining P₂ dumbbell in the C_{2v} -symmetrical β-P₄S₅ cage is bound to the metal chloride unit. The deviation of the adduct molecule from C_s symmetry is a bit larger than that in α-P₄S₄-containing molecules. As the two β-P₄S₅-containing adducts are similar, only the one with TaCl₅ will be referred to further.

In (TaCl₅)(α-P₄S₅) and (TaCl₅)(β-P₄S₆), the terminal sulfur atoms of the cages form coordinative bonds to the metal atoms. Since the free α-P₄S₅ cage is entirely unsymmetrical, the adduct molecules of (TaCl₅)(α-P₄S₅) are unsymmetrical as well. β-P₄S₆, in contrast, exhibits C_s symmetry. However, the adduct molecules (TaCl₅)(β-P₄S₆) also have only C_1 symmetry. The two compounds crystallize with

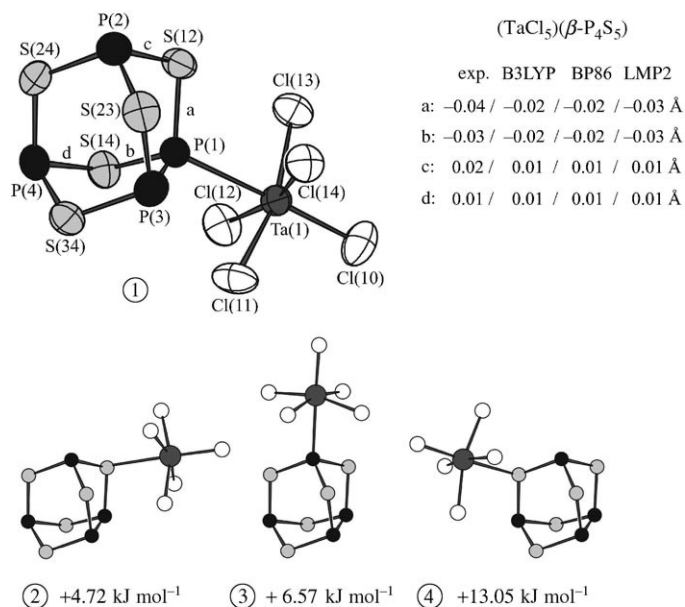


Figure 6.2: Experimental and calculated structures of (TaCl₅)(β-P₄S₅); see legend of Figure 6.1.

very similar packing of the molecules. The projections of the crystal structures along the [100] direction are given in Figure 6.5.

6.3.2 Conformation

Nonperiodic *ab initio* electronic-structure calculations were performed to assess the strength of the interaction between TaCl₅ and the individual cages and to study alternative conformers not observed experimentally. The geometry optimizations of the individual adduct molecules yielded structural parameters that are reasonably close to those observed in the crystal structures. Therefore, the orientations of the four equatorial chlorine atoms of the MCl₅ groups (anticipated to rotate almost freely), and the orientations of the whole MCl₅ units relative to the individual cages (for molecules with a terminal sulfur atom at the cages) observed experimentally are not primarily related to crystal formation but a property of the individual adduct molecules themselves.

Nevertheless, there are small deviations: In (TaCl₅)(α-P₄S₄) and (TaCl₅)(β-P₄S₅), the TaCl₅ unit is turned out of the "ideal" position for *C_s* symmetry by up to 10°, which cannot be considered as being the energetic minimum of the single molecule and which therefore has to be attributed to the influence of intermolecular forces or packing of molecules in the crystal.

6 Adducts of tantalum chlorides and phosphorus sulfide cages

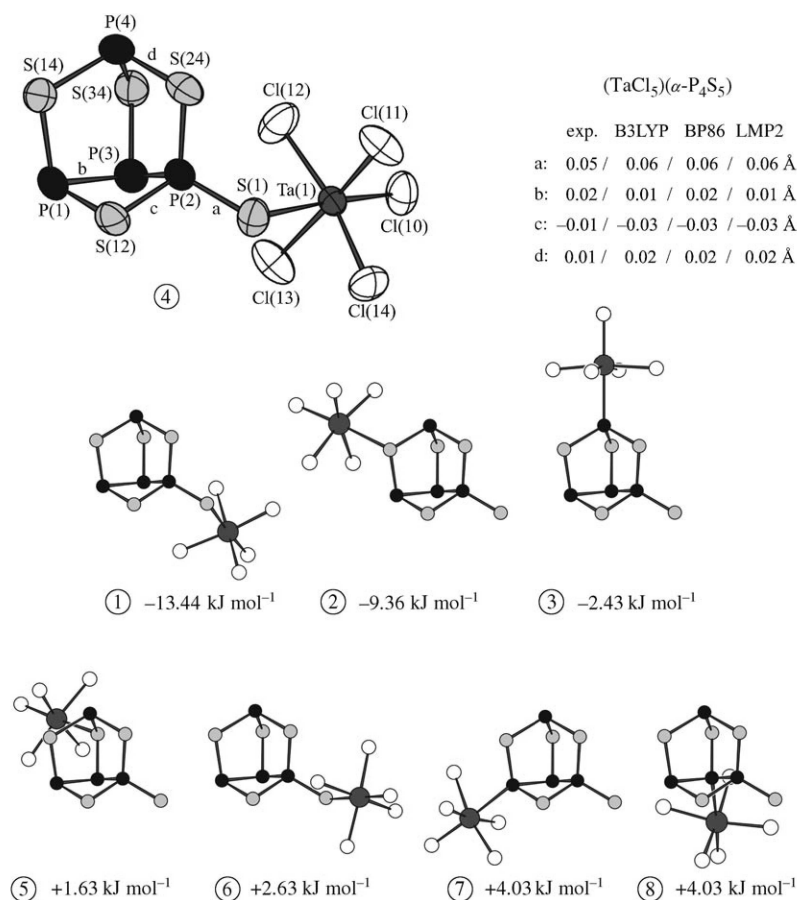


Figure 6.3: Experimental and calculated structures of (TaCl₅)(α-P₄S₅); see legend of Figure 6.1.

In the two adduct molecules with a terminal sulfur atom connected to the metal center, the TaCl₅ units possess greater flexibility because of the additional P–S_{terminal} rotation axis. Closer examination of the molecular conformation of (TaCl₅)(α-P₄S₅) and (TaCl₅)(β-P₄S₆) reveals that stabilizing intramolecular interactions may force the metal chloride units to arrange as observed. The closest chlorine atoms reach more or less into a cavity of the cage – a five-membered ring of phosphorus and sulfur of the α-P₄S₅ cage and a six-membered ring of the β-P₄S₆ cage. Thus, comparatively short distances between the nonbonded atoms S(1) and Cl(14) in α-P₄S₅ of 3.19 Å(exptl)/3.20 Å(calcd) and between S(1) and Cl(12) in β-P₄S₆ of 3.16 Å(exptl)/3.19 Å(calcd) result. Rotation about the P–S_{terminal} axis leads to conformers that display energetic minima as well (see below).

As already stated, the coordination octahedra of the metal atoms formed by chlorine and phosphorus or sulfur atoms are distorted. The angles (Cl_{equatorial}–

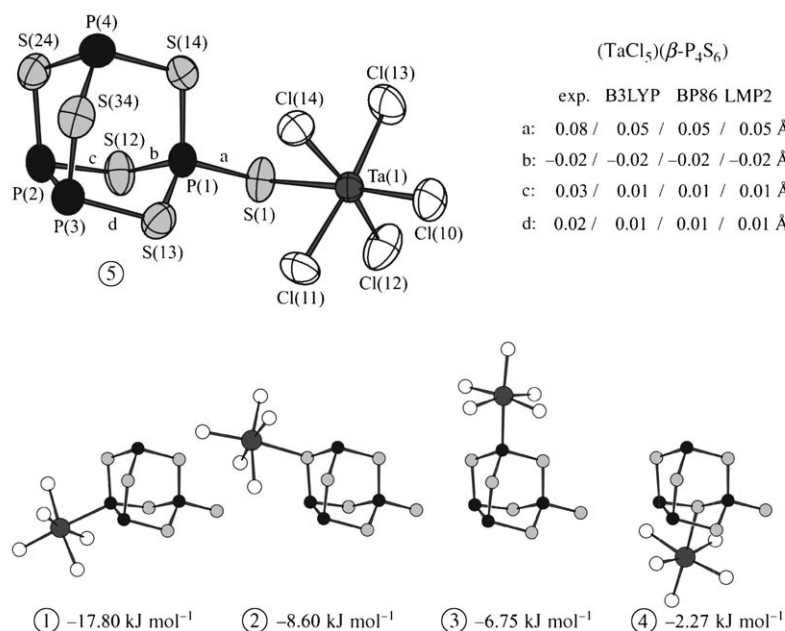


Figure 6.4: Experimental and calculated structures of (TaCl₅)(β-P₄S₆); see legend of Figure 6.1.

Ta–Cl_{axial}) are enlarged, which shifts the equatorial chlorine atoms towards the phosphorus or sulfur atoms, so the metal atoms lie about 0.2 to 0.4 Å from the Cl_{equatorial} plane. In addition, the P–Ta–Cl_{axial} or S–Ta–Cl_{axial} axis bends. The corresponding bond angles are 173.78 (exptl)/175.08 (calcd) for the α-P₄S₄ adduct, 175.18 (exptl)/174.98 (calcd) for the β-P₄S₅ adduct with Ta, 175.88 (exptl)/176.38 (calcd) for the α-P₄S₅ adduct, and 173.68 (exptl)/173.58 (calcd) for the β-P₄S₆ adduct. The distortion can be attributed to a second-order Jahn-Teller effect [176] usually observed, for example, in octahedral complexes of d⁰ transition metals (e.g. Na[TaCl₆]) [177].

6.3.3 Bond lengths

Bond lengths: The experimentally obtained and the calculated distances $d(\text{P-Ta})$ (or $d(\text{S-Ta})$), and the different bond lengths within the individual cages of the four adducts are compiled in Table 6.1. Evidently, the calculated LMP2 values for the distances $d(\text{P-Ta})$ of the isolated complexes are in good agreement with the values measured in the crystal. They deviate by 0.017 and 0.003 Å from the experimental values for (TaCl₅)(α-P₄S₄) and (TaCl₅)(β-P₄S₅), respectively. For DFT, the agreement is much worse; for example, for the B3-LYP case, the corresponding deviations amount to 0.138 and 0.133 Å.

6 Adducts of tantalum chlorides and phosphorus sulfide cages

		$\alpha\text{-P}_4\text{S}_4$			$(\text{TaCl}_5)(\alpha\text{-P}_4\text{S}_4)$			
Bond	Exptl ^a	B3LYP	BP86	LMP2	Exptl	B3LYP	BP86	LMP2
P(1) -P(3)	2.3530(8)	2.410	2.420	2.403	2.340(6)	2.397	2.404	2.375
-S(12)	2.1117(7)	2.139	2.141	2.146	2.104(5)	2.124	2.129	2.123
-S(14)	2.1095(7)	2.139	2.141	2.146	2.086(6)	2.124	2.129	2.123
P(2) -P(4)	2.3530(8)	2.409	2.419	2.403	2.379(6)	2.416	2.429	2.415
-S(12)	2.1068(8)	2.139	2.141	2.146	2.148(6)	2.141	2.142	2.155
-S(23)	2.1145(7)	2.139	2.141	2.146	2.117(9)	2.141	2.143	2.149
P(3) -S(23)	2.1145(7)	2.139	2.141	2.146	2.134(7)	2.137	2.140	2.148
-S(34)	2.1068(8)	2.139	2.141	2.146	2.089(7)	2.137	2.140	2.148
P(4) -S(14)	2.1095(7)	2.139	2.142	2.146	2.131(5)	2.141	2.142	2.155
-S(34)	2.1117(7)	2.139	2.141	2.146	2.141(7)	2.141	2.143	2.149
Ta(1) -P(1)					2.737(4)	2.875	2.812	2.754
		$\alpha\text{-P}_4\text{S}_5$			$(\text{TaCl}_5)(\alpha\text{-P}_4\text{S}_5)$			
Bond	Exptl	B3LYP	BP86	LMP2	Exptl	B3LYP	BP86	LMP2
P(1) -P(3)	2.269(1)	2.303	2.308	2.316	2.289(3)	2.314	2.324	2.330
-S(12)	2.179(1)	2.170	2.176	2.185	2.181(3)	2.180	2.185	2.196
-S(14)	2.130(1)	2.157	2.159	2.156	2.134(2)	2.151	2.155	2.153
P(2) -P(3)	2.240(1)	2.290	2.300	2.293	2.241(2)	2.298	2.305	2.300
-S(1)	1.950(1)	1.933	1.939	1.943	2.003(2)	1.988	1.999	2.003
-S(12)	2.098(1)	2.150	2.155	2.158	2.086(2)	2.121	2.125	2.126
-S(24)	2.100(1)	2.158	2.166	2.158	2.089(2)	2.133	2.138	2.127
P(3) -S(34)	2.080(1)	2.089	2.086	2.097	2.076(2)	2.087	2.086	2.094
P(4) -S(14)	2.122(1)	2.145	2.149	2.149	2.134(2)	2.144	2.146	2.151
-S(24)	2.134(1)	2.142	2.142	2.147	2.147(3)	2.157	2.161	2.162
-S(34)	2.145(1)	2.182	2.195	2.189	2.145(3)	2.174	2.183	2.180
Ta(1) -S(1)					2.665(2)	2.843	2.779	2.735
		$\beta\text{-P}_4\text{S}_5$			$(\text{TaCl}_5)(\beta\text{-P}_4\text{S}_5)$			
Bond	Exptl	B3LYP	BP86	LMP2	Exptl	B3LYP	BP86	LMP2
P(1) -P(3)	2.302(3)	2.346	2.361	2.343	2.304(1)	2.342	2.351	2.328
-S(12)	2.128(3)	2.144	2.145	2.150	2.092(1)	2.126	2.128	2.123
-S(14)	2.117(3)	2.144	2.145	2.150	2.090(2)	2.126	2.128	2.123
P(2) -S(12)	2.122(2)	2.147	2.153	2.152	2.144(2)	2.153	2.160	2.166
-S(23)	2.122(2)	2.147	2.153	2.152	2.126(2)	2.148	2.153	2.154
-S(24)	2.134(4)	2.163	2.167	2.164	2.120(2)	2.159	2.162	2.161
P(3) -S(23)	2.128(3)	2.144	2.145	2.150	2.118(2)	2.142	2.145	2.152
-S(34)	2.117(3)	2.144	2.145	2.150	2.113(2)	2.142	2.144	2.152
P(4) -S(14)	2.117(3)	2.147	2.153	2.152	2.131(2)	2.153	2.160	2.166
-S(24)	2.132(4)	2.163	2.167	2.164	2.116(2)	2.159	2.162	2.161
-S(34)	2.117(3)	2.147	2.153	2.152	2.115(2)	2.148	2.153	2.154
Ta(1) -P(1)					2.762(1)	2.895	2.822	2.765
		$\beta\text{-P}_4\text{S}_5$			$(\text{TaCl}_5)(\beta\text{-P}_4\text{S}_5)$			
Bond	Exptl ^b	B3LYP	BP86	LMP2	Exptl	B3LYP	BP86	LMP2
P(1) -S(1)	1.914(4)	1.930	1.937	1.942	1.990(2)	1.977	1.985	1.992
-S(12)	2.089(4)	2.142	2.149	2.143	2.074(2)	2.125	2.129	2.124
-S(13)	2.095(4)	2.142	2.150	2.143	2.104(3)	2.125	2.130	2.123
-S(14)	2.086(4)	2.136	2.135	2.134	2.080(2)	2.122	2.124	2.117
P(2) -P(3)	2.309(4)	2.360	2.369	2.362	2.305(3)	2.356	2.365	2.356
-S(12)	2.110(4)	2.139	2.141	2.147	2.143(2)	2.148	2.150	2.159
-S(24)	2.123(4)	2.146	2.150	2.150	2.118(3)	2.143	2.147	2.146
P(3) -S(13)	2.115(4)	2.139	2.141	2.147	2.138(3)	2.146	2.149	2.156
-S(34)	2.104(4)	2.146	2.150	2.150	2.146(3)	2.142	2.145	2.149
P(4) -S(14)	2.145(5)	2.188	2.201	2.187	2.159(3)	2.193	2.201	2.192
-S(24)	2.092(5)	2.135	2.138	2.142	2.098(3)	2.136	2.139	2.144
-S(34)	2.145(5)	2.135	2.138	2.142	2.121(3)	2.135	2.138	2.141
Ta(1) -S(1)					2.702(2)	2.912	2.846	2.798

a) Experimental data taken from Ref. 178.

b) Experimental data taken from Ref. 179.

Table 6.1: Bond lengths [\AA] in coordinated and noncoordinated cages.

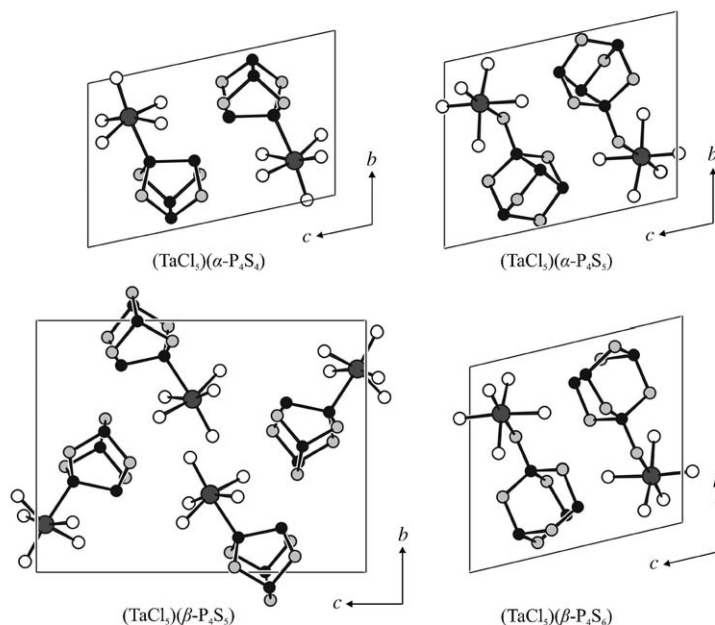


Figure 6.5: Projection of the crystal structures of $(\text{TaCl}_5)(\alpha\text{-P}_4\text{S}_4)$, $(\text{TaCl}_5)(\alpha\text{-P}_4\text{S}_5)$, $(\text{TaCl}_5)(\beta\text{-P}_4\text{S}_5)$, and $(\text{TaCl}_5)(\beta\text{-P}_4\text{S}_6)$ in the $[100]$ direction. Phosphorus: black, sulfur: light gray, tantalum: dark gray, chlorine: white.

For the distances $d(\text{S-Ta})$ in the adducts in which the free terminal sulfur atoms act as the donors of the cages, the deviations between the calculated LMP2 values and the experimental values measured in the crystal increase to 0.07 Å for $(\text{TaCl}_5)(\alpha\text{-P}_4\text{S}_5)$ and to 0.096 Å for $(\text{TaCl}_5)(\beta\text{-P}_4\text{S}_6)$. Again, the discrepancies for the corresponding B3-LYP results are significantly larger, amounting to 0.178 and to 0.21 Å, respectively. Since the latter complexes are more flexible (see above), the influence of crystal packing on their structural parameters is expected to be larger than for adducts with a direct linkage of Ta to a P atom of the cage. Hence, the bigger discrepancies between calculated and measured values for the distances $d(\text{S-Ta})$ are not surprising. The bad performance of DFT in comparison with LMP2 indicates that van der Waals dispersion (absent in DFT calculations employing the usual xc functionals) plays a crucial role in the binding between TaCl_5 and the individual cages. Furthermore, if van der Waals dispersion contributes substantially to the binding energy, then the LMP2 results are likely to improve further when the AO basis set is extended and the large core pseudopotential for tantalum is substituted by a small core pseudopotential (presently not available). The importance of van der Waals dispersion in the binding of these adducts will be discussed further in the next section.

6 Adducts of tantalum chlorides and phosphorus sulfide cages

Coordination causes certain bonds within the individual cages to contract or elongate, as is evident from experimental as well as theoretical data compiled in Figures 6.1–6.4 and Table 6.1. As known from other adduct molecules such as $(\text{SbCl}_5)(\text{S}_4\text{N}_4)$ [180] or $(\text{SbCl}_5)(\text{S}_8\text{O})$ [181], the formation of the coordinative bond between Lewis acid (electron-pair acceptor) and Lewis base (electron-pair donor, phosphorus sulfide in this case) not only weakens the adjacent bond but also alters the bond lengths throughout the whole cage molecule (Figure 6.6). In $(\text{SbCl}_5)(\text{S}_4\text{N}_4)$, this even leads to cleavage of the S–S bonds: the S_4N_4 molecule connected to SbCl_5 is merely annular [182].

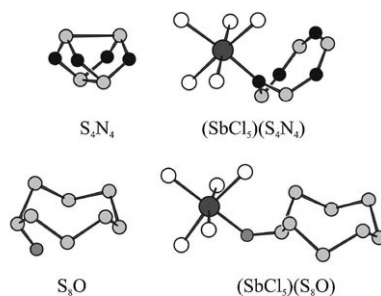


Figure 6.6: Molecules S_4N_4 [182], S_8 [183], and adducts $(\text{SbCl}_5)(\text{S}_4\text{N}_4)$ [180] and $(\text{SbCl}_5)(\text{S}_8\text{O})$ [181]. Antimony: dark gray, chlorine: white, sulfur: light gray, nitrogen: black, oxygen: medium gray.

For the adducts presented herein, it is notable that especially the bond between phosphorus and the terminal sulfur atoms, if present, lengthens considerably upon coordination, as do the second nearest bonds within the cages (this situation holds also for adducts linked through phosphorus), whereas the bonds in between are shortened slightly. In Figures 6.1–6.4, bonds that show the strongest alterations upon coordination of the metal chloride units are marked with a, b, c, and d. The scheme of alternate elongation and contraction of bonds is disturbed by the shape of the cages, being composed of concatenated rings of atoms. In $(\text{SbCl}_5)(\text{S}_8\text{O})$, the analogous sequence of bond elongation and shortening relative to the noncoordinated S_8O can be followed more explicitly because of the ring shape of the sulfur oxide [181, 183].

The local MP2 geometries mostly confirm these subtle changes of bond lengths (cf. Figures 6.1–6.4 and Table 6.1). For $(\text{TaCl}_5)(\alpha\text{-P}_4\text{S}_4)$, bonds of the phosphorus atom P(4) as well as the P(2)–S(12) bond are found to be significantly elongated, the P(1)–S(14) bond in contrast is shortened. In $(\text{TaCl}_5)(\beta\text{-P}_4\text{S}_5)$, bonds of the phosphorus atom P(1), which is directly connected to tantalum, is shortened, the adjacent bonds P(2)–S(12) and P(4)–S(14) are elongated, P(2)–S(24) again is shortened. $(\text{TaCl}_5)(\alpha\text{-P}_4\text{S}_5)$ and $(\text{TaCl}_5)(\beta\text{-P}_4\text{S}_6)$ show a quite pronounced elonga-

tion of the P-S_{terminal} bonds as mentioned earlier. Besides, bonds P(1)–P(3) and P(4)–S(24) in (TaCl₅)(α -P₄S₅) and P(2)–S(12) and P(3)–S(13) in (TaCl₅)(β -P₄S₆) are elongated, bonds P(2)–S(12) in (TaCl₅)(α -P₄S₅) and P(1)–S(12) in (TaCl₅)(β -P₄S₆) are shortened. Interestingly, LMP2 and DFT predict very similar changes in these bond lengths, as is evident from Figures 6.1–6.4. We conclude that these changes are primarily induced by the weak chemical bond formed between TaCl₅ and the individual cages, which is properly described both by LMP2 and DFT, whereas van der Waals dispersion, even though constituting an important fraction of the overall binding energy, does not induce any significant changes in the intramolecular bonds of the cages.

6.3.4 Alternative coordination modes

Alternative coordination modes: For all phosphorus sulfide cages, only one coordination type was observed experimentally. In contrast, in the α -P₄S₅, β -P₄S₅, and β -P₄S₆ cages, there are chemically different phosphorus atoms available as possible bonding partners, and all phosphorus sulfide cages could coordinate through sulfur atoms within the cage framework as well. However, phosphorus atoms connected to three sulfur atoms were not found to form a coordinative bond to the metal chlorides under investigation, in contrast to the case of P₄S₃ [149, 158–162]. In fact, coordination through bridging sulfur atoms of the cages could not be observed at all with the metal chlorides used, and only one example for such coordination type is known [158, 162].

Alternative coordination sites of the phosphorus sulfides were explored by locating the corresponding minimum energy geometries on the DFT and local MP2 potential energy hypersurfaces. Structural parameters and the related binding energies (with respect to dissociation of the adducts into their phosphorus sulfide and the TaCl₅ fragments) are compiled in Figures 6.1–6.4 and Tables 6.1 and 6.2. Table 6.3 demonstrates that the deviations between local and canonical MP2 are rather small, especially when extended domains are employed (as in the present work).

The binding between the TaCl₅ subunit and the individual phosphorus sulfide cages is rather delicate and needs some discussion. Comparison of the DFT and local MP2 binding energies in Table 6.2 reveals that DFT grossly underestimates the binding between the two subunits. In fact, the binding energy predicted by DFT is even substantially smaller than that of a hydrogen bond, occurring, for example, in the water dimer (about 20 kJ mol⁻¹). This is particularly true for the case of the hybrid functional, where self-interaction is reduced owing to admixing of nonlocal (Hartree-Fock) exchange. At the level of Hartree-Fock theory, similar

Adduct	coord. via	No. in Fig. 6.1–6.4	B3LYP				BP				LMP2 (ext. domains)			
			E_{int}	E_{rel} (TaCl ₅)	E_{rel} (cage)	E_{bind}	E_{int}	E_{rel} (TaCl ₅)	E_{rel} (cage)	E_{bind}	E_{int}	E_{rel} (TaCl ₅)	E_{rel} (cage)	E_{bind}
(TaCl ₅)(α -P ₄ S ₄)	P	(1)	-40.026	-26.874	-4.291	-8.861	-47.918	-25.296	-4.664	-17.959	-107.752	-13.219	-8.619	-85.914
	S	(2)	-21.376	-23.893	-3.121	+5.638	-31.058	-25.142	-4.262	-1.654	-97.421	-17.415	-5.584	-74.421
(TaCl ₅)(α -P ₄ S ₅)	S(1)	(4)	-50.432	-36.917	-7.756	-5.759	-57.828	-36.827	-8.618	-12.382	-123.589	-34.966	-12.432	-76.191
	S(1)	(1)	-53.384	-37.615	-6.545	-9.224	-59.581	-36.517	-6.565	-16.499	-127.951	-28.880	-9.441	-89.630
	S(1)	(6)	-48.448	-35.748	-6.585	-6.115	-54.184	-35.141	-7.080	-11.964	-116.378	-33.869	-8.950	-73.559
	P(1)	(7)	-31.148	-24.345	-2.896	-3.907	-44.667	-23.028	-3.600	-18.038	-98.138	-19.329	-6.650	-72.159
	P(4)	(3)	-27.748	-23.517	-2.933	-1.298	-37.121	-22.802	-2.951	-11.368	-95.903	-11.143	-6.136	-78.624
	S(14)		-4.936	-15.639	-1.265	+11.968	-21.465	-23.441	-3.827	+5.803	-88.155	-24.496	-4.603	-59.056
	S(14)	(2)	-29.655	-26.656	-4.389	+1.391	-41.390	-27.662	-5.697	-8.031	-110.258	-18.552	-6.154	-85.552
	S(34)		^a				-19.893	-21.976	-4.423	+6.506	-90.928	-13.695	-8.000	-69.234
	S(34)	(5)	-14.653	-21.278	-2.570	+9.195	-26.186	-23.926	-3.584	+1.324	-94.692	-15.307	-4.823	-74.563
	S(24)		^a				-23.583	-24.558	-5.010	+5.985	-95.710	-25.824	-7.275	-62.610
	S(24)		^a				-14.673	-21.426	-3.382	+10.135	-86.761	-23.669	-5.288	-57.804
	P(3)	(8)	-20.474	-23.783	-3.017	+6.326	-30.392	-23.459	-3.471	-3.462	-92.486	-12.518	-6.687	-72.159
	S(12)		-6.137	-15.212	-1.248	+10.322	-27.427	-24.700	-4.524	+1.797	-97.215	-19.119	-7.028	-71.068
	S(12)		^a				-14.888	-20.836	-2.520	+8.468	-86.840	-23.868	-3.941	-59.030
(TaCl ₅)(β -P ₄ S ₅)	P(1)	(1)	-39.850	-26.289	-3.973	-9.589	-48.580	-24.558	-4.445	-19.577	-114.329	-13.067	-8.165	-93.096
	P(2)	(3)	-33.495	-24.878	-3.323	-5.295	-42.040	-23.728	-3.360	-14.952	-105.287	-12.155	-6.603	-86.529
	S(12)		-13.076	-20.712	-2.140	+9.776	-26.174	-24.891	-3.583	+2.300	-90.458	-24.507	-4.657	-61.295
	S(12)	(2)	-30.422	-26.188	-4.400	+0.166	-41.859	-26.581	-5.632	-9.646	-112.881	-18.100	-6.404	-88.377
(TaCl ₅)(β -P ₄ S ₆)	S(24)	(4)	-29.650	-26.935	-5.371	+2.656	-40.348	-27.520	-6.649	-6.179	-106.424	-17.877	-8.504	-80.043
	S(1)	(5)	-38.171	-31.966	-5.594	-0.610	-43.062	-31.144	-5.765	-6.154	-106.156	-23.401	-6.910	-75.845
	S(1)		-34.958	-30.815	-4.673	+0.529	-40.354	-30.558	-4.937	-4.860	-101.485	-23.446	-6.574	-71.465
	S(1)		-37.271	-31.552	-5.678	-0.041	-42.034	-30.702	-5.848	-5.485	-105.206	-23.551	-6.979	-74.677
	P(2)	(1)	-35.320	-24.815	-3.653	-6.852	-44.613	-23.323	-3.916	-17.374	-113.429	-11.426	-8.358	-93.644
	P(4)	(3)	-27.975	-23.738	-2.793	-1.444	-37.891	-23.132	-2.905	-11.854	-100.367	-12.109	-5.666	-82.592
	S(12)		^a				-7.379	-17.577	-2.492	+12.690	-80.494	-21.377	-5.477	-53.640
	S(12)	(4)	^a				-24.548	-23.870	-4.130	+3.452	-101.250	-17.614	-5.521	-78.114
	S(14)		^a				-19.774	-22.669	-4.580	+7.475	-94.537	-24.207	-7.409	-62.920
	S(24)		^a				-19.559	-22.890	-3.587	+6.919	-86.616	-23.672	-4.167	-58.777
	S(24)	(2)	-23.462	-24.193	-3.752	+4.483	-36.056	-25.684	-5.313	-5.058	-108.202	-17.486	-6.272	-84.444
(TaCl ₅) ₂			-168.832	-85.345	-85.347	+1.859	-169.427	-79.832	-79.832	-9.763	-246.380	-82.706	-82.701	-80.974

a) Not bound on the corresponding potential energy surface.

Table 6.2: Interaction, relaxation and binding energies of the structures and their coordination alternatives, in kJ/mol.

6.3 Results and Discussion

Adduct	Coord. through	No. in Fig. 6.1–6.4	HF	LMP2	LMP2 (ext. domains)	MP2
(TaCl ₅)(α -P ₄ S ₄)	P	(1)	-29.728	-102.514	-107.752	-107.382
	S	(2)	-9.935	-89.782	-97.421	-97.991
(TaCl ₅)(α -P ₄ S ₅)	S(1)	(4)	-53.992	-117.157	-123.589	-123.479
	S(1)	(1)	-50.559	-122.561	-127.951	-127.709
	S(1)	(6)	-48.086	-110.063	-116.378	-116.285
	P(1)	(7)	-19.047	-92.321	-98.138	-97.885
	P(4)	(3)	-12.891	-89.570	-95.903	-95.804
	S(14)		3.461	-81.364	-88.155	-88.210
	S(14)	(2)	-11.343	-102.668	-110.258	-110.537
	S(34)		5.022	-82.133	-90.928	-89.850
	S(34)	(5)	-1.549	-87.345	-94.692	-95.105
	S(24)		12.039	-86.813	-95.710	-96.143
	S(24)		14.528	-81.656	-86.761	-86.453
	P(3)	(8)	-4.352	-86.084	-92.486	-92.910
	S(12)		0.002	-89.727	-97.215	-97.360
	S(12)		10.485	-81.789	-86.840	-86.565
(TaCl ₅)(β -P ₄ S ₅)	P(1)	(1)	-27.659	-106.232	-114.329	-114.996
	P(2)	(3)	-20.223	-99.920	105.287	-104.749
	S(12)		-0.249	-80.899	-90.458	-90.795
	S(12)	(2)	-11.868	-104.690	-112.881	-112.927
	S(24)	(4)	14.758	-97.414	-106.424	-106.665
(TaCl ₅)(β -P ₄ S ₆)	S(1)	(5)	-36.085	-101.883	-106.156	-106.016
	S(1)		-35.106	-96.003	-101.485	-101.626
	S(1)		-35.288	-98.307	-105.206	-105.648
	P(2)	(1)	-20.603	-107.319	-113.429	-112.913
	P(4)	(3)	-12.573	-94.615	-100.367	-99.935
	S(12)		17.938	-74.297	-80.494	-80.216
	S(12)	(4)	8.252	-93.683	-101.250	-101.313
	S(14)		11.314	-87.920	-94.537	-94.786
	S(24)		8.252	-78.819	-86.616	-86.767
	S(24)	(2)	-6.027	-101.071	-108.202	-108.151
(TaCl ₅) ₂			-169.072	-241.826	-246.380	-245.265

Table 6.3: Interaction energies, calculated with X=T basis set at Hartree-Fock, local (with normal and by 1 bond extended domains) and canonical MP2 level of theory, respectively, in kJ/mol.

binding energies are obtained as for DFT/B3-LYP. Nevertheless, a weak bond is formed between TaCl_5 and the individual cages at the Hartree-Fock level, which is, for example, reflected by the fact that the localization procedure (used for the subsequent local MP2 treatment; see above) generates a local bicentric orbital involving the Ta and the P (or S) atoms of the related cage (Figure 6.7). The gain in energy obtained by forming this bond, however, is to a large extent offset by exchange repulsion and geometrical deformation energies. Hence, the net energy gain due to formation of this bond is quite small. Nevertheless, this bond appears to be responsible for the subtle changes of the bond lengths within the individual cages resulting from coordination (see above).

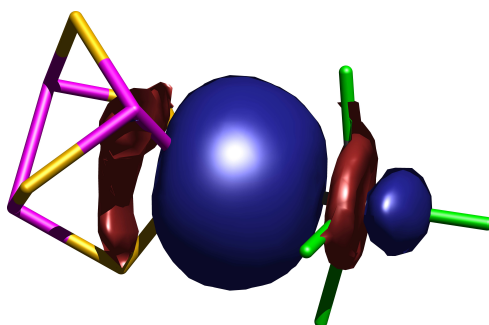


Figure 6.7: Isoplot of the binding orbital between (TaCl_5) and $(\alpha\text{-P}_4\text{S}_4)$ fragments of value 0.015. This orbital was obtained by the Pipek-Mezey localization procedure from the set of canonical Hartree-Fock orbitals.

At the MP2 level, however, substantially larger binding energies are obtained (76–93 kJ mol⁻¹). This difference could be attributed to long-range dispersion electron correlation effects (such as van der Waals forces), which are absent both at the Hartree-Fock level and in DFT (with presently available exchange-correlation functionals), but which are accounted for at the level of MP2. Considering the large polarizabilities of the individual subunits, noticeable van der Waals contributions to the binding energy are not too surprising. Taking into account the astonishingly small DFT binding energies, one may even argue that the major contributions to the binding energies of the individual adducts are actually indeed of van der Waals type. Van der Waals type interactions between closed-shell subunits are ubiquitous in inorganic chemistry (see Ref. 184 for a review). For example, they are clearly dominant in the aurophilic attraction between AuI ions [185, 186]. For a definite answer about the role of van der Waals forces in the adducts characterized in the present work, however, a more detailed study of the interactions between the phosphorus sulfide and the TaCl_5 subunits is required (e.g., based on a partitioning of the LMP2 correlation energy), as was done previously for dimers of coinage metal complexes [185, 186].

In any case, because of the poor description of the binding of the adducts by DFT, we will focus in the following discussion on the results obtained at the level of local MP2. In Figures 6.1–6.4, the different adduct isomers are enumerated in descending order with respect to their binding energies. For $(\text{TaCl}_5)(\alpha\text{-P}_4\text{S}_4)$ the alternative coordination mode (2) through a sulfur atom is $11.49 \text{ kJ mol}^{-1}$ less stable than the observed coordination through phosphorus.

For $(\text{TaCl}_5)(\beta\text{-P}_4\text{S}_5)$, the observed coordination through one of the phosphorus dumbbell atoms leads to the adduct with lowest energy. Coordination mode 2 through one of the four equivalent sulfur atoms and coordination mode 3 through an isolated phosphorus atom are 4.72 kJ mol^{-1} and 6.57 kJ mol^{-1} , respectively, less stable. The binding energies of adducts coordinated through the sulfur bridge (4) decrease even further (by $13.05 \text{ kJ mol}^{-1}$) relative to the global minimum.

For $(\text{TaCl}_5)(\alpha\text{-P}_4\text{S}_5)$, the coordination mode (4) through the terminal sulfur atom, observed in the conformation in the crystal, is according to the LMP2 calculations $13.44 \text{ kJ mol}^{-1}$ above the global minimum, conformation 1, obtained from 4 by rotation about the $\text{P-S}_{\text{terminal}}$ axis. As already stated, this rotation is not sterically hindered and requires only a small activation energy. The alternative – and most stable – conformer therefore is possibly not realized in the crystal for packing reasons but may also be the preferred one for the $\alpha\text{-P}_4\text{S}_5$ adduct in solution. Coordination mode 2 through the sulfur atom S(14) is still energetically favored relative to 4 by 9.36 kJ mol^{-1} , and even the coordination through the apical phosphorus atom P(4), variant 3, is more stable (by 2.43 kJ mol^{-1}) than the observed conformer. However, the coordination alternatives given as variants 5, 6, 7, and 8 (i.e., isomers coordinated through S(34), another conformational variant to the S(1) linkage) and coordination through the basal phosphorus atoms P(1) or P(3) are energetically less favored (by 1.63, 2.63, 4.03, and 4.03 kJ mol^{-1} , respectively). Notably, the three coordination modes through the terminal sulfur atom feature stronger binding at the (uncorrelated) Hartree-Fock level by about 20 kJ mol^{-1} relative to the remaining conformers. This result indicates that for such coordination modes, the covalent bond and eventually also electrostatic interactions play a more pronounced role in the binding than for the remaining conformers.

Finally, the global minimum for $(\text{TaCl}_5)(\beta\text{-P}_4\text{S}_6)$ features coordination through one of the phosphorus dumbbell atoms P(2) or P(3) (variant 1). The binding energy is $17.80 \text{ kJ mol}^{-1}$ larger than for the experimentally observed coordination through the terminal sulfur atom (variant 5). For this adduct there is a significant mismatch between the structural arrangements occurring in the crystal on the one hand and that of the isolated adduct predicted by theory on the other. Also, other adduct isomers coordinated through the sulfur atom S(24) (variant 2), the apical phosphorus atom P(4) (variant 3), or the sulfur atom S(12) (variant 4), are

energetically more stable by 8.60, 6.75, and 2.27 kJ mol⁻¹, respectively, relative to the β -P₄S₆ adduct observed experimentally. However, the alternative conformer for the linkage through the terminal sulfur atom given as variant 6 has a lower binding energy (1.17 kJ mol⁻¹) and is therefore less stable than the conformer observed.

Geometry optimizations for all possible coordination conformers were performed. Other coordination alternatives not listed here were found to be even less stable. Considering the LMP2 dissociation energy of (TaCl₅)₂, which amounts to 80.97 kJ mol⁻¹, the formation of all considered species presented herein is exothermic in the gas phase.

In conclusion, there is a general preference for coordination through basal/-dumbbell phosphorus atoms or terminal sulfur atoms (if present). Structural arrangements corresponding to such coordination modes are found to be most stable. A substantial part of the binding energy between the phosphorus sulfide cage and the TaCl₅ subunit can be ascribed to van der Waals dispersion. There is a mismatch between experimental results and theory for one case, where the experimentally found geometry does not correspond to the theoretically predicted global minimum. The existence of a structure corresponding to the global minimum cannot yet be ruled out, particularly as the differences in binding energy for the several adduct isomers are rather small.

6.4 Conclusions

Not only the smallest phosphorus sulfide cage molecule P₄S₃ [147–162] but also cage-like phosphorus sulfides with higher sulfur content can act as ligands in metal complexes. Adducts of α -P₄S₄, β -P₄S₄, α -P₄S₅, β -P₄S₅, β -P₄S₆, and monomeric TaCl₅ or NbCl₅ units could be obtained so far. Phosphorus or sulfur atoms of the sulfide cages in principle can be connected to Lewis acids. We found that the coordination to the cage molecule is favored either to phosphorus sites with one adjacent phosphorus atom or to terminal sulfur sites. Coordination to bridging sulfur sites or to phosphorus sites bound to three sulfur atoms was energetically less stable.

The cage constitution is not changed upon coordination; however, certain bond lengths within the cages change as a result of coordination to the metal.

Generally, bonds between phosphorus atoms and the coordinated terminal sulfur site lengthen considerably. However, bonds involving phosphorus, either directly coordinated or adjacent to a coordinated terminal sulfur site, shorten. The next nearest bonds then lengthen. These relative changes of the individual bond lengths

within the cages are rather well described by both DFT and LMP2, which suggests that they are primarily caused by the weak coordinative bond formed between the metal center and the cage. However, the contribution of this bond to the overall binding energy of the adduct is small, and the dominant component appears to be long-range van der Waals dispersion. The latter is not captured by DFT (in conjunction with the usual functionals), which consequently leads to much too small binding energies and too large lengths of the coordinative bond as predicted by this method. MP2, on the other hand, describes van der Waals dispersion at a level corresponding to the uncoupled Hartree-Fock representation of the underlying dynamical polarizabilities (which usually leads to significant overestimation of binding energy in complexes such as the benzene dimer or argon clusters). So, although not highly accurate, MP2 certainly paints a much more realistic picture of the energetics than DFT in a situation in which long-range van der Waals dispersion is of importance (of course, we were lucky that near degeneracy effects were absent in the present system; otherwise, perturbation theory based on a single reference would not be applicable). Hence, we are sure to describe the present system at least qualitatively correct. To further improve the accuracy, coupled cluster calculations with reasonably large basis sets must be performed, which is beyond the scope of the present study. DFT, however, qualitatively fails for the present systems with weak coordinative bonds.

6 Adducts of tantalum chlorides and phosphorus sulfide cages

7 Summary

In this project molecular clusters of phenol and 2-naphthol with water, and molecular aniline homoclusters were studied by means of *ab initio* electronic structure theory. These systems can be observed experimentally in supersonic beam experiments and measured mass-selectively by spectroscopic methods. Molecular clusters in such experimental setups serve as test beds to explore the intermolecular interactions, since they are vibrationally cold and isolated from environmental influences. The complementary treatment of these systems by *ab initio* methods allows for a more profound interpretation of the systems measured.

The **phenol-water**_{1≤n≤3} clusters were explored on the $S_1(\pi^* \leftarrow \pi)$ surfaces. Especially the spectroscopical behavior of $n = 2$ is remarkably different from the $n = \{1, 3\}$ cases, because it exhibits a weak, broad and congested band structure in its absorption spectrum, as well as low quantum yield and short lifetime, in comparison to the narrow line spectra with defined origins of the absorption spectra of the latter.

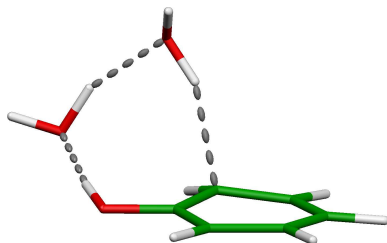


Figure 7.1: The global minimum structure of phenol-water₂ on the $S_1(\pi^* \leftarrow \pi)$ excited state.

It was found that for $n = 2$ the global minimum geometry (Fig. 7.1) in the excited state significantly differs from the ground state minimum. Whereas in the ground state the water molecules form a three membered ring with the hydroxy group of the phenol molecule, in the excited state the second water molecule acts as a H donor to the π system. Indeed similar structures could also be found for the $n = 3$ case, but in the $n = 2$ system no energetically competitive minimum exists in the vicinity of the Franck-Condon point, while this is the case for $n = 3$. Thus the small Franck-Condon factors explains both the weak intensity of the

7 Summary

band structure and the absence of the sharp line peaks in the spectrum of $n = 2$ in contrast to the spectra of $n = \{1, 3\}$. Furthermore, a conical intersection seam was located, which allows the systems to transfer a proton to the solvent molecules. The short lifetime of the $n = 2$ cluster can be explained by the rather high excess energy in the direction of out-of-plane modes, leading the system towards the conical intersection seam.

The **2-naphthol-water₂** system can be regarded as the larger relative of the phenol-water₂ cluster. Likewise its absorption spectrum also exhibits a peculiar structure. Two weak and congested bands structures along with two long progressions of line peaks can be observed. Depending on the orientation of the hydroxy group of the naphthol molecule, *trans* and *cis* conformers can be distinguished. It has been found that the two different kinds of hydrogen networks can coexist even in the ground state. Whereas the *trans* conformer energetically prefers the cyclic arrangement of the water molecules similar to phenol-water₂, for the *cis* conformer the cyclic arrangement and an arrangement where the second water molecule acts as a H donor to the π system are energetically almost equal. Upon excitation to the $S_1(\pi^* \leftarrow \pi)$ state the cyclic networks are no longer energetically competing, as it is the case in the phenol-water₂ cluster. Therefore, the cyclic conformers can be assigned to the weak and congested bands. The remaining *cis* conformer with the second water molecule interacting with the π system show much smaller changes in geometry upon excitation, and therefore can be assigned to the series of more structured peaks in the spectrum.

In contrast to the rather pronounced minima of the phenol- and naphthol-water_{*n*} systems, the potential energy surfaces of molecular **aniline homoclusters** involve a vast range of shallow minima. To locate the global and low-lying ground state minima a global optimization scheme was applied on a model potential, which was iteratively adapted to *ab initio* energies. It was found that the global minimum geometries of the dimer and trimer are energetically enough separated to be the only populated conformations within the typical vibrational temperatures in the experiment.

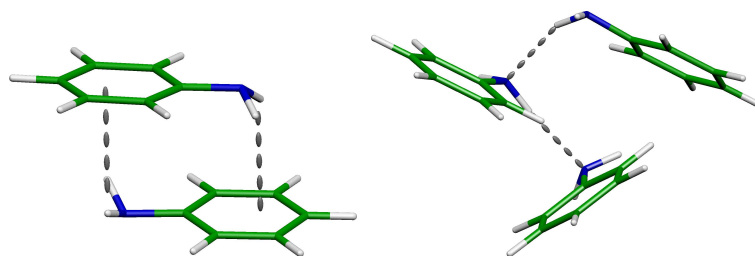


Figure 7.2: The global minimum structures of aniline₂ and aniline₃ in the ground state.

The dimer forms a head-to-tail arrangement (Fig. 7.2 on the left-hand side), with the amino groups of the almost equivalent molecules acting as double H donor to the π system of the opposing molecule, respectively. Due to the virtual equivalence of the monomers, two delocalized $\pi^* \leftarrow \pi$ excitations can be seen, of which the lower dark state leads to the formation of an excimer. The second, bright state can lead to a head-to-tail arrangement, but through the accessible conical intersection, the system is able to relax to the dark state and form the excimer.

The aniline trimer features two H bonds between the three amino groups, leading to three distinct monomers: Donor, both donor and acceptor, and acceptor monomer (Fig. 7.2 on the right-hand side). The three excited states are all local $\pi^* \leftarrow \pi$ excitations. The lowest excited state with the excitation localized on the donor monomer leads to a very similar geometry as the ground state geometry. The other two excited states relax to geometries significantly different from the Franck-Condon point, and thus, their origins are not anticipated to be visible in the spectrum.

Beside molecular clusters **adducts of tantalum chloride with the phosphorus sulfide cages**, α -P₄S₄, α -P₄S₅, β -P₄S₅ and β -P₄S₆, were investigated, too. As seen from experimental crystal structure data, the constitution of the cage molecules does not change upon coordination. A wide range of possible coordination modes have been screened and compared to the experimental data. *Ab initio* geometries without the crystal environment resemble the experimental geometries to a large extent, thus the crystal packing has only little effect on the obtained structures. Coordination to through basal/dumbbell phosphorus atoms or present terminal sulfur atoms is preferred and most stable.

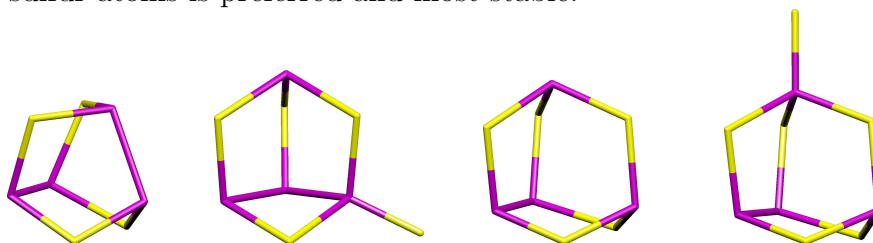


Figure 7.3: Uncoordinated phosphorus sulfide cage molecules, α -P₄S₄, α -P₄S₅, β -P₄S₅ and β -P₄S₆ (from left to right).

The weak coordinative bond between the cage and the tantalum chloride units causes a subtle change in the bond length pattern of the cage molecule. But it only represents a small contribution to the total binding energy between both subunits. The substantial part can be attributed to the long-range dispersion electron correlation effects, such as van der Waals forces. Considering the large polarizabilities of closed-shell compounds encountered in the inorganic chemistry,

7 *Summary*

the ubiquitous van der Waals forces render the investigation of those systems by means of density functional theory in conjunction with the frequently used functionals questionable, as they are not capable of describing these forces.

In conclusion, the spectra of phenol- and 2-naphthol-water clusters, whose interpretation was unclear for more than 15 years could finally be explained. Furthermore the delicate system of aniline homoclusters was interpreted. Also tantalum chloride adducts with phosphorus sulfide cages were investigated with the intriguing result, that the often neglected dispersion interaction occasionally plays an important role in inorganic systems.

Bibliography

- [1] Autumn, K.; Liang, Y. A.; Hsieh, S. T.; Zesch, W.; Chan, W. P.; Kenny, T. W.; Fearing, R.; Full, R. J. *Nature* **2000**, *405*, 681.
- [2] Jeziorski, B.; Moszynski, R.; Szalewicz, K. *Chem. Rev.* **1994**, *94*, 1887.
- [3] Stone, A. J. *The Theory of Intermolecular Forces*; Oxford University Press, 1996.
- [4] Chałasiński, G.; Szczęśniak, M. M. *Chem. Rev.* **2000**, *100*, 4227.
- [5] Eisenschitz, L.; London, F. *Z. Phys.* **1930**, *60*, 491.
- [6] Van der Avoird, A. *Chem. Phys. Lett.* **1967**, *1*, 24.
- [7] Van der Avoird, A. *Chem. Phys. Lett.* **1967**, *1*, 411.
- [8] Van der Avoird, A. *J. Chem. Phys.* **1967**, *47*, 3649.
- [9] Jeziorski, B.; Moszynski, R.; Ratkiewicz, A.; Rybak, S.; Szalewicz, K.; Williams, H. L. SAPT: a program for many-body symmetry-adapted perturbation theory calculations of intermolecular interaction energies. In *Methods and Techniques in Computational Chemistry: METECC94*; Clementi, E., Ed.; STEF: Cagliari, 1993; Vol. B, p 79.
- [10] Heßelmann, A.; Jansen, G.; Schütz, M. *J. Chem. Phys.* **2005**, *122*, 014103.
- [11] Korona, T.; Werner, H.-J. *J. Chem. Phys.* **2003**, *118*, 3006.
- [12] Elrod, M. J.; Saykally, R. J. *Chem. Rev.* **1994**, *94*, 1975.
- [13] Xantheas, S. S. *J. Chem. Phys.* **1994**, *100*, 7523.
- [14] Axilrod, B. M.; Teller, E. *J. Chem. Phys.* **1943**, *11*, 299.
- [15] Muto, Y. *Proc. Phys.-Math. Soc. Japan* **1943**, *17*, 629.
- [16] *Chem. Rev.* **1988**, *88*, 815–988.

Bibliography

- [17] *Chem. Rev.* **1994**, *94*, 1721–2160.
- [18] *Chem. Rev.* **2000**, *100*, 7–4264.
- [19] Brutschy, B. *Chem. Rev.* **2000**, *100*, 3891.
- [20] Saykally, R. J.; Blake, G. A. *Science* **1992**, *257*, 1937.
- [21] Liu, K.; Cruzan, J. D.; Saykally, R. J. *Science* **1996**, *271*, 929.
- [22] Braun, J. E.; Grebner, T. L.; Neusser, H. J. *J. Phys. Chem.* **1998**, *102*, 3273.
- [23] Buck, U.; Huisken, F. *Chem. Rev.* **2000**, *100*, 3863.
- [24] Buck, U.; Gu, X. J.; Lauenstein, C.; Rudolph, A. *J. Chem. Phys.* **1990**, *92*, 6017.
- [25] Behrens, M.; Fröchtenicht, R.; Hartmann, M.; Siebers, J. G.; Buck, U.; Hagemeister, F. C. *J. Chem. Phys.* **1999**, *111*, 2436.
- [26] Sadlej, J.; Buch, V.; Kazimirski, J. K.; Buck, U. *J. Phys. Chem. A* **1999**, *103*, 4933.
- [27] Bruderer, J.; Melzer, M.; Buck, U.; Kazimirski, J. K.; Sadlej, J.; Bush, V. *J. Chem. Phys.* **1999**, *110*, 10649.
- [28] Borho, N.; Suhm, M. A. *Phys. Chem. Chem. Phys.* **2002**, *4*, 2721.
- [29] Born, M.; Oppenheimer, R. *Annalen der Physik* **1927**, *84*, 457.
- [30] Hellmann, H. *J. Chem. Phys.* **1935**, *3*, 61.
- [31] Reiher, M.; Wolf, A. *Relativistic Quantum Chemistry*; WILEY-VCH, 2009.
- [32] T. H. Dunning, J. *J. Chem. Phys.* **1989**, *90*, 1007.
- [33] T. H. Dunning, J.; Hay, P. J. In *Modern theoretical chemistry*; Schaefer, H. F., Ed.; Plenum Press: New York, 1977; Vol. 3, Chapter 1, pp 1–27, Gaussian Basis Sets for Molecular Calculations.
- [34] Kendall, R. A.; Dunning, T. H.; Harrison, R. J. *J. Chem. Phys.* **1992**, *96*, 6796.
- [35] Helgaker, T.; Jørgensen, P.; Olsen, J.; John Wiley & Sons Ltd.: Baffins Lane, Chichester, 2000; p 323.
- [36] Hartree, D. R. *Rep. Prog. Phys.* **1948**, *11*, 113.

- [37] Seitz, F. In *The Modern Theory of Solids*; McGraw-Hill Book Company, Inc., New York, 1940; Chapter VI and VII.
- [38] Paldus, J.; Li, X. *Adv. Chem. Phys.* **1999**, *110*, 1.
- [39] Møller, C.; Plesset, M. S. *Phys. Rev.* **1934**, *46*, 618.
- [40] Boys, S. F.; Bernardi, F. *Mol. Phys.* **1970**, *19*, 553.
- [41] Schütz, M.; Rauhut, G.; Werner, H.-J. *J. Phys. Chem. A* **1998**, *102*, 5997.
- [42] Bowman, J. M.; Christoffel, K.; Tobin, F. *J. Phys. Chem.* **1979**, *83*, 905.
- [43] Christoffel, K. M.; Bowman, J. M. *Chem. Phys. Lett.* **1982**, *85*, 220.
- [44] Christoffel, K. M.; Bowman, J. M. *Theor. Chim. Acta* **1998**, 191.
- [45] Hrenar, T.; Werner, H.-J.; Rauhut, G. *J. Chem. Phys.* **2007**, *126*, 134108.
- [46] Christiansen, O.; Koch, H.; Jørgensen, P. *Chem. Phys. Lett.* **1995**, *243*, 409.
- [47] Christiansen, O.; Jørgensen, P.; Hättig, C. *Int. J. Quantum Chem.* **1997**, *68*, 1.
- [48] Grimme, S. *J. Chem. Phys.* **2003**, *118*, 9095.
- [49] Hellweg, A.; Grün, S. A.; Hättig, C. *Phys. Chem. Chem. Phys.* **2008**, *10*, 4119.
- [50] Kucharski, S. A.; Bartlett, R. J. *Adv. Quant. Chem.* **1986**, *18*, 281.
- [51] Crawford, T. D.; III, H. F. S. *Rev. Comp. Chem.* **2000**, *14*, 33.
- [52] Bachorz, R. A.; Bischoff, F. A.; Höfener, S.; Klopper, W.; Ottiger, P.; Leist, R.; Frey, J. A.; Leutwyler, S. *Phys. Chem. Chem. Phys.* **2008**, *10*, 2758.
- [53] Jung, Y.; Lochan, R. C.; Dutoi, A. D.; Head-Gordon, M. *J. Chem. Phys.* **2004**, *121*, 9793.
- [54] Almlöf, J. *Chem. Phys. Lett.* **1991**, *181*, 319.
- [55] Saebø, S.; Pulay, P. *Annu. Rev. Phys. Chem.* **1993**, *44*, 213.
- [56] Pulay, P. *Chem. Phys. Lett.* **1983**, *100*, 151.
- [57] Hampel, C.; H.-J.-Werner, *J. Chem. Phys.* **1996**, *104*, 6286.

Bibliography

- [58] Schütz, M.; Hetzer, G.; Werner, H.-J. *J. Chem. Phys.* **1999**, *111*, 5691.
- [59] Schütz, M.; Werner, H.-J. *J. Chem. Phys.* **2001**, *114*, 661.
- [60] Schütz, M. *J. Chem. Phys.* **2000**, *113*, 9986.
- [61] Schütz, M. *J. Chem. Phys.* **2002**, *116*, 8772.
- [62] Pipek, J.; Mezey, P. *J. Chem. Phys.* **1989**, *90*, 4916.
- [63] Baerends, E. J.; Ellis, D. E. *Chem. Phys.* **1973**, *2*, 41.
- [64] Whitten, J. L. *J. Chem. Phys.* **1973**, *58*, 4496.
- [65] Dunlap, B. I.; Connolly, J. W. D.; Sabin, J. R. *J. Chem. Phys.* **1979**, *71*, 3396.
- [66] Häser, M.; Almlöf, J. *J. Chem. Phys.* **1992**, *96*, 489.
- [67] Feyereisen, M.; Fitzgerald, G.; Komornicki, A. *Chem. Phys. Lett.* **1993**, *208*, 359.
- [68] Fuke, K.; Kaya, K. *Chem. Phys. Lett.* **1983**, *94*, 97.
- [69] Oikawa, A.; Abe, H.; Mikami, N.; M.Ito, *J. Phys. Chem.* **1983**, *87*, 5083.
- [70] Lipert, R. J.; Colson, S. D. *J. Chem. Phys.* **1988**, *89*, 4579.
- [71] Lipert, R. J.; Colson, S. D. *J. Phys. Chem.* **1989**, *93*, 135.
- [72] Lipert, R. J.; Colson, S. D. *Chem. Phys. Lett.* **1989**, *161*, 303.
- [73] Stanley, R. J.; A. W. Castleman, J. *J. Chem. Phys.* **1991**, *94*, 7744.
- [74] Schütz, M.; Bürgi, T.; Leutwyler, S.; Fischer, T. *J. Chem. Phys.* **1993**, *98*, 3763.
- [75] Leutwyler, S.; Bürgi, T.; Schütz, M.; Taylor, A. *Farad. Discuss. Chem. Soc.* **1994**, *97*, 285.
- [76] Bürgi, T.; Schütz, M.; Leutwyler, S. *J. Chem. Phys.* **1995**, *103*, 6350.
- [77] Jacoby, C.; Roth, W.; Schmitt, M.; Janzen, C.; Spangenberg, D.; Kleiner-manns, K. *J. Phys. Chem. A* **1998**, *102*, 4471.
- [78] Watanabe, T.; Ebata, T.; Tanabe, S.; Mikami, N. *J. Chem. Phys.* **1996**, *105*, 408.

- [79] Schütz, M.; Bürgi, T.; Leutwyler, S. *J. Mol. Struct. THEOCHEM* **1992**, *276*, 117.
- [80] Feller, D.; Feyereisen, M. *J. Comput. Chem.* **1993**, *14*, 1027.
- [81] Gerhards, M.; Kleinermanns, K. *J. Chem. Phys.* **1995**, *103*, 7392.
- [82] Watanabe, H.; Iwata, S. *J. Chem. Phys.* **1996**, *105*, 420.
- [83] Fang, W.-H. *J. Chem. Phys.* **2000**, *112*, 1204.
- [84] Fang, W.-H.; Liu, R.-Z. *J. Chem. Phys.* **2000**, *113*, 5253.
- [85] Kryachko, E.; Nakatsuji, H. *J. Phys. Chem. A* **2002**, *106*, 731.
- [86] Benoit, D. M.; Clary, D. C. *J. Phys. Chem. A* **2000**, *104*, 5590.
- [87] Lüchow, A.; Spangenberg, D.; Janzen, C.; Jansen, A.; Gerhards, M.; Kleinermanns, K. *Phys. Chem. Chem. Phys.* **2001**, *3*, 2771.
- [88] Sobolewski, A. L.; Domcke, W. *J. Phys. Chem. A* **2001**, *105*, 9275.
- [89] Sobolewski, A. L.; Domcke, W.; Dedonder-Lardeux, C.; Jouvet, C. *Phys. Chem. Chem. Phys.* **2002**, *4*, 1093.
- [90] Hättig, C. *J. Chem. Phys.* **2003**, *118*, 7751.
- [91] Köhn, A.; Hättig, C. *J. Chem. Phys.* **2003**, *119*, 5021.
- [92] Ragazos, I.; Robb, M.; Bernardi, F.; Olivucci, M. *Chem. Phys. Lett.* **1992**, *197*, 217.
- [93] Köhn, A.; Tajti, A. *J. Chem. Phys.* **2007**, *127*, 044105.
- [94] Kats, D.; Korona, T.; Schütz, M. *J. Chem. Phys.* **2006**, *125*, 104106.
- [95] Kats, D.; Korona, T.; Schütz, M. *J. Chem. Phys.* **2007**, *127*, 064107.
- [96] Werner, H.-J. et al. *MOLPRO, version 2009.1, a package of ab initio programs*, 2010, see <http://www.molpro.net>.
- [97] Celani, P.; Werner, H.-J. *J. Chem. Phys.* **2003**, *119*, 5044.
- [98] Dunning, Jr., T. H.; Hay, P. J. In *Methods of electronic structure theory*; H. F. Schaefer III, Ed.; Plenum Press, 1977; Vol. 2.
- [99] Weigend, F.; Köhn, A.; Hättig, C. *J. Chem. Phys.* **2002**, *116*, 3175.

Bibliography

- [100] Klopper, W.; Schütz, M.; Lüthi, H.-P.; Leutwyler, S. *J. Chem. Phys.* **1995**, *103*, 1085.
- [101] Schütz, M.; Werner, H.-J.; Lindh, R.; Manby, F. R. *J. Chem. Phys.* **2004**, *121*, 737.
- [102] Schemmel, D.; Schütz, M. *J. Chem. Phys.* **2007**, *127*, 174304.
- [103] Salman, S. *Org. Magn. Reson.* **1984**, *22*, 385.
- [104] Hollas, J. M.; bin Hussein, M. Z. *J. Mol. Spectrosc.* **1988**, *127*, 497.
- [105] Johnson, J.; Jordan, K.; Plusquellic, D.; Pratt, D. *J. Chem. Phys.* **1990**, *93*, 2258.
- [106] Ebata, T.; Kouyama, K.; Mikami, N. *J. Chem. Phys.* **2003**, *119*, 2947.
- [107] Kouyama, K.; Miyazaki, M.; Mikami, N.; Ebata, T. *J. Chem. Phys.* **2006**, *124*, 054315.
- [108] Droz, T.; Knochenmuss, R.; Leutwyler, S. *J. Chem. Phys.* **1990**, *93*, 4520.
- [109] Schütz, M.; Bürgi, T.; Leutwyler, S.; Fischer, T. *J. Chem. Phys.* **1993**, *99*, 1469.
- [110] Weller, A. *Prog. React. Kinet.* **1970**, *5*, 273.
- [111] Plusquellic, D.; Tan, X.-Q.; Pratt, D. *J. Chem. Phys.* **1992**, *96*, 8026.
- [112] Matsumoto, Y.; Ebata, T.; Mikami, N. *J. Chem. Phys.* **1998**, *109*, 6303.
- [113] Matsumoto, Y.; Ebata, T.; Mikami, N. *J. Phys. Chem. A* **2001**, *105*, 5727.
- [114] Niehaus, T. *J. Chem. Phys.* **2007**, *126*, 034303.
- [115] Hättig, C.; Köhn, A. *J. Chem. Phys.* **2002**, *117*, 6939.
- [116] Mata, R. A.; Werner, H.-J. *Mol. Phys.* **2007**, *105*, 2753.
- [117] Schütz, M.; Bürgi, T.; Leutwyler, S.; Bürgi, H. *J. Chem. Phys.* **1993**, *99*, 5228.
- [118] Schemmel, D.; Schütz, M. *J. Chem. Phys.* **2008**, *129*, 034301.
- [119] Yeh, J.-H.; Shen, T.-L.; Nocera, D. G.; Leroi, G.; Suzuka, I.; Ozawa, H.; Namuta, Y. *J. Phys. Chem.* **1996**, *100*, 4385.

- [120] Yamamoto, N.; Hino, K.; Mogi, K.; Ohashi, K.; Sakai, Y.; Sekiya, H. *Chem. Phys. Lett.* **2001**, *342*, 417.
- [121] Sugawara, K.-I.; Miyawaki, J.; Nakanaga, T.; Takeo, H.; Lembach, G.; Djafari, S.; Barth, H.-D.; Brutschy, B. *J. Phys. Chem.* **1996**, *100*, 17145.
- [122] Hoare, M. R. *Adv. Chem. Phys.* **1979**, *40*, 49.
- [123] Wille, L. T.; Vennik, J. *J. Phys. A* **1985**, *18*, L419.
- [124] Hartke, B. *Chem. Phys. Lett.* **1996**, *258*, 144.
- [125] Hartke, B.; Schütz, M.; Werner, H.-J. *Chem. Phys.* **1998**, *239*, 561.
- [126] Kirkpatrick, S.; Gelatt, C. D. J.; Vecchi, M. P. *Science* **1983**, *220*, 671.
- [127] Černý, V. *Journal of Optimization Theory and Applications* **1985**, *45*, 41.
- [128] Dueck, G.; Scheuer, T. *J. Comput. Phys.* **1990**, *90*, 161.
- [129] Hu, T. C.; Kahng, A. B.; Tsao, C.-W. A. *ORSA J. Comput.* **1995**, *7*, 417.
- [130] Vanderbilt, D.; Louie, S. G. *J. Comput. Phys.* **1984**, *56*, 259.
- [131] Applequist, J. *J. Chem. Phys.* **1985**, *83*, 809.
- [132] Werner, H.-J.; Manby, F. R.; Knowles, P. J. *J. Chem. Phys.* **2003**, *118*, 8149.
- [133] Schütz, M.; Werner, H.-J. *Chem. Phys. Lett.* **2000**, *318*, 370.
- [134] Schütz, M.; Manby, F. R. *Phys. Chem. Chem. Phys.* **2003**, *5*, 3349.
- [135] Grüning, M.; Gritsenko, O.; van Gisbergen, S.; Baerends, E. *J. Chem. Phys.* **2001**, *114*, 652.
- [136] Weigend, F. *Phys. Chem. Chem. Phys.* **2002**, *4*, 4285.
- [137] Boughton, J. W.; Pulay, P. *J. Comput. Chem.* **1993**, *13*, 736.
- [138] Lindh, R.; Bernhardsson, A.; Schütz, M. *Chem. Phys. Lett.* **1999**, *303*, 567.
- [139] Chałasiński, G.; Szcześniak, M. M.; Kendall, R. A. *J. Chem. Phys.* **1994**, *101*, 8860.
- [140] Sadeghian, K.; Bocola, M.; Schütz, M. *J. Am. Chem. Soc.* **2008**, *130*, 12501.
- [141] Sadeghian, K.; Bocola, M.; Schütz, M. *Phys. Chem. Chem. Phys.* **2010**, *12*, 8840.

Bibliography

- [142] Riley, K. E.; Pitoňák, M.; Jurečka, P.; Hobza, P. *Chem. Rev.* **2010**, *110*, 5023.
- [143] Schemmel, D.; Schütz, M. *J. Chem. Phys.* **2010**, *132*, 174303.
- [144] Ohashi, K.; Inokuchi, Y.; Izutsu, H.; Hino, K.; Yamamoto, N.; Nishi, N.; Sekiya, H. *Chem. Phys. Lett.* **2000**, *323*, 43.
- [145] Ohashi, K.; Inokuchi, Y.; Nishi, N.; Sekiya, H. *Chem. Phys. Lett.* **2002**, *357*, 223.
- [146] *TURBOMOLE V6.2 2010, a development of University of Karlsruhe and Forschungszentrum Karlsruhe GmbH, 1989-2007, TURBOMOLE GmbH, since 2007; available from <http://www.turbomole.com>.*
- [147] Riess, J. G.; J. R. Van Wazer, *J. Am. Chem. Soc.* **1966**, *88*, 2166.
- [148] Ashley, P. J.; Torrible, E. G. *Can. J. Chem.* **1969**, *47*, 2587.
- [149] Cordes, A. W.; Joyner, R. D.; Shores, R. D.; Dill, E. D. *Inorg. Chem.* **1974**, *13*, 132.
- [150] Walker, M. L.; Mills, J. L. *Inorg. Chem.* **1975**, *14*, 2438.
- [151] Alange, G. G.; Banister, A. J. *J. Inorg. Nucl. Chem.* **1978**, *40*, 203.
- [152] M. Di Vaira,; Peruzzini, M.; Stoppioni, P. *J. Chem. Soc. Chem. Commun.* **1983**, 903.
- [153] M. Di Vaira,; Peruzzini, M.; Stoppioni, P. *J. Chem. Soc. Dalton Trans.* **1985**, 291.
- [154] Thewaldt, U.; Holl, K. *Z. Naturforsch. B* **1988**, *43*, 467.
- [155] Wachter, J. *Angew. Chem.* **1998**, *110*, 782.
- [156] Wachter, J. *Angew. Chem. Int. Ed.* **1998**, *37*, 750.
- [157] Aubauer, C.; Irran, E.; Klapötke, T. M.; Schnick, W.; Schulz, A.; Senker, J. *Inorg. Chem.* **2001**, *40*, 4956.
- [158] Adolf, A.; Gonsior, M.; Krossing, I. *J. Am. Chem. Soc.* **2002**, *124*, 7111.
- [159] Guidoboni, E.; I. de Los Rios,; Ienco, A.; Marvelli, L.; Maelli, C.; Romerosa, A.; Rossi, R.; Peruzzini, M. *Inorg. Chem.* **2002**, *41*, 659.

- [160] I. de Los Rios,; Mani, F.; Peruzzini, M.; Stoppioni, P. *J. Organomet. Chem.* **2004**, *689*, 164.
- [161] M. Di Vaira,; I. de Los Rios,; Mani, F.; Peruzzini, M.; Stoppioni, P. *Eur. J. Inorg. Chem.* **2004**, 293.
- [162] Raabe, I.; Antonijevic, S.; Krossing, I. *Chem. Eur. J.* **2007**, *13*, 7510.
- [163] Nowotnick, H.; Stumpf, K.; Blachnik, R.; Reuter, H. *Z. Anorg. Allg. Chem.* **1999**, *625*, 693.
- [164] Pfitzner, A.; Hoppe, D. *Z. Anorg. Allg. Chem.* **2006**, *632*, 1771.
- [165] Hoppe, D.; Pfitzner, A. *Z. Naturforsch. B* **2009**, *64*, 58.
- [166] Perdew, J. P. *Phys. Rev. B: Condens. Matter Mater. Phys.* **1986**, *33*, 8822.
- [167] Becke, A. D. *J. Chem. Phys.* **1993**, *98*, 5648.
- [168] Andrae, D.; Haeussermann, U.; Dolg, M.; Stoll, H.; Preuss, H. *Theor. Chim. Acta* **1990**, *77*, 123.
- [169] Martin, J. M. L.; Sundermann, A. *J. Chem. Phys.* **2001**, *114*, 3408.
- [170] Hellweg, A.; Hättig, C.; Höfener, S.; Klopper, W. *Theor. Chim. Acc.* **2007**, *117*, 587.
- [171] Eichkorn, K.; Treutler, O.; Öhm, H.; Häser, M.; Ahlrichs, R. *Chem. Phys. Lett.* **1995**, *240*, 283.
- [172] Eichkorn, K.; Weigend, F.; Treutler, O.; Ahlrichs, R. *Theor. Chim. Acc.* **1997**, *97*, 119.
- [173] Stålring, J.; Schütz, M.; Lindh, R.; Karlström, G.; Widmark, P.-O. *Mol. Phys.* **2002**, *100*, 3389.
- [174] Hoppe, D.; Schemmel, D.; Schütz, M.; Pfitzner, A. *Chem. Eur. J.* **2009**, *15*, 7129.
- [175] Hoppe, D. Ph.D. thesis, Universität Regensburg, 2007.
- [176] Kunz, M.; Brown, I. D. *J. Solid State Chem.* **1995**, *115*, 395.
- [177] Henke, H. *Z. Kristallogr.* **1992**, *198*, 1.
- [178] Chang, C. C.; Haltiwanger, R. C.; Norman, A. D. *Inorg. Chem.* **1978**, *17*, 2056.

Bibliography

- [179] Blachnik, R.; Peukert, U.; Czediwoda, A.; Engelen, B.; Boldt, K. *Z. Anorg. Allg. Chem.* **1995**, *621*, 1637.
- [180] Neubauer, D.; Weiss, J. *Z. Anorg. Allg. Chem.* **1960**, *303*, 28.
- [181] Steudel, R.; Sandow, T.; Steidel, J. *J. Chem. Soc. Chem. Commun.* **1980**, 180.
- [182] Clark, D. *J. Chem. Soc.* **1952**, 1615.
- [183] Luger, P.; Bradaczek, H.; Steudel, R.; Rebsch, M. *Chem. Ber.* **1976**, *109*, 180.
- [184] Pyykkö, P. *Chem. Rev.* **1997**, *97*, 597.
- [185] Runeberg, N.; Schütz, M.; Werner, H.-J. *J. Chem. Phys.* **1999**, *110*, 7210.
- [186] Magnko, L.; Schweizer, M.; Rauhut, G.; Schütz, M.; Stoll, H.; Werner, H.-J. *Phys. Chem. Chem. Phys.* **2002**, *4*, 1006.

Erklärung

Ich erkläre hiermit an Eides statt, dass ich diese Arbeit selbst verfasst und keine anderen als die angegebenen Hilfsmittel verwendet habe. Alle aus anderen Quellen direkt oder indirekt übernommenen Daten und Konzepte sind unter Angabe des Literaturzitats gekennzeichnet.

Regensburg, September 2010

Dominik Schemmel